THE EFFECT OF ARYL HYDROCARBON RECEPTOR SIGNALING ON COLONIC STEM CELL BIOLOGY

A Dissertation

by

HUAJUN HAN

Submitted to the Office of Graduate and Professional Studies of
Texas A&M University
in partial fulfillment of the requirements for the degree of

DOCTOR OF PHILOSOPHY

Chair of Committee,	Vishal Gohil
Committee Members,	Robert S. Chapkin
	Lanying Zeng
	Stephen H. Safe
Head of Department,	A. Joshua Wand

August 2020

Major Subject: Biochemistry

Copyright 2020 Huajun Han

ABSTRACT

The aryl hydrocarbon receptor (AhR) is a ligand-activated basic helix-loop-helix transcription factor that binds and senses cues from promiscuous ligands including environmental toxicants and dietary/microbiota-derived physiologically relevant compounds. Emerging studies have indicated that AhR plays a suppressive role in colorectal cancer (CRC) tumorigenesis, the second leading cause of cancer death in the United States. However, mechanistic insights into how AhR activation prevents colon tumorigenesis are ill-defined. Since dysregulation in colonic stem cells is generally assumed to be the most efficient sequelae of tumorigenesis, it is important to define the role of AhR signaling in the regulation of colonic stem cells.

Here, we observed that the inducible deletion of AhR in $Lgr5^{+}$ stem cells increased the percentage of colonic stem cells and enhanced organoid initiating capacity and growth of both sorted stem and progenitor cells. Furthermore, intestinal specific AhR KO increased cell proliferation, and promoted colon tumorigenesis in a preclinical colitis-associated tumor model by upregulating FoxM1 signaling. Moreover, to further characterize the effect of AhR signaling on human colon adenoma transition, mice carrying $Apc^{S580/+}$; $Kras^{G12D/+}$ mutations, the most common mutations in CRC, were utilized. The combination of mutations in Apc, Kras, and AhR (triple mutant) increased organoid forming efficiency and growth of colonic stem/progenitor cells, and accelerated cell proliferation compared with the controls harboring only Apc and Kras mutations (double mutant). Importantly, the triple mutant organoids can grow independently of Wnt3a, R-Spondin1 and EGF growth factors by upregulating Wnt and EGF signaling

and loss of AhR promoted cecum and colon tumorigenesis. Finally, AhR deficiency desensitized the response of colonic stem/progenitor cells to IL-22 signaling by upregulating expression of SOCS3, a negative regulator of IL-22 signaling, and this resulted in an impaired DNA damage repair response. Deletion of SOCS3 in AhR KO organoids restored the effect of IL-22 treatment on the DNA damage repair response pathway.

In summary, our findings indicate that AhR plays a crucial role in colon tumorigenesis by modulating colonic stem/progenitor cell behavior and provide a rationale for targeting AhR as a new potential therapeutic strategy to prevent and treat colon cancer.

ACKNOWLEDGEMENTS

I would first like to express my sincere gratitude toward my research supervisor, Dr. Robert S. Chapkin, for his systematic and kind guidance, encouragement and support during my doctoral studies. I was really impressed each time when Dr. Chapkin helped me proofread my writings, with which red circles were always filled. I never met with such a supervisor or instructor to do proofreading in this way before. I kept all records. I think that is my treasure. Moreover, I am really inspired by the positive and shining attitude of Dr. Chapkin toward research and life. I also appreciate Dr. Chapkin's support for students to attend high-quality conferences every year. Dr. Chapkin's training has provided a strong foundation for my career.

I would also like to thank Dr. Stephen Safe, who is one of my committee members, for providing his invaluable expertise in aryl hydrocarbon receptor filed, and giving me immediate research discussion and support when needed. In addition, I acknowledge my committee members, Dr. Vishal Gohil and Dr. Langyin Zeng, for their insightful discussion and guidance during my annual research presentation meeting.

Thanks also go to the members of the Dr. Chapkin's lab, especially Dr. Laurie Davidson for her research coordination and support. Without their help, my research would not have continuously moved forward. In this lab, I not only benefited from the technique training, but also the overall lab organization.

In addition, I also appreciate the help and encouragement from my friends. Their warm welcome and sense of humor always sparks my life. With them, I know how lucky I am.

Finally, I deeply thank my parents and sister for their endless love and encouragement, which provided a powerful driving force at all times. Even though my parents did not provide direct guidance to my academic studies, their wisdom, determination, hardworking optimism and integrity are all encrypted in my mind, enabling me to tackle future challenges.

CONTRIBUTORS AND FUNDING SOURCES

Contributors

This work was supervised by a dissertation committee consisting of Professor Dr. Robert S. Chapkin [advisor] of the Department of Nutrition, Professor Dr. Vishal Gohil [Committee Chair] and Professor Dr. Lanying Zeng of the Department of Biochemistry and Biophysics and Professor Dr. Stephen Safe of the Department of Veterinary Physiology and Pharmacology.

In chapter 2, Dr. Grace Yoon and Jennifer Goldsby from Dr. Chapkin's lab performed RNA sequencing analysis. Dr. Laurie Davidson of Dr. Chapkin's lab performed experiments in Figure 6D&E and Figure 11J. Dr. Yang-Yi Fan of Dr. Chapkin's lab performed Seahorse and cell toxicity experiments in Figure 15, 16C and Table 1. Rachel Wrights of Dr. Chapkin's lab created artistic illustrations in Figure 1-4. Dr. Un-Ho Jin of Dr. Safe's lab performed ChIP experiments in Caco2 cells in Figure 16M&N. Dr. Bradley R. Weeks of Department of Veterinary Pathobiology provided pathological scoring analysis in AOM/DSS tumor study.

All other work conducted for the dissertation was completed by the student independently.

Funding Sources

This work was granted by Texas AgriLife Research, the Sid Kyle Chair Endowment, the Allen Endowed Chair in Nutrition & Chronic Disease Prevention, the

Cancer Prevention Research Institute of Texas (RP160589), and the National Institutes of Health (R01-ES025713, R01-CA202697, R35-CA197707 and T32-CA090301).

TABLE OF CONTENTS

Page

LIST OF FIGURES

Page

LIST OF TABLES

Page

1. INTRODUCTION

1.1. AhR signaling

The aryl hydrocarbon receptor (AhR) was initially identified as a hepatic cytosolic protein that bound a series of halogenated aromatic hydrocarbons including 2,3,7,8-tetrachlorodibenzo-p-dioxin (TCDD), and structurally similar polychlorinated dibenzo-p-dioxins, biphenyls, dibenzofurans, and polycyclic aromatic hydrocarbons, including 3-methylcholanthrene (3MC), β-naphthoflavone (BNF) and benzo[a]pyrene (**Fig. 1**). The bound AhR complex subsequently induces AhR-dependent expression of xenobiotic metabolizing genes including several forms of cytochrome P450 (CYP1A1, CYP1A2, CYP1B1), UDP-glucuronosyl transferases (UGT1A1) and other phase II drug metabolizing enzymes [1,2]. In the absence of ligands, the AhR is bound to several chaperone proteins in the cytoplasm including heat shock proteins 90 (Hsp90), p23 and immunophilin related protein XAP2 (**Fig. 2**). Upon ligand binding, XAP2 dissociates from the cytosolic AhR complex [3], and the AhR-ligand complex is then translocated into the nucleus. Once in the nucleus, Hsp90 and p23 are displaced by AhR nuclear translocator (ARNT) [4,5] to form a nuclear heterodimer, which then interacts with cis-acting dioxin response elements (DREs) within the core sequence 5'-TNGCGTG-3' or 5'-CACGCNA-3' on promoters of AhR-responsive genes [6]. In addition to the genes for xenobiotic metabolizing enzymes and monooxygenases, several genes such as AhR repressor (AHRR), Bax, Oct4, c-myc and SOX2 have also been identified as target genes for the AhR/ARNT system [7-10]. Following transcription, AhR is then exported from the nucleus and degraded by the cytoplasmic proteasome [11]. The AhR

independent of ARNT also regulates expression of genes that lack canonical DREs in their promoter regions, such as plasminogen activator inhibitor 1 (PAI-1) [12]. The recognition of non-canonical DREs in the PAI-1 promoter requires the interaction between AhR and the Kruppel-like factor (KLF) family member KLF6 [13]. In addition, there is also evidence that the AhR alone regulates non-genomic pathways and this resembles similar effects observed for some steroid hormone receptors that also activate both genomic and non-genomic pathways. In the past decade, the focus on AhR function has also been bifurcated into its (i) initially recognized xenobiotic metabolizing role, and (ii) other adaptive roles, such as organ development, cancer biology and immune regulation.

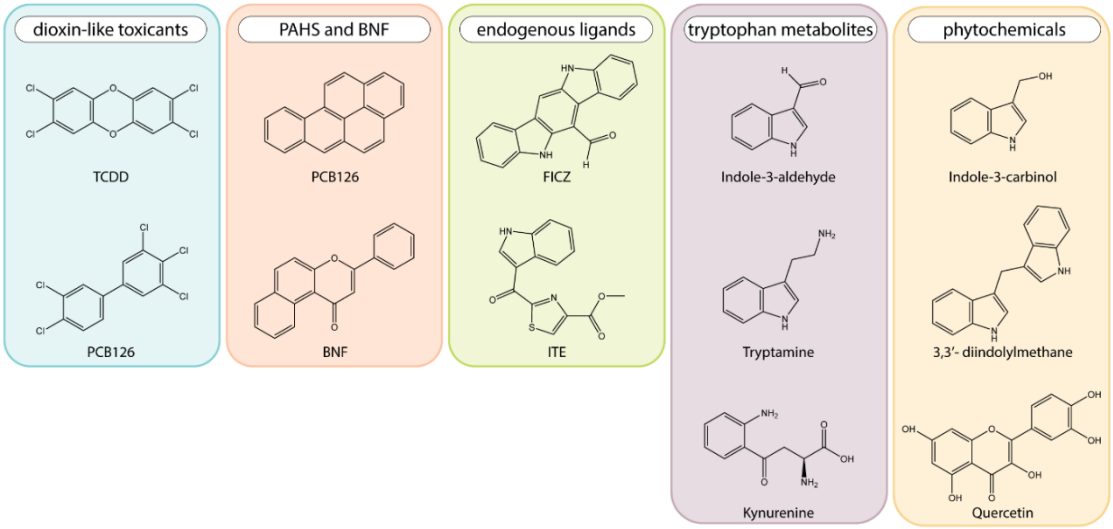

Figure 1. Structure of different classes of AhR ligands.
Dioxin-like toxicants and polycyclic aromatic hydrocarbons belong to synthetic AhR ligands with binding affinity ranging from pM to nM. Endogeous ligands, such as FICZ and ITE, tryptophan metabolites and phytochemicals represent naturally occurring AhR ligands with relatively lower binding affinity (nM to µM). PAHS: polycyclic aromatic hydrocarbons, BNF: β-naphthoflavone, TCDD: 2,3,7,8-tetrachlorodibenzo-p-dioxin, PCB126: 3,3',4,4',5-pentachlorobiphenyl, FICZ: 6-formylindolo [3,2-b]carbazole, ITE: 2-(1'H-indole-3-carbonyl)-thiazole-4-carboxylic acid methyl ester.

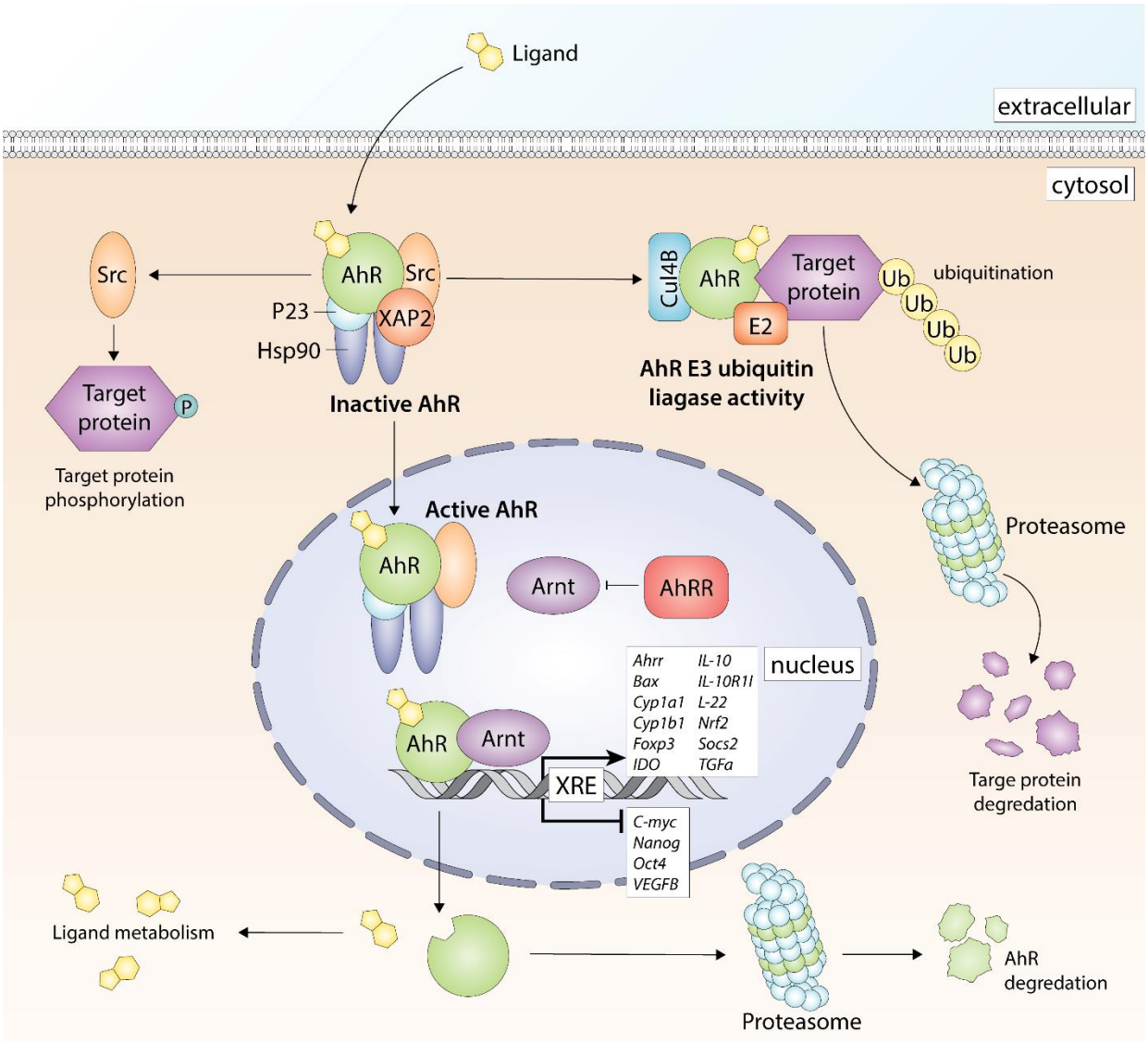

Figure 2. AhR signaling pathways.
AhR signaling pathways. Inactive AhR is sequestrated within the AhR chaperone complex containing heat shock protein 90 (Hsp90), immunophilin related protein XAP2, p23, and Src. Upon ligand binding, the AhR-ligand complex translocates to the nucleus, where Hsp90 and p23 are displaced by the AhR nuclear translocator (ARNT)[4,5], to form a heterodimer with AhR, which then binds to the xenobiotic response elements (XREs) to regulate the expression of genes that are involved in various cellular functions, including xenobiotic metabolism, cell apoptosis and proliferation, self-renewal and differentiation of stem cells, immune regulation, and redox biology. Following transcription, AhR is exported from the nucleus and degraded by the cytoplasmic proteasome. Activated AhR can function as an E3 ubiquitin ligase, inducing the ubiquitination and proteasomal degradation of target proteins[14]. In addition, AhR ligand binding induces phosphorylation of Src kinase, initiating SRC driven phosphorylation cascades[15].

1.1.1. AhR functional domains and ligand diversity

AhR belongs to a member of the basic-helix-loop-helix-Per-Arnt-Sim (bHLH-PAS) transcription factor superfamily, which play key roles in developmental biology, circadian rhythmicity, and environmental homeostasis[16-18]. The bHLH and PAS domains in the N terminus (**Fig. 3**) are relatively well-conserved, e.g., *C. elegans* AhR (CeAhR) shares 38% amino acid identity over the first 395 amino acids with human AhR. The bHLH domain of AhR forms a homodimeric structure, containing basic-rich amino acids, and heterodimerizes with ARNT to recognize an atypical E-box DNA sequence 5'-TNGCGTG-3', thereby activating the transcription of numerous gene targets, such as xenobiotic-metabolic enzymes[19](**Fig. 2**). The AhR has two PAS domains, PAS-A and PAS-B (**Fig. 3**). This is noteworthy, because bHLH and PAS-A domains contribute to the dimerization and stability of the AhR-ARNT complex and is largely dictated by hydrophobic contacts [20-22]. The PAS-B domain contains a ligand binding motif and ligand binding induces conformational changes in the AhR that enhances AhR-ARNT dimerization and exposes the nuclear localization sequences (NLS) for subsequent translocation of the AhR-ligand complex into the nucleus [20]. In contrast to the relatively conserved bHLH-PAS domains, the C terminal region of the AhR exhibits wide variations across species. For example, the CeAhR does not contain a glutamine (Q)-rich domain in the C-terminal region even though it still functions as a transcription factor, while *D. melanogaster* and mammalian AhRs contain a Q-rich domain. Interestingly, both CeAhR and DmAhRdimerize with their ARNT orthologs, independent of AhR ligands, and act as transcriptional activators [23,24]. Deletion analysis has revealed that removal of the Q-rich subdomain results in the complete inactivation of the

hAhR [25], which is in contrast with CeAhR. The C-terminal transactivation domain regulates cellular localization and nucleocytoplasmic shuttling of AhR. For instance, the nuclear export sequence (NES) in the N-terminal region, which mediates hAhR export out of nucleus, requires the V647 residue within the Q-rich domain. Substitution of V647 to alanine promotes an exclusive nuclear retention [26]. In addition, the C-terminal domain uniquely confers transactivation potential of AhR across species by differentially recruiting cell context-specific LXXLL-containing coactivators, thus resulting in divergent expression of target genes [27,28].

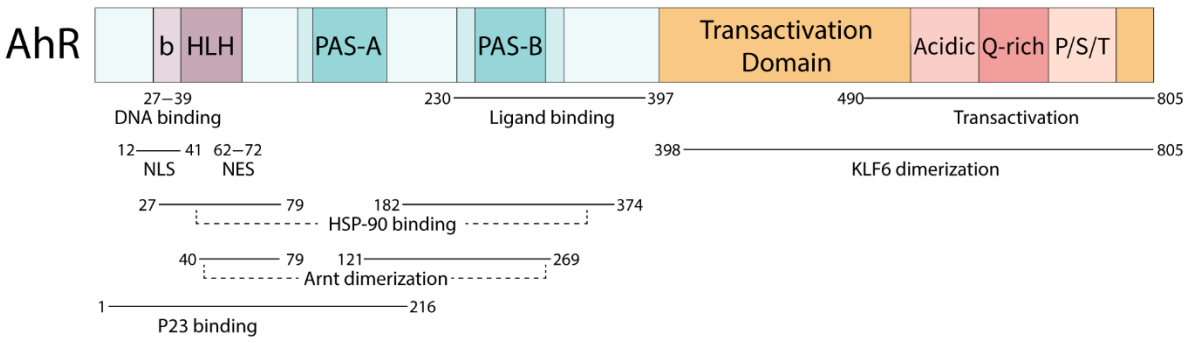

Figure 3. Schematic representation of murine AhR functional domains and the location mapping of the amino acid sequences that interact with other proteins.
bHLH: basic helix-loop-helix, PAS: Per-ARNT-Sim homology domain, NLS: nuclear localization sequence, NES: nuclear export sequence, P/S/T: Proline/Serine/Threonine. The figure is adapted from [29]

Initial studies showed that the AhR binds TCDD and structurally related polychlorinated aromatic compounds containing chlorine substitution in their lateral 2,3,7 and 8 positions [1,30]. The K_D value for TCDD is in the 10^{-12} M range and the binding is almost irreversible even though there is no evidence for TCDD-AhR covalent binding [31]. The chlorinated aromatic compounds induce a common set of toxic responses including thymic atrophy, body weight loss, hepatic porphyria, cleft palate in mice and acnegenic responses in humans, rabbit ear and certain strains of mice [1,30]. In contrast, this pattern of toxic responses is not observed for BNF or PAHs and the unique toxicities associated with TCDD and related compounds has been ascribed to persistent occupation of the receptor. Subsequent studies have shown that the AhR binds structurally diverse compounds including multiple classes of aromatics and heteroaromatic, pharmaceuticals, phytochemicals, multiple kinase inhibitor and a host of endogenous compounds including microbiota-derived tryptophan metabolites and 1,4-dihydroxy-2-naphthoic acid (DHNA) and serotonin [5,32-35] (**Fig. 1**). Although endogenous ligands for the AhR have not been unequivocally assigned, two possibilities are the tryptophan-derived compounds 6-formylindolo [3,2-b]carbazole (FICZ) and 2-(1'H-indole-3-carbonyl)-thiazole-4-carboxylic acid (ITE). These structurally diverse AhR ligands do not cause TCDD-like toxicities and many of these compounds induce beneficial health-promoting responses and are selective AhR modulators (SAhRMs) [36,37]. Selective receptor modulators are observed for many of the nuclear receptors and differences in their tissue/cell-specific activities are due to multiple factors including ligand-receptor conformations, expression of nuclear co-factors and chromatin/nuclear factors such as cell- and gene- specific histone modifications [38]. Evidence for ligand

structure-dependent differences in ligand-AhR interactions has been based on the modeling of ligand binding to the ligand binding domain of the AhR and mutagenesis of different amino acids within this domain that are necessary for AhR ligand binding and transactivation [5]. One study showed that F318 mutations results in remarkable differences in ligand interactions with the AhR and transactivation and this was dependent on both ligand structure and the substituted amino acid for F318 [5]. Similar results were observed for other amino acids and this explains, in part the ligand structure-dependent functional differences in AhR ligands which may vary from highly toxic (TCDD) to health promoting (flavonoids and tryptophan metabolites).

1.1.2. AhR diversification

The AhR is an ancient protein, present throughout metazoans and identification of AhR homologs in nematodes, anthropods and molluscs, indicating that the AhR dates back to the earliest bilateral metazoans, over 600 million years ago [39]. The genetic diversification of AhR is likely due to multiple rounds of whole genome duplication early in vertebrate evolution, from a single AhR homology in the first chordates, to at least three AhR homologs (AHR1, AHR2, and AHRR) found in extant vertebrate groups. The earliest identified function of the AhR was as the cognate receptor for halogenated aromatic hydrocarbons, such as TCDD and BNF, resulting in the induction of xenobiotic-metabolizing enzymes. However, invertebrate AhR is unable to bind TCDD or BNF and induce the expression of their enzymes, and this feature distinguishes invertebrate AhRs from their vertebrate homologs [40]. Interestingly, invertebrate AhR-ARNT dimerization is independent of AhR ligands.

What is the ancestral role of AhR? Studies in *C. elegans* have revealed that orthologs of AhR (ahr-1) and ARNT mediate GABAergic motor neuron fate specification, thereby regulating neuronal development. Specifically, loss of AhR in RMEL and RMER neurons promotes differentiation into RMED/RMEV-like neurons, while ectopic expression of ahr-1 in RMED/RMEV neurons promotes a RMEL/RMER-like cell fate [41]. Defects in neuronal differentiation, aberrant cell migration, and axon branching have also been observed in ahr-1-deficient *C. elegans* [42]. With respect to *Drosophila* retinal patterning as determined by the stochastic expression of Spineless (ss), the AhR ortholog acts as a binary switch that converts the homogenous compound eye into a mosaic pattern required for color vision [43]. In addition, loss of ss or the *Drosophila* ortholog of ARNT, Tango, leads to transformation of distal antenna to leg, deletion of distal leg structures, and reduction of bristle size in *Drosophila* [23,44]. Similarly, ss was found to play a role in neuronal development by controlling the diversification of dendrite morphology in dendritic arborization sensory neurons, independent of its cofactor tango [45]. Therefore, the functions of AhR in the development and chemosensory neural systems may reflect its ancestral roles, while the regulation of xenobiotic-metabolizing enzymes and immune response are evolutionarily adaptive functions.

1.2. Natural AhR ligands

In addition to initially identified synthetic AhR ligands, many naturally occurring endogenous AhR ligands have been discovered in the past few decades. In general, these AhR ligands are non-toxic and exhibit relatively low AhR binding affinity with short metabolic half-lives. The major sources of natural AhR ligands are plant-derived dietary

compounds, gut microbiota metabolites of poorly digestable plant-derived dietary ingredients, and host metabolism of tryptophan. Flavonoids and indole-based glucobrassicin represent two main classes of plant derived phytochemical AhR ligands[46,47]. Flavonoids are a large class of polyphenolic secondary metabolites that are widely present in fruits and vegetables. A subset of flavonoids, such as quercetin, taxifolin and robinetin can activate AhR [48]. Some flavonoids such as Luteolin act as AhR antagonists[49], as determined by dioxin response element (DRE)-driven cell based reporter systems, downstream target gene expression, such as Cyp1a1 and UTG1A1, and promoter binding assays. A major structural determinant for AhR activation is the number of hydroxyl groups with pentahydroxyflavonoids showing maximal potency [48]. In addition, Brassicaceae family plants, such as Chinese cabbage, broccoli, Brussel sprouts and cauliflower, are rich sources of glucobrassicin, the glucosinolate precursor of indole-3-carbinol (I3C). Glucobrassicin can be enzymatically hydrolyzed and converted into I3C by myrosinase (β-thioglucosidase), which is present in intact plant cells and gut microbiota [50,51]. I3C itself activates AhR but exhibits low binding affinity (~mM). However, I3C undergoes acid catalyzed condensation in the stomach to generate a variety of more potent AhR ligands, such as 3.3'-diindolylmethane (DIM), [2-(indol-3-ylmethyl)-indol-3-yl]indol-3-ylmethane (LTr1) and indolo[3,2-b] carbazole (ICZ)[52,53]. ICZ exhibits highly potent AhR activation (~0.2-3.6 nM)[54]. In addition, indigo and indirubin, present in the traditional Chinese medicine and the dried leaves of the flowering plant Isatis tinctoria serving as dyes for textile coloring, robustly activate AhR and induces Cyp1a1 expression in mammals[55].

1.3. Gut microbiota and AhR ligands

The human gastrointestinal (GI) tract represents one of the largest interfaces (250–400 m^2) between the host and its external milieu in the human body. In the healthy adult, it has been estimated that ~3.8 x 10^{13} microorganisms (microbiota), including bacteria, archaea, and eukarya, inhabit the large intestine [56]. The gut microbiota consists of thousands of bacterial species dominated by four phyla, Firmicutes (50~70%), Bacteroidetes (10~30%), Proteobacteria (up to 10%), and Actinobacteria (up to 5%) [57]. Notably, these microorganisms provide a range of beneficial properties to the host, including the fermentation of undigested carbohydrates, and biosynthesis of vitamins and generation of tryptophan metabolites. Since a number of recent reviews can be found concerning the role of gut microbiota in health and disease [58-61], we will confine our discussion to the role of microbiota with respect to the biosynthesis of tryptophan metabolites, which serve as endogenous AhR ligands.

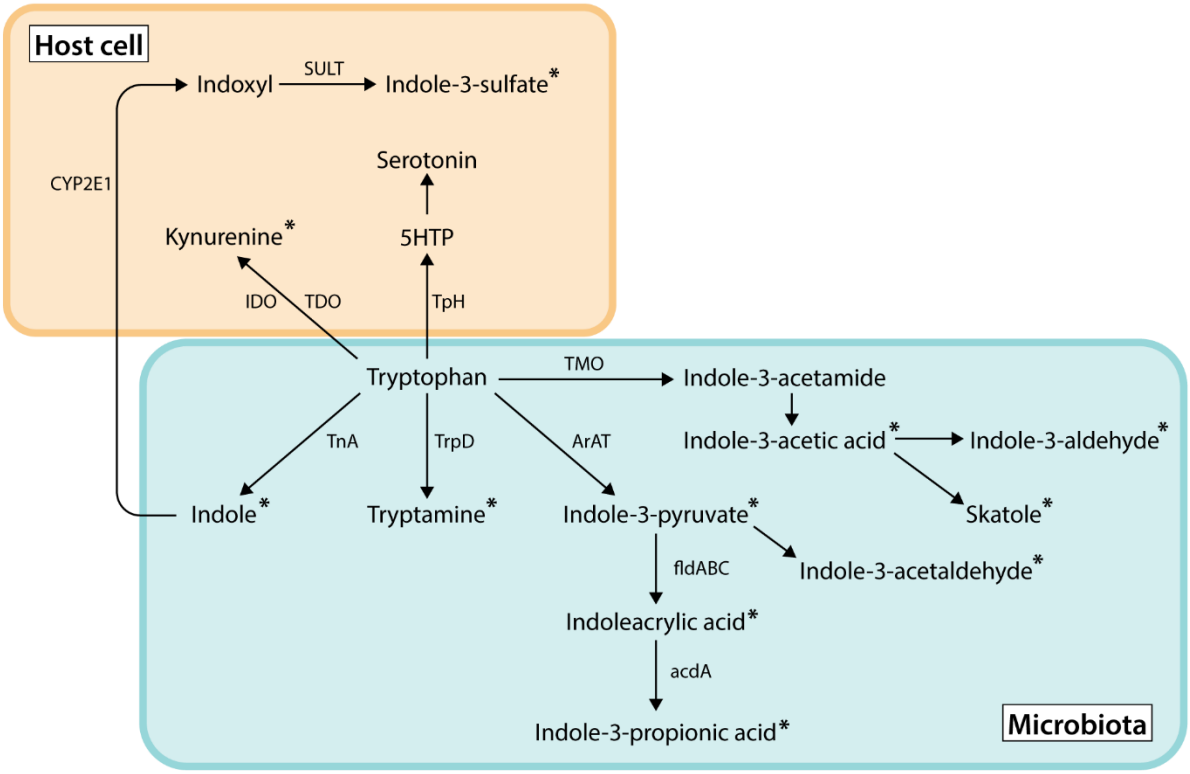

Figure 4. Pathways of tryptophan catabolite in human host cells and gut microbiota.
TMO: Tryptophan 2-Monooxygenase; TnA: Tryptophanase; TrpD: Tryptophan Decarboxylase; ArAT: Aromatic amino acid Aminotransferase; fldABC: phenyllactate dehydratase gene cluster; acdA: acyl-COA dehydrogenase; TpH: Tryptophan Hydroxylase; IDO: Indoleamine 2,3-Dioxygenase; TDO: Tryptophan 2,3-Dioxygenase; SULT: Sulfotransferases. Asterisk symbols represent AhR ligands.

Tryptophan is an essential and limiting amino acid in proteins and cells. Average serum concentrations of tryptophan in healthy humans is in the range of 70 ± 10 µmol/L for males and 65 ± 10 µmol/L for females [62]. Transformation of tryptophan by intestinal microbiota produces several metabolites, including indole, indole-3-acetic acid, and tryptamine (**Fig. 4**). These tryptophan metabolites which are also found in the mammalian blood steam, are primarily generated by gut microbiota, as evidenced by decreased or undetectable levels of tryptophan metabolites in germ-free mice,

compared with conventional mice [63]. Numerous species capable of producing indole and other tryptophan metabolites have been identified and described in previous reviews [64,65]. Thus, we briefly discuss pathways for the formation of tryptophan catabolites. Although indole itself is capable of activating human AhR at its physiological concentration (250-1100 μM) in human feces [66], it has minimal effects on mouse AhR [67]. In contrast, most of the indole derivatives, such as 3-methylindole (skatole), tryptamine (TPM), indole-3-acetate (IAA), indole-3-aldehyde (IAld), indole-3-acetaladehyde (IAAld), indoleethanol (IE), indole-3-pyruvate (IPyA), indole-3-propionic acid (IPA), and indoleacrylic acid (IA), are considered bioactive AhR ligands in the gut (**Fig. 4**). Indole is synthesized from tryptophan exclusively by tryptophanase (TnA) in ~85 Gram-positive and Gram-negative bacterial species, including Bacteroides spp, Clostridium spp. and *Escherichia coli* [68-71]. Alternatively, bacterial toluene *o*-monooxygenase activity can also convert indole to hydroxyindoles[72], although their prevalence in the intestinal community is unknown. The production of tryptamine from tryptophan by decarboxylation is mediated by members of the Firmicutes phylum (*Clostridium sporogenes* and *Ruminococcus gnavus*) in the human gut [73]. Indole pyruvate (IPyA) is a major intermediate for the production of IAAld and IPA from tryptophan and is carried out by the catalytic activity of the aromatic amino acid aminotransferase (ArAT) enzyme expressed in many bacterial species, including Lactobacilli. Lactobacilli can further convert IPyA into IAld by ArAT [74]. Several species belonging to the Peptostreptococcus genus, *Clostridium sporogenes*, and *Clostridium cadaveris* containing the phenyllactate dehydratase gene cluster (fldABC) can synthesize IA and IPA from IPyA [75,76]. In addition, tryptophan can be directly converted

into indole-3-acetamide by the enzyme tryptophan 2-monooxygenase (TMO) by Actinobacteria [77-79].

Mounting evidence indicates that reduced blood and fecal levels of gut microbiota-derived AhR ligands are associated with many human diseases, such as inflammatory bowel diseases (IBDs), obesity, Type 2 diabetes, and high blood pressure [80-82]. This is consistent with the fact that the diversity of gut microbiota is decreased in these patient populations, e.g., reduced abundance of Lactobacillus spp, Bifidobacterium spp and *Faecalibacterium prausnitzii*, and elevated abundance of *E. coli* and *Clostridium difficile*, compared with healthy individuals [83]. Interestingly, modulation of AhR activation can contribute to gut microbial community alterations possibly by affecting the maintenance of gut immune cells, including intraepithelial lymphocytes, ILCs and Th17 cells [84-87]. For instance, dietary exposure to 2,3,7,8-tetrachlorodibenzofuran (TCDF) can produce a shift from Firmicutes to Bacteroidetes in the gut microbiota, thereby altering host metabolism[88]. Moreover, treatment with TCDD and PCB126, has been linked to dysbiosis of gut microbiota and the deterioration of gut health in Zebrafish and mice[89-91]. However, AhR activation by natural AhR ligands, e.g., I3C, has been shown to prevent pathogenic gut microbial dysbiosis and restore gut microbiome composition in mice with colitis [92]. This is consistent with reports that depletion of AhR ligands in the diet decreased α diversity of gut microbiota, while I3C supplementation restored microbiota composition[93]. Similarly, significant alterations in phyla abundance of gut microbiota accompanied by functional shift in bacterial metabolism has been observed in AhR null mice, predisposing the host to chronic inflammation and/or a metabolic stress state [84,94].

Therefore, AhR acts at the bidirectional interface between the host and gut microbial communities and their AhR active metabolites.

1.4. Host metabolism of tryptophan

Endogenous AhR ligands can also be produced by host cells and the most well-characterized ligand is Kynurenine (Kyn). In the host, more than 95% of dietary tryptophan is degraded via the Kyn pathway, while less than 5% of tryptophan is metabolized into serotonin by tryptophan hydroxylase. The rate limiting reaction step in the Kyn pathway is catalyzed by the enzyme tryptophan 2,3-dioxygenase (TDO) or indoleamine 2,3-dioxygenase (IDO). TDO is constitutively expressed mainly in the liver and brain, while IDO is inducibly expressed in a number of tissues or cells in response to pro-inflammatory cytokines, such as IFN-γ. Induction of the Kyn-IDO pathway plays an important role in immune tolerance/suppression and tumor pathogenesis[95,96]. The serum concentration of Kyn in healthy humans is ~1.8±0.4 μM, which is within the dose range of AhR activation, even though Kyn binds to mouse liver AhR with an apparent Kd of ~4 μM [96,97]. Kyn can be further metabolized into Kynurenic acid (KA), Xanthurenic acid (XA), and Cinnabarinic acid (CA), which all serve as endogenous AhR ligands [98,99]. In addition, another potent AhR ligand, 6-formylindolo[3,2-b]carbazole (FICZ), can be produced in human keratinocytes from L-tryptophan under UV irradiation and FICZ activates AhR at nanomolar concentrations, which is comparable with TCDD [100]. In addition, gut microbiota derived indole can be further processed in host liver tissue, where it is hydroxylated into 3-hydroxyindole by hepatic cytochrome P450 enzymes,

including CYP2E1 [101], and subsequently sulfated by sulfotransferases into indole-3-sulfate (I3S) [102], an important uremic toxin and potent endogenous AhR ligand [103].

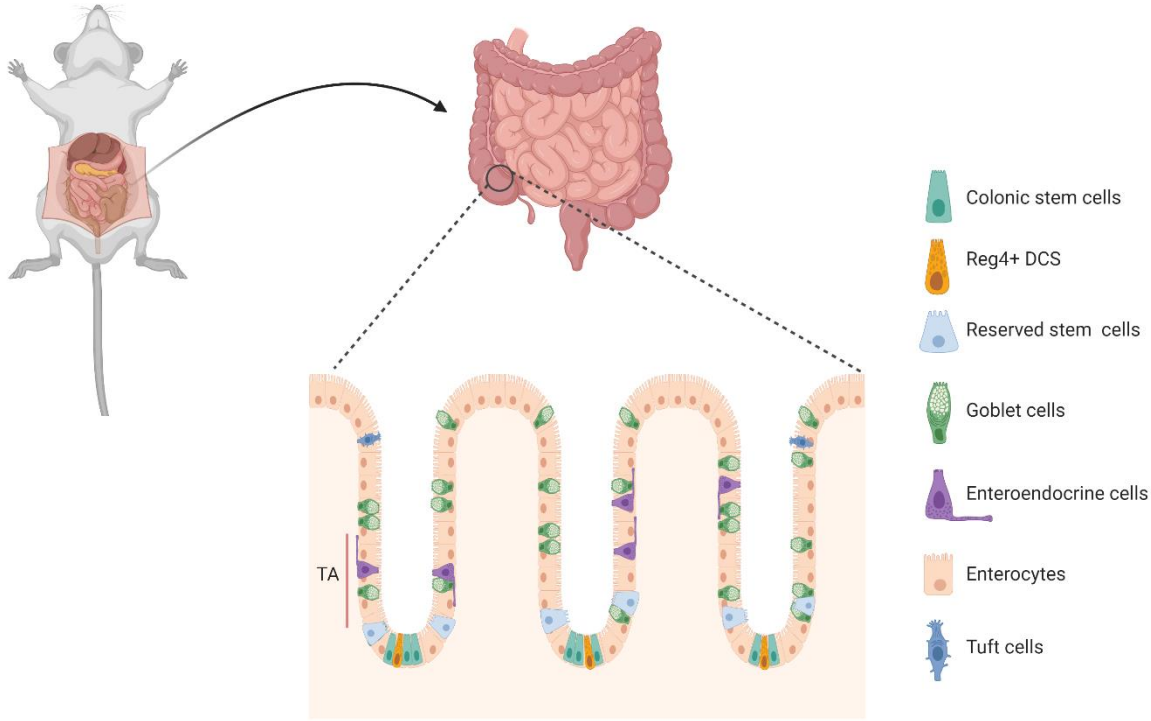

Figure 5. Schematic representation of mouse colon anatomy.
TA: transient amplifying region; DCS: deep crypt secretory cells. Created with BioRender.com.

1.5. Colon physiology

The colon is the part of the large intestine that extends from the cecum to the rectum, and is lined with a single layer of columnar epithelial cells whose primary function is to absorb water and salt, and constitutes a natural barrier surface against the invasion of pathogens and microorganisms in the gut lumen[104]. The intestinal epithelial

cells make up the most vigorously self-renewing tissue of adult mammals with a self-renewal cycle of 3-5 days[105], and form finger-like invaginations into the underlying connective tissue as the basic functional structure, the crypt. The crypt is composed of several different cell types, including rapidly cycling colonic stem cells, reserve stem cells, transient amplifying (TA) cells, goblet cells, enteroendocrine cells, Tuft cells, and enterocytes (**Fig. 5**). Rapid cycling stem cells, marked by Lgr5 (leucine-rich-repeat-containing G-protein-coupled receptor 5, also known as Gpr49), reside at the bottom of crypts and self-renew every day. Linear tracing experiment revealed that Lgr5+ stem cells are capable of producing all cell lineages in vivo[106]. The maintenance of colonic stem cells (CSCs) is highly dependent on their complex microenvironment, which mainly consists of the epithelial niche and mesenchymal niche. Reg4+ deep crypt secretory cells are intermingled with CSCs, and provide several growth factors, such as epidermal growth factor (EGF) and Notch ligands, to nurse CSC cell renewal[107]. CSCs are lost in vivo upon depletion of Reg4+ deep crypt secretory cells[107]. In addition, CSCs are also in close proximity with subepithelial myofibroblasts underneath the crypt, which not only provide structural support but also important growth factors, including WNT, bone morphogenic protein (BMP), BMP antagonists and cytokines, to maintain CSC homeostasis[108].

Most Lgr5+ CSCs double their number every day and stochastically adopt stem or TA cell fates, due to their neutral competition in occupying the stem cell niche[109]. The daughter cells become TA cells when leaving the stem cell niche and migrate upwards along the crypt. The newly formed TA cells, also referred to as progenitor cells, typically undergo a limited round of rapid cell divisions and are then committed to produce

terminally differentiated cells[110]. Upon the loss of CSCs in the injury state, such as irradiation or colitis, TA cells exhibit high plasticity, and can dedifferentiate into CSCs to re-establish the new homeostasis[111-113]. In addition, reserved stem cells, a rare cell population located in +4 location, are quiescent in homeostasis, but also could revert into rapid cycling CSCs upon injury[114,115]. Therefore, the cellular hierarchy in the crypt is not constant, but is dynamically interchangeable. The differentiation of secretory cells is driven by inhibition of Notch signaling. Hes1, a well-characterized Notch signaling target, represses the expression of the Atoh1 and neurogenin 3, which are main regulators that direct goblet cell and enteroendocrine cell differentiation, respectively[116-118]. Goblet cells are the cellular source of mucins, which constitute the major component of mucus layers to defend gut microorganisms from invasion and reduce mechanical stress by lubricating the gut lumen[119]. Enteroendocrine cells are the hormone-producing secretory cells and act as the key sensors of luminal nutrients and sensory sentinels of the intestinal environment, even though they only account for 1% of intestinal epithelial cells[120]. Enterocytes represent the majority of intestinal epithelial cells and are mainly responsible for ion and water absorptions in the colon[108].

Intestinal epithelial cells are frequently challenged by mechanical and chemical stress. Environmental pollutants, pathogenic gut bacteria and their metabolites place the intestinal epithelium at high risk. In particular, rapidly cycling stem cells are exquisitely sensitive to extrinsic (genotoxic carcinogen and dietary) factors that modulate colon cancer risk[121]. Dysregulation of CSCs are generally presumed to be the earliest step in colon tumorigenesis. For instance, deletion of the Wnt negative regulator Apc in $Lgr5^+$ stem cells leads to their transformation and progressively growing

neoplasia, indicating that crypt Lgr5^{+} stem cells are the cells-of-origin of intestinal and colonic cancer[122].

1.6. AhR and colon cancer

Studies from rats, mice and hamsters provide evidence that chronic activation of AhR promotes tumor incidence in multiple tissue sites [123]. Recent epidemiologic studies show that higher blood levels of TCDD as markers of exposure are associated with increased risk of cancers in all sites combined, and several specific cancers, including lymphoma, small intestine and liver [124-127]. Thus, TCDD is now classified as a Group 1 human carcinogen based on increased risk of all cancers combined [128]. However, laboratory animal studies demonstrate that the AhR can function as a tumor-type dependent promoter or inhibitor of carcinogenesis indicating that SAhRMs acting as agonists or antagonists have potential as cancer chemotherapeutic drugs [129,130]. Emerging studies using mouse models have suggested that AhR signaling plays an important role in regulating intestinal cancer [131-134].

Colorectal cancer (CRC) is the third most commonly diagnosed cancer and the second leading cause of cancer death in men and women combined in the United States. The lifetime risk of developing CRC is slightly lower in women than in men (https://www.cancer.org/cancer/colon-rectal-cancer/about/key-statistics.html). The risk of developing CRC is affected by both environmental and genetic factors [135]. Ultimately, genetic alterations following CRC progression involve the inactivation of tumor suppressor genes and DNA mismatch repair genes, and/or activation of oncogenes, in which Adenomatous polyposis coli (Apc) serves as an initiating event, accompanied by

the mutations of other common genes, such as Kirsten RAS (Kras), Sma- and Mad-related protein 4 (SMAD4) and TP53[136].

Since AhR acts as an environmental sensor, it is capable of integrating external environmental stimuli and host responses to modulate intestinal epithelial cells. Kawajiri and coworkers were the first to report that global deletion of AhR promotes the spontaneous development of cecal tumors, and enhanced expression of β-catenin and c-myc in epithelial cells of the ileum, colon and cecum. In addition, administration of natural AhR ligands I3C or DIM significantly reduced the number of tumors in the cecum and small intestine and dramatically downregulated β-catenin levels in $Apc^{Min/+}$ mice, but not in $Apc^{Min/+}$; $AhR^{-/-}$ mice [131]. Consistent with these findings, global AhR KO promotes tumor incidence and multiplicity in colitis-associated colorectal tumorigenesis, and supplementation of I3C reduces the number of colorectal tumors in WT mice, but not in $AhR^{-/-}$ mice [132]. Of note, no changes in β-catenin and c-myc were observed, and spontaneous tumor development was extremely low and did not reach statistical significance in $AhR^{-/-}$ mice [132]. Interestingly, germ free $AhR^{-/-}$ mice or compound mice lacking AhR and apoptosis-associated speck-like protein containing a CARD (ASC), exhibit a reduction in tumor development compared with $AhR^{-/-}$ mice [134], implying that the mechanism by which global AhR KO enhances intestinal tumorigenesis in $AhR^{-/-}$ mice may be linked to a perturbation in immune function or dysregulated intestinal epithelial cells or both. Recently, Metidji et al. found that intestinal specific deletion of AhR (Villin-Cre) promotes carcinogen induced and colitis-associated colon tumorigenesis [133]. Intestinal specific AhR loss also enhances intestinal stem cell expansion and impaired intestinal stem cell differentiation, e.g., reduced goblet cells and

absorptive enterocytes, resulting in defective gut barrier and upregulation of IL-6. Chromatin immunoprecipitation analysis indicates that AhR can interact with the promoter of the Wnt negative regulator, Rnf43, and inhibit its expression, consequently stabilizing Wnt signaling, as evidenced by increased β-catenin level and its target genes[133]. Collectively, the results from animal models suggest that AhR should be considered a chemoprevention target to reduce intestinal cancers. With regard to human subjects with CRC, it remains controversial whether changes in AhR expression are linked to tumor incidence [131,137]. However, the expression of AhR is upregulated in colonic tumors, compared with normal tissue based on the TCGA database (https://xena.ucsc.edu/).

With respect to colon cancer cell culture models, whether AhR inhibits or promotes tumor growth remains controversial. For example, AhR activation by two piperidone analogs of curcumin, RL66 and RL118, has been shown to promote apoptosis in human DLD1, HCT116, LS513 and RKO colon cancer cell lines [138]. siRNA-mediated AhR knockdown promotes cell growth in HCT116 and HT29 [137]. In addition, FICZ treatment decreases cell proliferation by inducing G1 cell cycle arrest but exhibits no effect on cell apoptosis in human LoVo colon cancer cells [139]. Reduced cell proliferation and induction of p53, retinoblastoma, p21 and regucalcin is also observed in RKO cells treated with TCDD [140]. However, in human colon cancer cell lines, H508 and SNU-C4, TCDD incubation induces phosphorylation of Src, subsequently promoting phosphorylation of EGFR and ERK1/2, thereby promoting cell proliferation [15]. The variable results from those studies suggest that cell response is highly dependent on

cell line sources, tumor types, and AhR ligands. Hence, the mechanism by which AhR signaling modulates the intestinal tumorigenesis warrants further exploration.

1.7. AhR and IL-22

Interleukin-22 (IL-22) belongs to a member of the IL-10 family of cytokines that plays various roles in cell proliferation, host defense, inflammation and tissue regeneration[141]. IL-22, a potential therapeutic target for acute inflammatory diseases, is elevated in patients with inflammatory bowel diseases[142]. Recent study provided very exciting insights that IL-22 signaling was required to initiate efficiency DNA damage response after exposure to genotoxic stress, and impaired IL-22 signaling promoted colon tumorigenesis due to accumulation of DNA mutations[143]. In the gut, many different types of immune cells, including innate lymphoid cells, NK T cells, γδ T cells, Th17 cells neutrophils and CD4+ T cells, are capable of producing IL-22 [144-149]. AhR is one of the main regulators of IL-22 production[74,80,150]. Global AhR deficient mice exhibit reduced IL-22 expression and RORγt+ group 3 innate lymphoid cells (ILC3) development as well as increased intestinal Th17 cell numbers[150]. Selective depletion of Thy1.2+ ILCs in Rag1-/- mice after adoptive T cell transfer promotes Th17 cell response, suggesting a role for AhR in balancing ILCs and Th17 cell responses in the gut [150]. This is consistent with the fact that AhR activation by FICZ treatment ameliorates TNBS-, DSS- and T-cell transfer induced colitis in part by up-regulating IL-22 and downregulating the expression of pro-inflammatory cytokines, such as IFN-γ, IL-17α and TNF-α [80]. Intestinal lamina propria mononuclear cells (LPMCs) from patients with IBD treated with FICZ also exhibit a decrease in IFN-γ and increased IL-22 production [80]. Interestingly, AhR activation by

TCDD decreases methylation of the CpG island of FoxP3, a master regulator in the development of Treg cells, as well as demethylation of the IL-17 promoter in mesenteric lymph nodes and lamina propria cells during colitis, thereby inducing Treg cell differentiation and inhibiting Th17 cell production [151]. Thus, AhR can control Treg cell differentiation by directly targeting the expression of Foxp3 [152], affecting IL-22 production. In addition, alpinetin, an AhR agonist, has been shown to decrease the methylation level of Foxp3 in CD4+ T cells by promoting the expression of miR-302, subsequently reducing DNA methytransferase 1 (DNMT-1) expression. miR-15a/16-1 has also been shown to regulate the expression of AhR, and overexpression of miR-15a/16-1 decreases IL-22 production by inhibiting AhR expression in CD4+ T cells [153]. The direct regulation of IL-22 production by AhR has also been observed in mouse CD4+ T cells and RORɣt(+) ILCs [87,154]. Interestingly, global AhR KO mice accumulated more DNA mutations after exposure to carcinogen e.g., azoxymethane (AOM) and promoted AOM/DSS induced colon tumorigenesis[69], which is phenocopied with intestinal specific IL-22R1 KO mice[143], implying that defective IL-22 signaling played a role in carcinogen induced colon tumorigenesis in AhR null mice. In addition, intestinal specific AhR KO still enhanced AOM induced colon tumorigenesis. However, the epithelial specific role of the AhR signaling on the response to IL-22 is not appreciated yet.

2. LOSS OF ARYL HYDROCARBON RECEPTOR POTENTIATES FOXM1 SIGNALING TO ENHANCE SELF-RENEWAL OF COLONIC STEM AND PROGENITOR CELLS*

2.1. Introduction

The AhR is a ligand-activated transcription factor widely expressed in various cell types [18]. While 2,3,7,8-tetrachloro-dibenzo-p-dioxin (TCDD) and structurally related halogenated and polynuclear aromatic hydrocarbons have been extensively investigated as AhR ligands , it is now appreciated that AhR also binds ligands unrelated to TCDD and other halogenated aromatics, including dietary botanical-derived ligands such as flavonoids, indole-3-carbinol (I3C), diindolylmethane (DIM), formylindolo-[3,2-b]-carbazole (FICZ), and a growing number of gut microbial-derived tryptophan metabolites [155-158].

The role of AhR activation in the critical stages of intestinal epithelium development, intestinal immunity, and tumorigenesis is an intense area of investigation [85,131,159-161]. For example, several studies have recently demonstrated a critical role for the AhR and its ligands in mediating gastrointestinal integrative physiology and pathogenesis [85,131,161]. Consistent with these findings, reports show that TCDD decreases inflammation associated with Crohn's disease and that other AhR agonists protect

*This chapter is reprinted with permission from "Loss of aryl hydrocarbon receptor potentiates FoxM1 signaling to enhance self-renewal of colonic stem/progenitor cells" by Huajun Han, Laurie A. Davidson, Yang-Yi Fan, Jennifer S. Goldsby, Grace Yoon, Un-Ho Jin, Gus A. Wright, Kerstin K. Landrock, Bradley R. Weeks, Rachel C. Wright, Clinton D. Allred, Arul Jayaraman, Ivan Ivanov, Jatin Roper, Stephen H. Safe, and Robert S. Chapkin. EMBO J, Copyright (2020) by the Author(s).

against inflammatory bowel disease [161-163]. It has also been reported that AhR silencing or lack of AhR ligands compromises the maintenance of intraepithelial lymphocytes and regulatory T cells in the skin and intestine [85,86,95], thereby disrupting mucosal immunity and integrity. Thus, AhR ligands, such as I3C and other intestinal microbiota derived agonists/antagonists, may uniquely modulate the gastrointestinal immune system. With regard to colorectal cancer (CRC), whole body knockout of AhR enhances intestinal tumor formation in the *Apc*$^{Min/+}$ model, while phytochemical-derived AhR ligands such as I3C and its metabolite DIM inhibit tumor formation [131]. In addition, it has recently been demonstrated that AhR plays a protective role in colitis-associated CRC, suggesting that the AhR acts as a tumor suppressor in inflammation-associated intestinal neoplasia [160]. Since global AhR KO mice were utilized in the majority of studies to date, it remains to be determined whether effects of AhR silencing on intestinal cancer incidence result indirectly from a globally dysregulated immune and metabolic systems or via direct effects on intestinal epithelial cells.

Crypt-base stem cells are the cells-of-origin of intestinal cancer [122] and Lgr5-expressing cancer cells exhibit the properties of tumor-initiating cells, i.e., cancer stem cells, which retain high capacity for self-renewal [164,165]. Thus, Lgr5 stem cells are an attractive therapeutic target for the prevention and/or treatment of gastrointestinal cancers [166]. There is evidence showing a role for the AhR in modulating the dynamics and functionality of stem cell populations, including hematopoietic stem cells (HSCs) and neural stem cells [167,168]. Studies on the stabilization of HSCs and their expansion identified a compound SR1, an AhR antagonist, that induced a 50-fold increase in cells expressing CD34 (hematopoietic stem cell marker) [168]. SR1 and other synthetic AhR

antagonists are now being used for expansion of HSCs and clinical applications of HSC therapy. Collectively, these findings suggest that AhR plays an important role in stem cell biology and the effects of AhR agonists and antagonists are stem cell-specific.

The contribution of AhR with respect to colonic stem cell homeostasis remains to be established. Since transformation of adult stem cells is an extremely important mechanism for intestinal cancer initiation [122], we interrogated the effect of AhR ligands on intestinal stem cell homeostasis in the presence or absence of AhR. Herein, we report that AhR signaling has a role in controlling colonic stem and progenitor cell homeostasis. These results suggest that AhR may be a critical dietary/pharmacological target for modulating stem cell biology in the gut epithelium, and the subsequent inflammation-induced development of colorectal cancer.

2.2. Materials and methods

2.2.1. Mice

Animals were housed under conventional conditions, adhering to the guidelines approved by the Institutional Animal Care and Use Committee at Texas A&M University. Stem cell targeted Lgr5-EGFP-IRES-Cre^{ERT2}, colon targeted CDX2P-Cre^{ERT2}, intestine targeted Villin-Cre, tdTomato$^{f/f}$, AhR$^{f/f}$ and tdTomato$^{f/f}$ mouse strains have all been previously described [18,106,169-172]. The mouse genotypes used in this study include: tamoxifen inducible - Lgr5-GFP-Cre^{ERT2} X Tomato$^{f/f}$ (GT, control), AhR$^{f/f}$ X Lgr5-GFP-Cre^{ERT2} X Tomato$^{f/f}$ (HGT), Lgr5-GFP-Cre^{ERT2} X CDX2P-Cre^{ERT2} (GC, control), AhR$^{f/f}$ X Lgr5-GFP-Cre^{ERT2} X CDX2P-Cre^{ERT2} (HGC); constitutive - AhR$^{f/f}$ (H, control), AhR$^{f/f}$ X Villin-Cre AhR$^{f/f}$ (HV), AhR$^{f/f}$ X Lgr5-GFP-Cre^{ERT2} (HG), and AhR$^{f/f}$ X Lgr5-GFP-CreERT2

X Villin-Cre (HVG). Male and female mice in an age range of 5-10 weeks were intraperitoneally injected with 2.5 mg of tamoxifen (Sigma, T5648) dissolved in corn oil (25 mg/ml) once a day for four consecutive days, unless otherwise specified. To inhibit cell proliferation in vivo, mice were intraperitoneally injected with a FoxM1 inhibitor Thiostrepton [173] (Sigma, T8902) at 50 mg/kg bw daily for 2 consecutive days. Mice were maintained on an AIN-76A semi-purified diet (Research Diets, D12450B), fed ad libitum and housed on a 12 h light-dark cycle. For all experiments, littermate controls were cohoused with the knockout mice, unless specifically indicated.

2.2.2. *Crypt and single cell isolation and cell sorting*

Colons were removed, washed with cold PBS without calcium and magnesium (PBS-/-), everted on a disposable mouse gavage needle (Instech Laboratories) and incubated in 15 mM EDTA in PBS-/- at 37°C for 35 min as previously described [174]. Subsequently, following transfer to chilled PBS-/-, crypts were mechanically separated from the connective tissue by rigorous vortexing. Crypts were embedded in Matrigel and overlaid with crypt culture media as previously described [174]. For intestinal stem cell isolation, crypt suspensions were dissociated to individual cells with 0.25% Trypsin-EDTA containing 200 U/ml DNase. Cell suspensions were then filtered through a 40-µm mesh and GFP-expressing cells were collected using a MoFlo Astrios Cell Sorter (Beckman Coulter) or a Bio-Rad S3e Cell Sorter. Dead cells were excluded by staining with propidium iodide or 7-AAD. Sorting purity was routinely examined and over 95%. Sorted cells were collected in RNA lysis buffer (for RNA isolation) or crypt culture medium (for culturing).

2.2.3. Organoid culture

Isolated mouse colonic crypts were counted and embedded in growth factor reduced Matrigel (Corning, 356231) at 3-6 crypts per µl and cultured in crypt culture medium containing Advanced DMEM/F12 (Gibco) supplemented with 2 mM glutamax, penicillin/streptomycin, 10 mM HEPES, 50 ng ml^{-1} EGF (Life Technologies), 100 ng ml^{-1} Noggin (Peprotech) or 0.2 µM LDN-193189 (Stemgent), 10% R-spondin conditioned medium, 1 µM N-acetyl-l-cysteine (Sigma), 1X N2 (Life Technologies), 1X B27 (Life Technologies) and 50% Wnt conditioned medium as described previously [175]. Isolated intestinal stem cells (GFF^{high}) or progenitor cells (GFP^{low}) were centrifuged for 3 min at 500xg, resuspended in the appropriate volume of crypt culture medium (100-250 cells $µl^{-1}$), then seeded (500 cells) onto 30 µl Matrigel containing 1 µM Jagged-1 (Ana-Spec) in flat bottom 24-well plates. Following Matrigel polymerization, cells were overlaid with 300 µl of crypt culture medium supplemented with 10 µM Y-27632 (Sigma Y0503), 1 µM Jagged-1 and 2.5 µM CHIR99021 (Stemgent, 04-0004). Y-27632, Jagged-1 and CHIR99021 were withdrawn from the crypt culture medium 2 d after plating. The crypt media was changed every 2 d. Organoids were quantified on day 5 of culture, unless otherwise specified. For AhR-related treatments, DMSO, TCDD (10 nM) or CH223191 (10 µM) were added to cultures for 3 d. In some experiments, colonic organoids were cultured in 50% WRN conditioned medium derived from L-WRN cells (ATCC, CRL-3276), and 10% FBS (WRN medium) [176]. For human organoid cultures, Advanced DMEM/F12 was supplemented with penicillin/streptomycin, 2 mM glutamax, 10 mM HEPES, 40 ng ml^{-1} EGF (Life Technologies), 3 µM SB202190 (Sigma), 500 nM A83-01 (Tocris), 10 mM nicotinamide (Sigma), 1 µM N-acetyl-l-cysteine (Sigma-Aldrich),

1X N2 (Life Technologies), 1X B27 (Life Technologies), 50% WRN conditioned medium,10 nM gastrin I (Sigma) and 100 µg/ml Primocin (Invitrogen). To assay organoid forming efficiency, human organoids were dissociated with 0.25% Trypsin-EDTA, filtered through 20 µm mesh, and sorted on a BioRad S3e cell sorter. Dead cells were excluded by propidium iodide staining. Subsequently, cells were centrifuged and plated as described above. Following Matrigel polymerization, cells were overlaid with culture media supplemented with 10 µM Y-27632. To measure organoid viability, CellTiter-Blue reagent (Promega) was used according to the manufacturer's instructions. Fluorescence was measured on a CLARIOstar microplate reader.

2.2.4. Colitis associated colon cancer

At 8 to 12 weeks of age, male and female mice were given a single s.c. injection of azoxymethane (AOM) (10 mg/kg bw), followed by three cycles of 2% DSS exposure and subsequently terminated 6 wk after final DSS treatment. On the day of euthanasia, the colon was harvested, colon lesions were measured, mapped, excised, routinely processed and paraffin embedded. Hematoxylin and eosin (H&E) stained sections were examined using light microscopy by a board-certified veterinary pathologist in a blinded manner. Tumor volume was calculated as 0.523 x length x width x width.

2.2.5. RNA isolation and quantitative real-time PCR

RNA from sorted cells was isolated using the Quick-RNA MicroPrep Kit (Zymo, R1050) and further processed using a DNA removal kit (DNA Free, Ambion, AM1906). RNA integrity was assessed on a Bioanalyzer 2100 (Agilent Technologies), quantified

by Nanodrop and stored at minus 80°C. Real-time PCR was performed on an AB 7900 PCR system (Applied Biosystems) or QuantStudio 3 System (Applied Biosystems) using TaqMan Universal PCR Master Mix (Applied Biosystems) or SYBR Green mix (Applied Biosystems). Specific primer/probe mix for each gene was obtained from Life Technologies: AhR (Mm00478930_m1), Lgr5 (Mm00438890_m1; Hs00969422_m1), Olfm4 (Hs00197437_m1), Muc2 (Hs03005103_g1), Fabp2 (Hs01573164_g1), Cyp1a1 (Mm00487218_m1; Hs01054796_g1) and Gapdh (Mm99999915_g1), β-actin (Mm00607939_s1), Tbp (Hs00427620_m1), Foxm1 (Mm00514924_m1; Hs01073586_m1), Plk1 (Mm00440924_g1; Hs00983227_m1), Ccnd1 (Mm00432359_m1), Cdc25B (Mm00499136_m1; Hs01556934_m1), Ccnb2 (Mm01171453_m1), Birc5 (Mm00599749_m1), Cdca8 (Mm01182198_m1), AurkA (Mm01248177_m1), AurkB (Mm01718146_g1), Bub1B (Mm00437811_m1), IL-1β (Mm00434228_m1), IL-6 (Mm00446190_m1), IL-17α (Mm00439618_m1), IL-22 (Mm01226722_g1), and TNF-α (Mm00443258_m1). The primers for SYBR Green PCR were: FoxM1 (5'-TCACCGGGAACTGGATAGGT-3' and 5'-TGTTTAAGCAGCAGAAACGACC-3'), and TBP (5'- GATCAGAACAACAGCCTGCC-3' and 5'- TTCTGAATAGGCTGTGGGGT-3'). Results were calculated using the ΔCt method.

2.2.6. In situ hybridization (ISH)

Paraffin-embedded colon or colonic organoids sections (5 µm) were processed for RNA in situ detection using the RNAscope 2.5 HD detection kit (Advanced Cell Diagnostics (ACD), 322360) according to the manufacturer's instructions. RNAscope

probes used were: AhR (ACD, 452091), FoxM1 (ACD, 503581), LGR5 (ACD, 311021). Images were scanned using a Aperio CS2 instrument or all-in-one BZ-X800 Keyence fluorescence microscope. FoxM1 *in situ* images were quantified using ImageJ in a blinded manner.

2.2.7. Immunohistochemistry

In order to assess cell proliferation in the colon, mice were intraperitoneally injected with EdU 2 h prior to termination as previously described [177]. Colonic cell proliferation was measured using a Click-IT EdU kit (Life Technologies, C10340). Antigen retrieval was performed by sub-boiling in 10 mmol/L sodium citrate (pH 6.0) for 20 min. Antibodies used were goat polyclonal antibody to GFP (Abcam, ab6673) followed by Alexa-488 rabbit anti-goat secondary antibody (Life Technologies, A-21222), mouse monoclonal antibody to β-catenin (BD 610154) followed by Alexa-546 conjugated secondary antibody against mouse (Life Technologies, A10036). Prolong Gold antifade with DAPI (Life Technologies, P36935) was used to coverslip the slides. Images of colonic crypts were captured on an inverted TE 300 Nikon Eclipse fluorescence microscope equipped with a Photometrics Cool Snap EZ digital CCD camera. Images were processed using NIS Image software, version 3.2. For enumeration of immunohistochemical staining, a minimum of 30 crypts (typically >40) or 160 GFP^+ stem cells (typically >200) were assessed from at least three animals per treatment. Immunofluorescence images of the entire colon were captured on an all-in-one BZ-X800 Keyence fluorescence microscope. Images were processed using Keyence™ software.

2.2.8. Western blotting

Organoids were extracted from Matrigel by washing in cold $PBS^{-/-}$, then lysed in lysis buffer (50 mM Tris-HCl pH 7.2, 250 mM sucrose, 2 mM EDTA pH 7.6, 1 mM EGTA pH 7.5, 1% Triton X-100, 10 mM β-mercaptoethanol) supplemented with protease inhibitor cocktail (Sigma) and 1x phosphatase inhibitor (Life Technologies). Nuclear and cytoplasmic extraction was performed as per manufacturer's instructions (Life Technologies, 78833). Lysates were subjected to standard SDS-PAGE and Western blotting procedures using primary antibodies against β-catenin (1:2000, BD 610154), non-phospho β-catenin (1:2000, 8814S, Cell Signaling Technology), β-actin (1:4000, ab8227, Abcam), pERK1/2 (1:1000, 4370S, Cell Signaling Technology), ERK1/2 (1:1000, ,9107S, Cell Signaling Technology), AhR (1:2000, BML-SA210, Enzo), GAPDH (1:1000, 8884S, Cell Signaling Technology), human FoxM1 (1:1000, ab207298, Abcam), mouse FoxM1 (1:100, sc-376471, Santa Cruz Biotechnology Inc.), and PLK1 (1:500, Life Technologies, 37-7100). Secondary anti-mouse or rabbit conjugated to horseradish peroxidase were used to detect primary antibodies. Signal was detected using ECL substrate (Bio-Rad), imaged with the Bio-Rad Chemidoc System and protein bands quantified using Image Lab 6.0 (Bio-Rad).

2.2.9. Dual-luciferase reporter assay

pEZX-PG04 FoxM1 Dual-Luc plasmids were purchased from GeneCopoeia (HPRM39173-PG04; MPRM39500-PG04). Cells were transfected using Lipofectamine 3000 (Life Technologies) according to the manufacturer's instructions. Following transfection, cells were incubated with 10 nM TCDD for YAMC cells, or 25 nM TCDD for

human colon cancer cell lines Caco2 and SW48. Cell media was collected and assayed for luciferase activity 1 d after treatment. Secreted alkaline phosphatase was used as an internal control for normalizing transfection efficiency.

2.2.10. Chromatin immunoprecipitation (ChIP)

ChIP analysis was performed as per manufacturer's instructions (Active Motif 53040). Organoids or cells were treated with DMSO (vehicle) or 10 nM TCDD in culture medium for 2 h. In addition, mice were gavaged with DMSO or TCDD (25 μg/kg, bw) 2.5 h prior to termination, and crypts were subsequently harvested. Organoids or crypts were chemically crosslinked using 1% formaldehyde for 15 min at room temperature. 5% of each chromatin preparation was retained as input. The chromatin preparation was then immunoprecipitated overnight at 4°C with 2 μg of anti-AhR antibody (BML-SA210, Enzo, or sc-5579, Santa Cruz Biotechnology) or 2 μg of anti-IgG antibody (2729S, Cell Signaling, or sc-2027, Santa Cruz Biotechnology) per reaction. After washing, reversal of cross-linking, and DNA purification steps, DNA fragments were analyzed by qPCR or PCR and normalization relative to input DNA. The following primers were used for the mouse FoxM1 promoter: forward 5'-CGCTGTATCCTCCGCTCTT-3'; reverse 5'-TAGACTTGCGGTTACGTGGC-3'; human FoxM1 promoter: forward 5'- AGCAGACGATCGTTCACTGT-3'; reverse 5'-GGGAGAGTTTGGGGACGC-3', and mouse negative control primer (Active Motif 71011).

2.2.11. RNA sequencing and gene expression analysis

Isolated total RNA (5 ng) from each sample was prepared for sequencing using the NuGen Ovation® Single Cell RNA-Seq System (0342HV, San Carlos, CA) following manufacturer's instructions. Samples were sequenced on a NextSeq 500 (Illumina,) 75 bases, single ended. There was an average of 18.7 million reads per sample. Reads were mapped to the grcm38 mouse genome from Ensembl using STAR (ver. 2.4.0j) with default settings. Using only the 22,219 genes that had a count of more than 3 for all samples, EdgeR was used to identify differentially expressed genes. Differentially expressed genes (FDR<0.1) were included in pathways and function analyses performed using Ingenuity Pathway Analysis software (IPA). To determine the enrichment of intestinal stem cell signatures, PID_FoxM1 Pathway or KEGG Wnt signaling pathway gene sets, unbiased gene set enrichment analysis was performed using Gene Set Enrichment Analysis (GSEA v3.0; http://www.broadinstitute.org/gsea) and normalized enrichment scores (NES) with FDRs were generated. RNAseq analysis results from normal human colon tissues using the GTEx dataset were downloaded from UCSC Xena (http://xena.ucsc.edu).

2.2.12. *Study approval*

Animal studies were approved by the Institutional Animal Care and Use Committee at Texas A&M University. The use of normal human colonic organoids was approved by the Institutional Review Board at Texas A&M University. Normal human colonic organoids were originally isolated from a resected colon segment derived from 4 female

individuals (patient 1, age 30; patient 2, age 71; patient 3, age 56; patient 4, age 60) and 2 male individuals (patient 5, age 32; patient 6, age 58).

2.2.13. Statistics

Two-tailed Student's t-tests were used to assess statistical significance of the differences between means across experimental groups. One-way or two-way ANOVA with Tukey's multiple comparisons test were used to compare more than 2 groups. Tumor incidence was assessed using Chi Square analysis. Tumor volume was assessed using the Mann-Whitney U test. Paired student t-tests were used to examine the statistical significance of the differences between treatments within genotypes in organoids, unless otherwise specified. No samples or animals were excluded from the analyses. All data are presented as mean ± SE, and all analyses were conducted using Prism 8 statistical software (GraphPad Software, Inc.).

2.3. Results

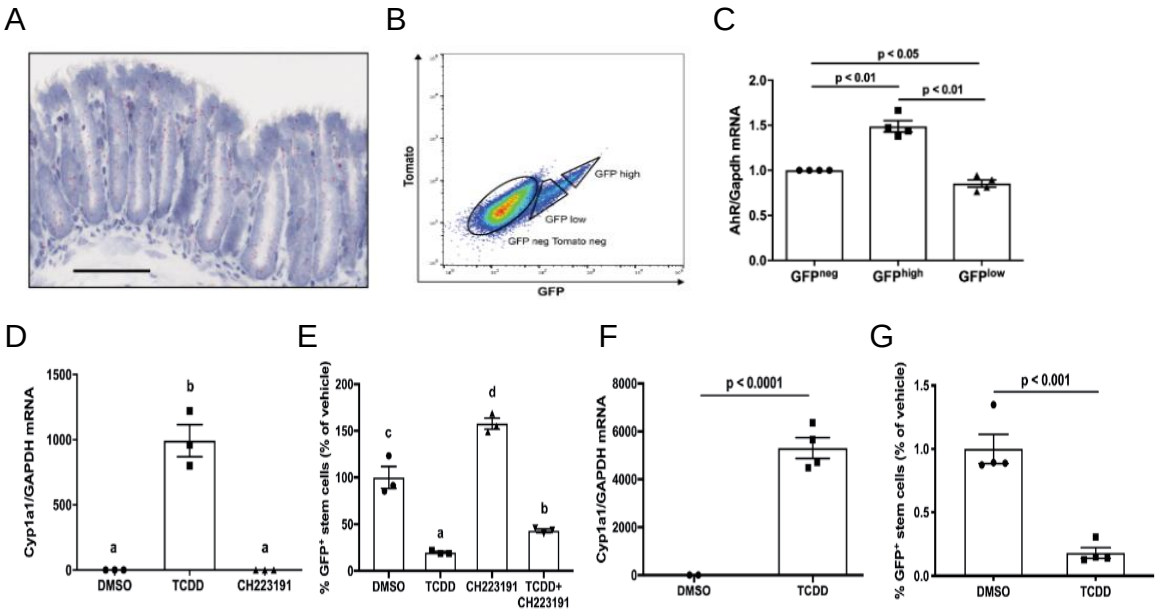

Figure 6. AhR signaling modulates the percentage of stem cells in colonic crypts.
(A) Representative image of AhR in situ hybridization in mouse colon. Scale 50 µm. (B) Flow cytometry gating profiles of Lgr5-EGFP-IRES-Cre^{ERT2} mice. (C) Expression of AhR in the indicated cell fractions from Lgr5-EGFP-IRES-Cre^{ERT2} mice. (D-E) Colonic organoids grown from Lgr5-EGFP-IRES-Cre^{ERT2} mice were treated with an AhR agonist (10 nM TCDD) or antagonist (10 µM CH223191) for 3 d. (D) Induced Cyp1a1 mRNA expression in response to different treatments (n=3 per group). DMSO (control) was set to 1. (E) Assessment of GFP$^+$ stem cell percentages (n=3 replicates per treatment). Bars with different letters are significantly different ($p<0.05$). (F-G) Mice were gavaged every other day, 4 times total, with vehicle or TCDD (25 µg/kg bw) and terminated 1 d later. Colons were subsequently resected and GFP$^+$ stem cell percentages assessed. (F) Induced Cyp1a1 mRNA expression in stem cells after oral gavage with TCDD (n=4). DMSO (control) was set to 1. (G) Percentage of GFP$^+$ stem cells (n=4 mice per group).

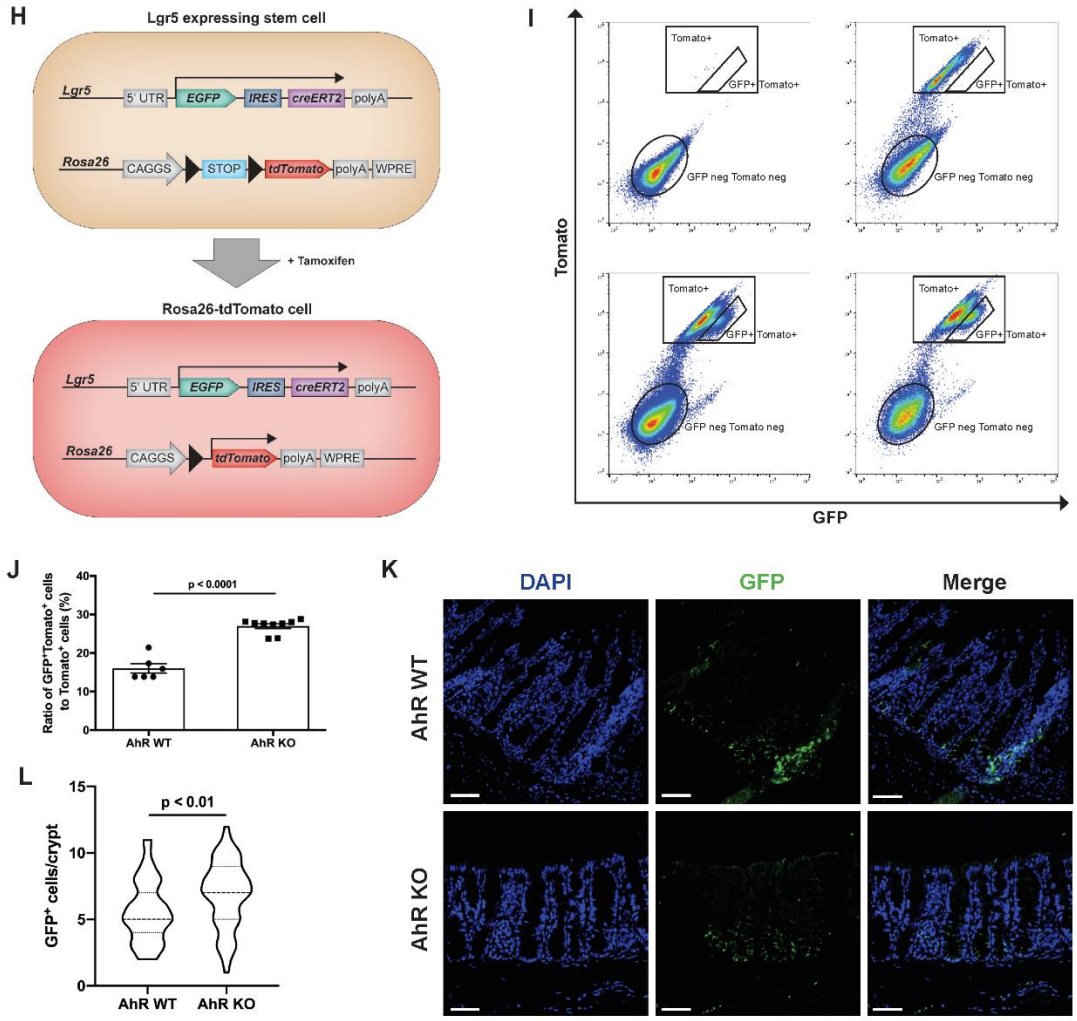

Figure 6. Continued.
(H) Scheme of the generation of transgenic Lgr5-GFP^{CreERT2} X Tomato$^{f/f}$ mice. eGFP and CreERT2 expression are controlled by the intestinal stem cell specific marker Lgr5 promoter, and the tdTomato reporter cassette is knocked into the Rosa26 locus. A floxed STOP cassette is upstream of the tdTomato gene, thus preventing tdTomato expression in the absence of tamoxifen. Upon tamoxifen exposure, CreERT2 recombinase will be translocated into the nucleus, and the STOP sequence between the loxP sites is excised and the tdTomato reporter is permanently and constitutively expressed in intestinal stem cells and their progeny. (I) Flow cytometry analysis of GFP^{+}Tomato^{+} and Tomato^{+} cells in the large intestine of AhR wild type (Lgr5-GFP^{CreERT2} X Tomato$^{f/f}$, GT) and AhR knock out (AhR$^{f/f}$ X Lgr5-GFP^{CreERT2} X Tomato$^{f/f}$, HGT) mice. Top left panel shows representative cells from WT negative control animal (no GFP or Tomato expression). Top right panel shows Tomato only control (CDX2P-Cre^{ERT2} X Tomato$^{f/f}$). Bottom left panel is from a representative AhR WT mouse and bottom right panel is from a representative AhR KO mouse. (J) Quantitative analysis of the percentage of Lgr5^{+} stem cells from FACS experiments in (I), n=6-9 mice per group. (K-L). Representative immunohistochemistry and violin plots of GFP^{+} stem cells per crypt, n=3 mice per group. Scale 50 µm.

2.3.1. *AhR signaling modulates the percentage of colonic stem cells*

Although several studies have linked AhR signaling and stem cell dynamics [168,178], there is a paucity of data describing how this environmental sensor modulates colonic stemness and the functional properties of intestinal stem and progenitor (i.e., transit amplifying) cells. Therefore, we initially assessed the expression of AhR in the mouse colon. Results from AhR RNA in situ hybridization (ISH) showed that AhR was ubiquitously expressed across the entire colonic epithelial cells (**Fig. 6A**). Moreover, AhR mRNA was moderately enriched in sorted colonic stem cells from Lgr5-EGFP-IRES-Cre^{ERT2} reporter mice (**Fig. 6B&C**). We subsequently treated colonic organoids generated from Lgr5-EGFP-IRES-Cre^{ERT2} reporter mice with a prototypical AhR agonist TCDD or antagonist CH223191 for 3 d. Cyp1a1 induction was used as a biomarker of AhR activation (**Fig. 6D**). AhR activation by TCDD dramatically decreased the percentage of colonic stem cells marked by GFP, while AhR inhibition by CH223191 had the opposite effect (**Fig. 6E**). Moreover, cotreatment with TCDD plus CH223191 showed that the TCDD-dependent decrease in the percentage of colonic stem cells was attenuated by the AhR antagonist. Similarly, Cyp1a1 was induced and there was a decreased percentage of colonic stem cells in vivo after mice were treated with TCDD by oral gavage (**Fig. 6F and G**). To further confirm that the decreased percentage of colonic stem cells by TCDD was mediated exclusively through AhR, inducible and intestinal-specific AhR knockout (KO) mice were generated by crossing AhR$^{f/f}$ mice with Lgr5-EGFP-IRES-Cre^{ERT2} mice. To address the confounding effects of mosaicism in Lgr5-EGFP-IRES-Cre^{ERT2} mice, tdTomato reporter alleles were introduced into our inducible stem cell targeted AhR KO mouse model (**Fig. 6H**). In this model, the

resulting tomato-positive cells are derived from recombined $GFP^{+}Tomato^{+}$ stem cells. AhR KO efficiency in sorted $tdTomato^{+}$ cell populations was ~85%. These findings demonstrate that tomato expression is a high-fidelity marker to track recombined cell populations. Tamoxifen-induced AhR KO significantly increased the percentage of stem cells, compared to wildtype (WT) control (**Fig. 6I&J**). In addition, immunohistochemical analysis of colonic stem cell marker proxy, GFP, showed that AhR KO enhanced the number of colonic stem cells per crypt (**Fig. 6K&L**). Overall, these results suggest that AhR signaling plays a direct role in modulating the proportion of stem cells in the colonic crypt.

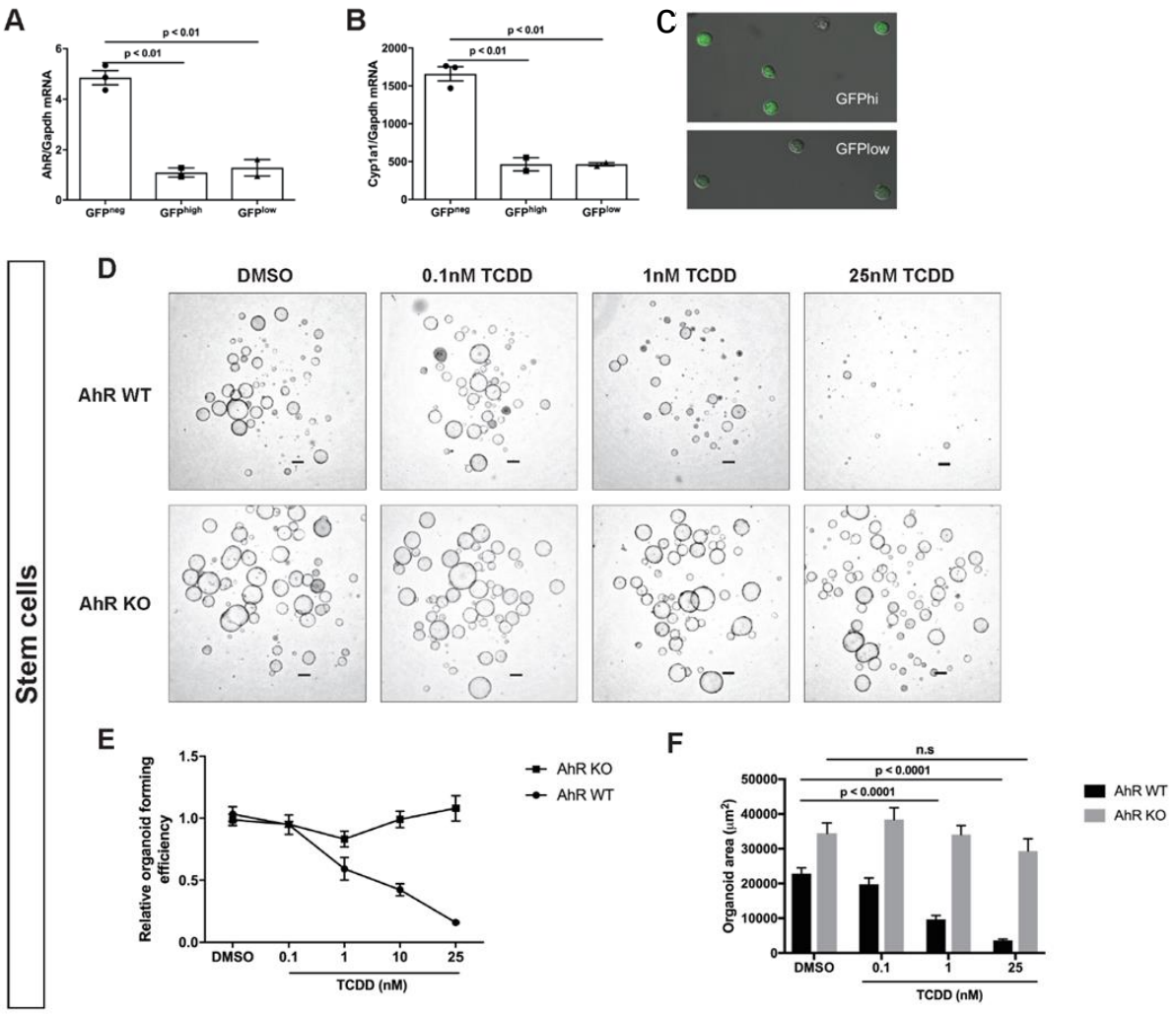

Figure 7. Functional characterization of AhR signaling in mouse colonic stem and progenitor cells.

Expression of (A) AhR and (B) Cyp1a1 in the indicated cell fractions from AhR$^{f/f}$ X Lgr5-GFP^{CreERT2} X CDX2P-Cre^{ERT2} (HGC) mice 2 wk post tamoxifen injection. Data represent mean ± SE (n=3 mice per group). (C) Representative fluorescence microscopy images of sorted GFP^{high} stem cells and GFP^{low} progenitor cells from Lgr5-EGFP-IRES-Cre^{ERT2} mice. (D) representative brightfield images of organoids generated from mouse colonic stem cells treated with different doses of TCDD. (E-F) Quantification of organoid forming efficiency and organoid size derived from colonic stem cells.

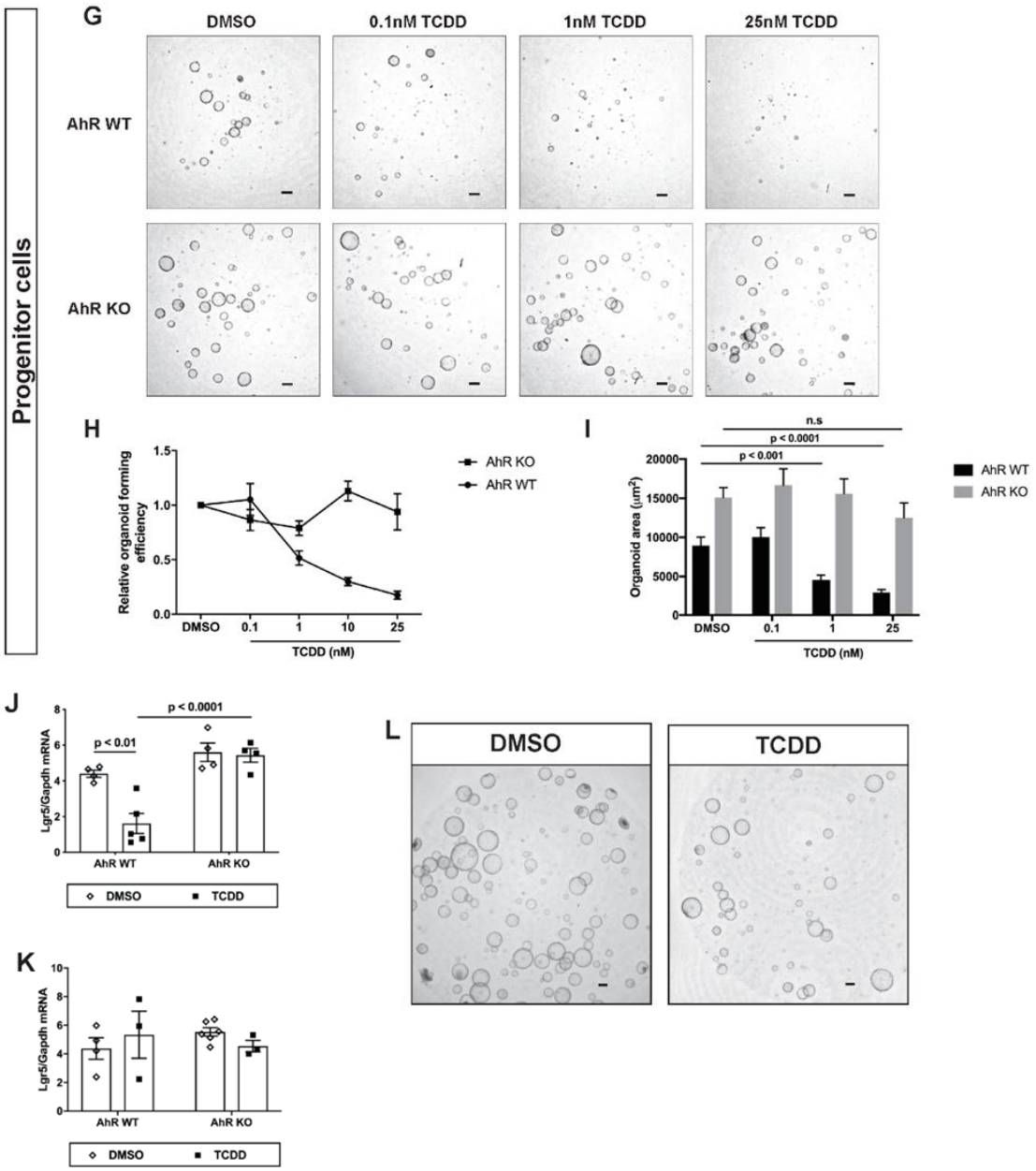

Figure 7. Continued.
(G) representative brightfield images of organoids generated from mouse progenitor cells treated with different doses of TCDD. (H)(I) Organoid forming efficiency and organoid size derived from colonic progenitor cells. Data represent mean ± SE, n=6 from 2 mice per treatment. (J) Lgr5 expression in organoids and (K) sorted stem cells in the absence or presence of TCDD treatment (n≥4 independent samples per group). (L) Representative brightfield images for secondary organoid formation pretreated with DMSO or 10 nM TCDD for 2d. Scale 200 µm. A 2-way ANOVA with Tukey's multiple comparisons was carried out in (F) (I) (J) and (K).

2.3.2. *AhR signaling regulates the functionality of colonic stem and progenitor cells*

To more broadly delete AhR in colonic epithelial cells, mice expressing the $AhR^{f/f}$ allele were crossed with mice expressing a Cre^{ERT2} transgene driven by Lgr5 and CDX2 promoters [169]. AhR deletion was subsequently characterized (**Fig. 7A&B**). Next, we determined whether AhR signaling impacts the function of stem cells and transit amplifying progenitor cells. For this purpose, fluorescence-activated cell sorting (FACS) was used to sort stem cells (defined as GFP^{high}) and progenitor cells (GFP^{low}) based on GFP expression (**Fig. 6B**). The intensity of the GFP signature and quality of the isolation of the two sorted cell populations were confirmed using confocal microscopy (**Fig. 7C**). Since intestinal stem cells are uniquely capable of generating long-lived organoids in vitro [175], and progenitor cells have a much lower capability to drive organoid formation in vitro (exhibit dynamic plasticity and can revert to stem cells upon crypt damage [111,112]), we determined the organoid forming efficiency of sorted stem and progenitor cells with and without AhR in the presence or absence of TCDD. AhR activation by TCDD dramatically decreased the organoid forming efficiency of WT stem cells in a dose-dependent fashion, compared with vehicle, while AhR KO exhibited a remarkably high organoid forming efficiency and abrogated the effect of TCDD (**Fig. 7D&E**), demonstrating that TCDD effects were exclusively mediated by AhR. As expected, organoid growth, i.e., organoid diameter, was positively correlated with organoid forming efficiency (**Fig. 7F**). Surprisingly, AhR KO significantly promoted organoid formation and growth in wells containing sorted progenitor cells, while AhR activation by TCDD inhibited organoid formation and growth of WT progenitor cells in dose-dependent manner, but not KO progenitor cells (**Fig. 7G-I**). The organoids from

sorted progenitor cells were morphologically similar with those from sorted stem cells except for smaller size at day 5.

To exclude the possibility that larger organoid size following AhR KO results from increased cell differentiation, we examined the expression of Lgr5 in organoids. As expected, Lgr5 mRNA expression was increased in AhR KO vs WT organoids derived from these mice (**Fig. 7J**). In addition, Lgr5 expression was decreased in WT organoids following TCDD treatment in comparison to DMSO (control), but not in AhR KO organoids (**Fig. 7J**). However, Lgr5 expression was not altered in sorted stem cells regardless of DMSO or TCDD treatment or AhR KO (**Fig. 7K**), indicating that decreased Lgr5 expression by TCDD in organoids resulted from diminished stem cell pools, as opposed to reduced Lgr5 expression itself in stem cells. Analysis of secondary organoid clonogenicity further demonstrated that TCDD treatment decreased functional colonic stem cell populations (**Fig. 7L**). Together, these results show that AhR signaling regulates the clonogenic capacity of mouse colonic stem and progenitor cells.

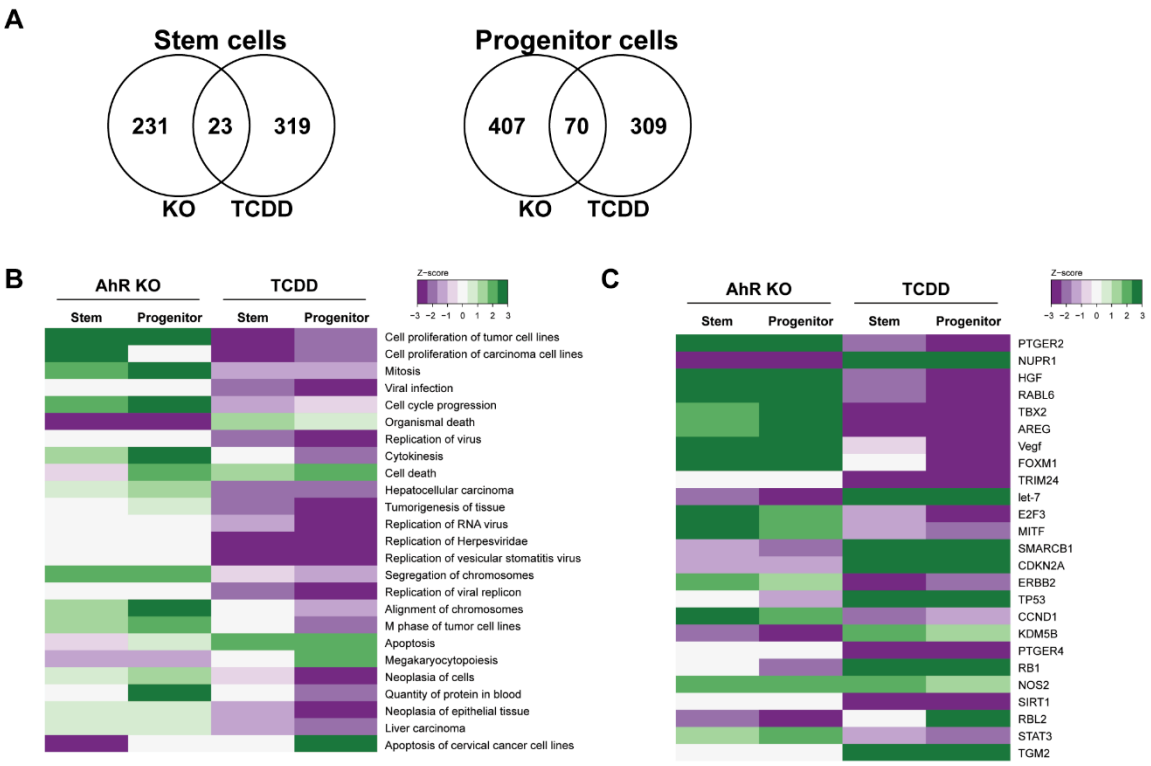

Figure 8. FoxM1 pathway affected by AhR in mouse colonic stem and progenitor cells.
(A) Venn diagrams of differentially expressed genes following comparison of AhR KO (KO/WT) and TCDD effects (TCDD/vehicle in WT mice) in sorted stem and progenitor cells; KO (HGC mice); WT (GC mice). An FDR<0.1 cutoff was used. (B) Heatmap comparison of the top 25 enriched Diseases and Biological Functions in AhR KO (KO/WT) and TCDD (TCDD/vehicle in WT mice) treated cells as identified by IPA. (C) Heatmap comparison of the top 25 upstream regulators between AhR KO (KO/WT) and TCDD (TCDD/vehicle in WT mice) treated cells.

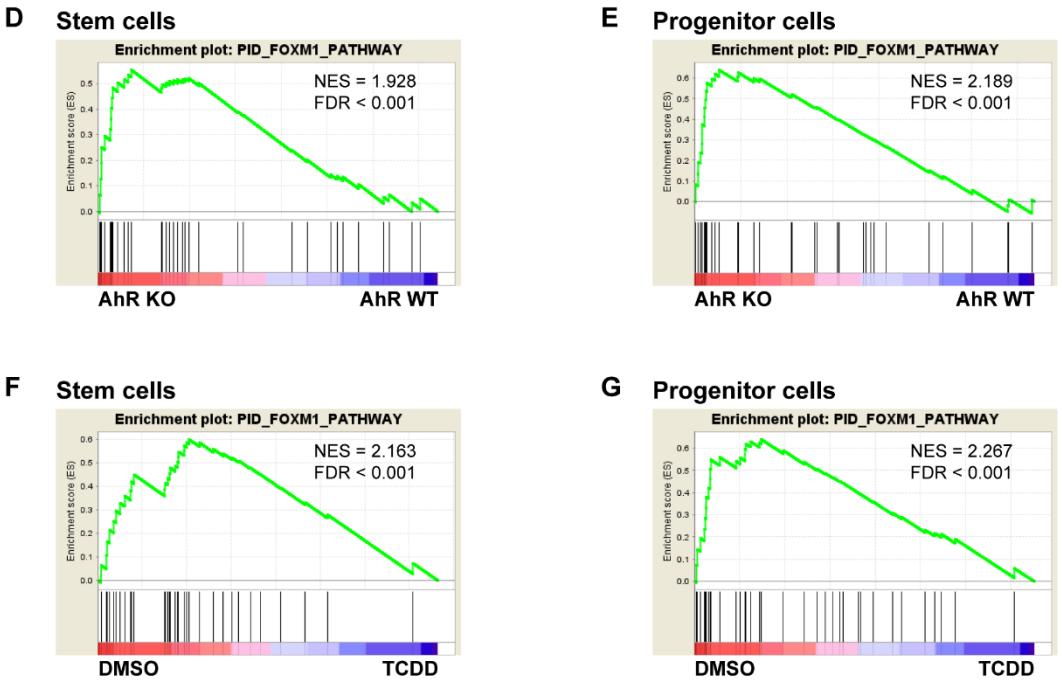

Figure 8. Continued.
(D-G) Gene Set Enrichment Analysis (GSEA) was performed in sorted stem and progenitor cells from AhR WT (n=3) and KO (n=4) mice (D&E) and in WT mice in response to vehicle and TCDD treatment (F&G). Normalized enrichment scores (NES) and FDRs were calculated using the Public Interaction Database (PID) for the FoxM1 Pathway gene set.

2.3.3. *AhR KO upregulates FoxM1-mediated cell proliferation associated genes*

To gain mechanistic insight into how AhR modulates organoid forming efficiency and organoid growth of stem and progenitor cells, gene expression profiling by RNAseq was performed. For this purpose, cell signaling networks in sorted stem and progenitor cells harvested from tamoxifen-injected mice treated with TCDD or DMSO vehicle were compared. The number of differentially expressed genes (DEGs) was 254 and 477 in AhR KO stem and progenitor cells, respectively, compared with corresponding controls, while the number of DEGs was 342 and 379 in TCDD challenged WT stem and

progenitor cells, respectively (**Fig. 8A**). Pathway (Diseases and Function) **(Fig. 8B)** and Upstream Analysis **(Fig. 8C)** by Ingenuity Pathway Analysis (IPA) revealed that AhR signaling had a major impact on cell proliferation, cell cycle progress and cell death or apoptosis. Stem cells and progenitor cells exhibited similar expression patterns in either AhR KO (KO/WT) or TCDD challenged (TCDD/vehicle) conditions. Interestingly, there was little overlap with respect to DEGs between AhR KO and TCDD treatments, implying differences in AhR regulated versus TCDD-induced gene expression. However, the affected cell signaling pathways were highly conserved, implying that AhR regulates cellular signaling at different nodes of the same signaling pathway. In contrast, stem cells shared many DEGs with progenitor cells, irrespective of AhR KO and TCDD treatment (not shown). Of note, FoxM1, a pivotal regulator of cell proliferation, was consistently identified as an upstream regulator in stem cells and progenitor cells in response to AhR KO and AhR activation (**Fig. 8C**). GSEA was subsequently performed to examine whether AhR signaling affects FoxM1 pathway. For this purpose, RNAseq data was examined with respect to FoxM1 gene signatures in both stem and progenitor cells with/without AhR in the absence or presence of TCDD. FoxM1 signature genes were primarily enriched in AhR KO stem and progenitor cells, compared with WT counterparts (**Fig. 8D&E**), and in vehicle treated stem and progenitor cells, compared with TCDD treatment (**Fig. 8F&G**). In addition, we also tested the effect of prostaglandin E_2 (PGE_2) supplementation on organoid growth, since prostaglandin E receptors 2/4 (PTGER2/4) were identified as top upstream regulators. However, PGE_2 treatment had no effect on organoid growth (**Fig. 9**). Collectively, our

global transcriptomic analyses suggest that AhR KO upregulates FoxM1-mediated cell proliferation pathways both in stem and progenitor cells.

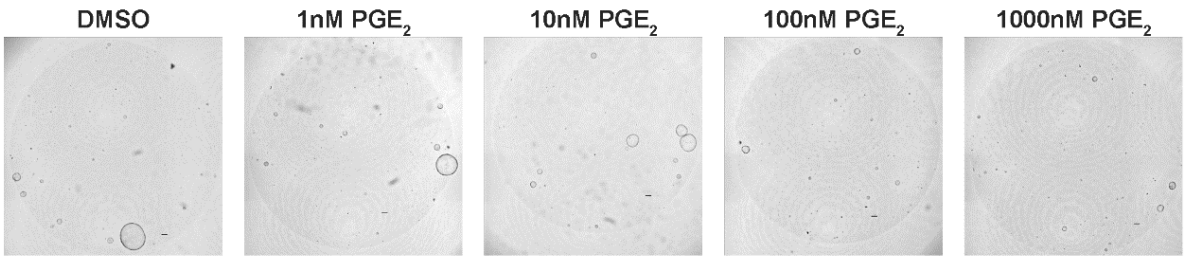

Figure 9. Lack of an effect of PGE2 on organoids derived from WT mice.
Representative images of organoids derived from sorted colonic stem cells, scale 200 μm. Experiments were conducted in triplicate.

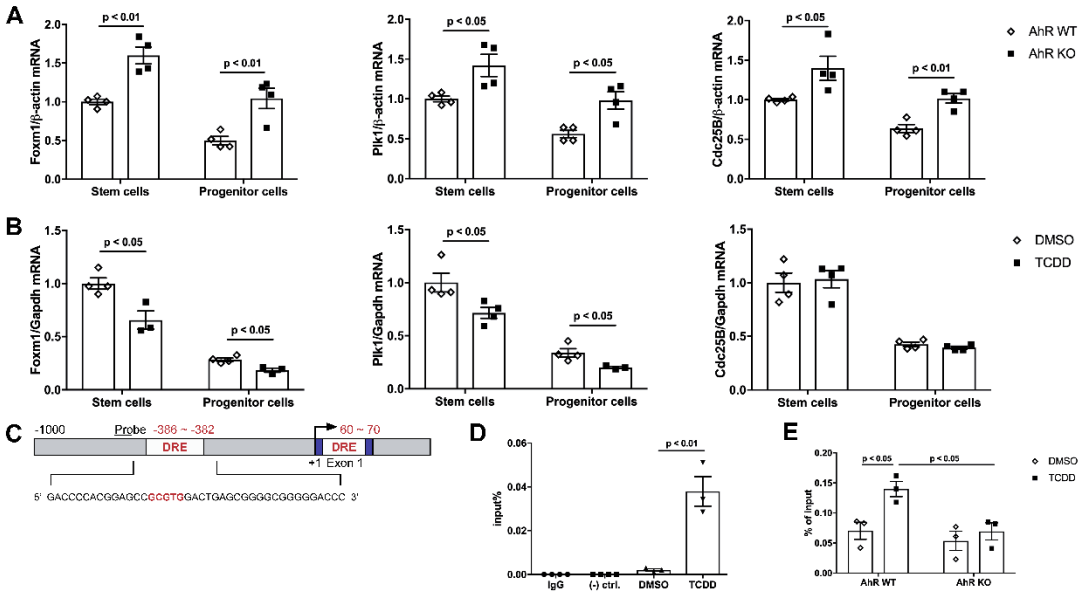

Figure 10. FoxM1 is a direct target of AhR.
(A) FoxM1, Plk1, and Cdc25B mRNA expression in stem and progenitor cells with and without AhR, n=4 mice per group. (B) FoxM1, Plk1, and Cdc25B mRNA expression in WT stem and progenitor cells with and without TCDD, n=4 mice per group. (C) Schematic representation of the FoxM1 promoter region containing a putative dioxin response element. (D-E) Chromatin immunoprecipitation (ChIP) analysis of AhR and FoxM1 promoter interaction using WT colonic organoids (D) or WT and KO crypts (E) treated with DMSO or TCDD, n=3 or 4 per group. A DNA fragment amplified in a gene desert on mouse chromosome 6 was used as a negative control.

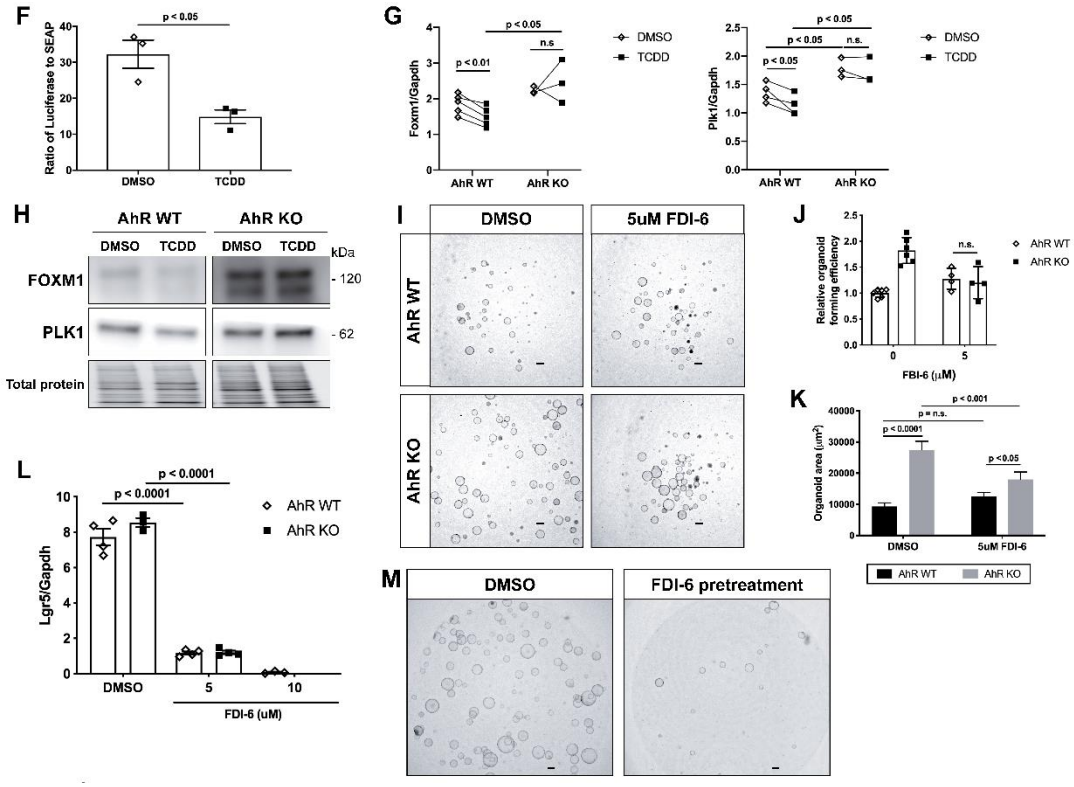

Figure 10. Continued.
(F) FoxM1 luciferase activity determination for young adult mouse colonocytes (YAMCs) treated with DMSO or 10 nM TCDD for 1 d, n=3 per group. (G)(H) Expression of FoxM1 and PLK1 at mRNA and protein level, respectively, n>=3 independent organoids per treatment. (I) Representative brightfield images of mouse colonic organoids generated from WT Lgr5^{+}-GFP^{hi} stem cells treated with DMSO or 5μM FDI-6. Scale bar 200 μm. Quantification of organoid forming efficiency (J) and organoid area (K) from WT colonic stem cells treated with DMSO or 5μM FDI-6. (L) Organoid expression of Lgr5 in response to FDI-6. Lgr5 expression level was dramatically suppressed by FDI-6 in a dose-dependent manner, n>=3 per treatment. (M) Representative brightfield images for secondary organoid formation following treatment with DMSO or 5 μM FDI-6 for 2 d. Scale 200 μm. A 2-way ANOVA with Tukey's multiple comparisons test was carried out in (E)(J)(K) and (L). Paired student t-test was performed within genotype in (G).

2.3.4. *FoxM1 is a direct target of AhR*

Since the FoxM1 pathway is affected by AhR signaling, qPCR was performed to confirm the expression of a subset of genes in the FoxM1 pathway. FoxM1 expression was significantly altered in response to AhR KO and TCDD treatment in both stem and progenitor cells, including its targets, Plk1 and Cdc25B (**Fig. 10A&B**). To test our hypothesis that FoxM1 is a direct target of AhR, we first performed an *in silico* search for canonical dioxin response elements (DREs) in the FoxM1 promoter within 1kb of the transcription start site. Two putative DREs were identified in the FoxM1 promoter (**Fig. 10C**). Next, chromatin immunoprecipitation (ChIP) was performed to examine AhR-FoxM1 promoter interaction both in organoids and colonic crypts. TCDD treatment significantly enhanced the enrichment of AhR at the FoxM1 promoter in WT but not AhR KO mice (**Fig. 10D&E**). Moreover, TCDD treatment decreased FoxM1 luciferase reporter activity (**Fig. 10F**), indicating that FoxM1 is a direct target of AhR. Next, the expression of FoxM1 and its target gene Plk1 in response to TCDD treatment were examined. Importantly, AhR activation decreased the expression of FoxM1 and Plk1 at the mRNA and protein levels in WT organoids, but not in AhR KO organoids (**Fig. 10G&H**). To determine whether upregulation of the FoxM1-mediated signaling could account for the increased organoid forming efficiency mediated by AhR KO, a FoxM1 inhibitor, FDI-6, was supplemented into the organoid medium used for plating sorted stem and progenitor cells. Interestingly, 5 μM FDI-6 abrogated AhR KO effects with respect to organoid forming efficiency in stem cells (**Fig. 10I&J**), significantly suppressed organoid growth from AhR KO colonic stem cells, and had no effect on WT counterparts (**Fig. 10I&K**). Finally, suppression of FoxM1 also significantly reduced Lgr5

expression in dose-dependent manner (**Fig. 10L**) and robustly suppressed secondary organoid formation (**Fig. 10M**), recapitulating the TCDD-mediated phenotype. Taken together, our data suggest that AhR binding to the FoxM1 promoter suppressed its expression, and thus the effects of AhR KO on organoid formation are mediated in part by upregulation of the FoxM1 pathway.

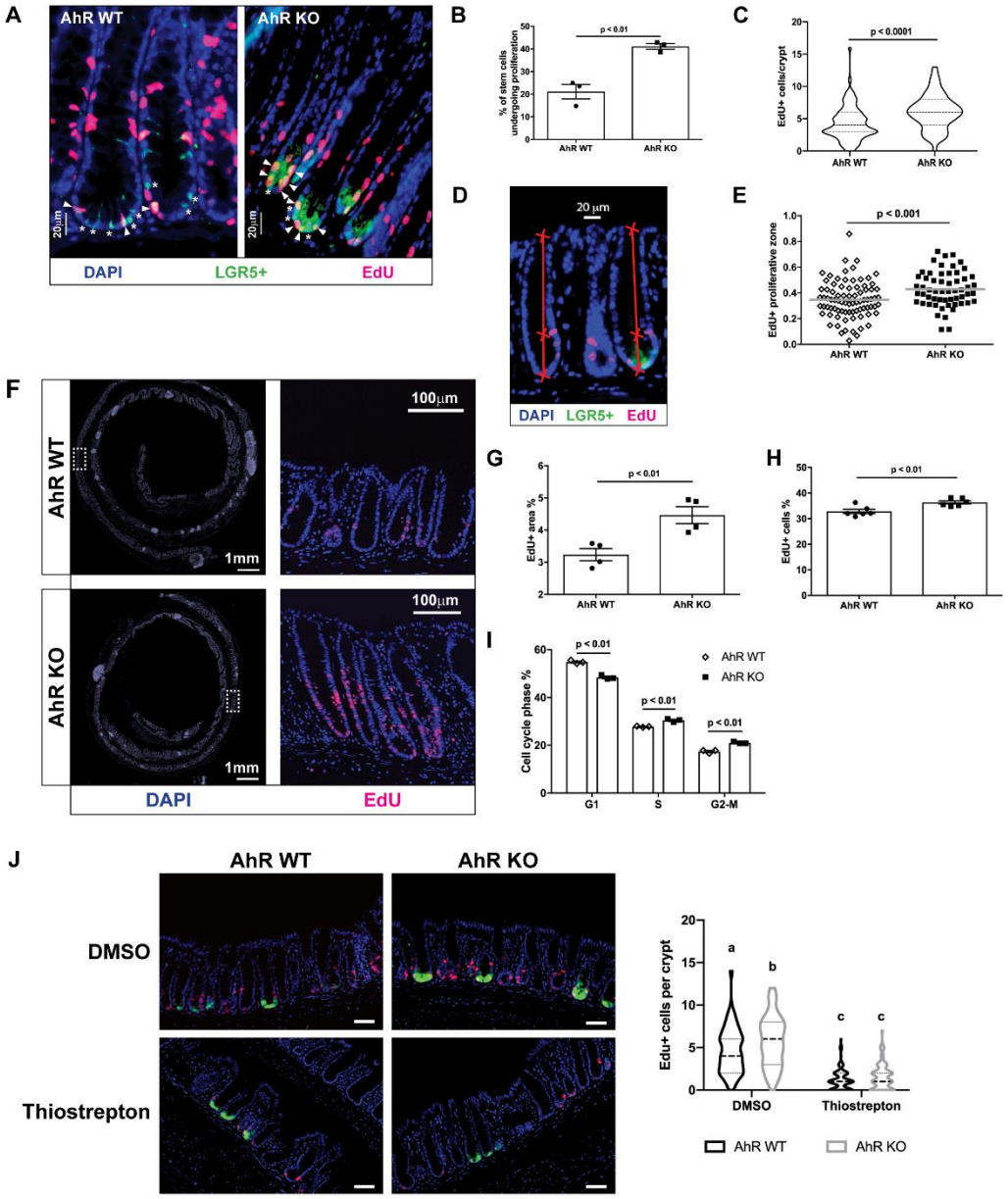

Figure 11. Effects of AhR KO on colonic cell proliferation.
(A and B) Proliferating Lgr5^{+} stem cells marked by EdU in the distal colon from AhR WT (GT) and KO (HGT) mice. Arrowhead and star symbols denote proliferating stem cells (GFP^{+}EdU^{+}) and static stem cells (GFP^{+}EdU^{-}), respectively, during a 2 h EdU pulse, n=3 per treatment. (C) Total number of EdU^{+} cells per crypt in the distal colon of AhR WT and KO (HGT) mice, n=3 per treatment. (D&E) Crypt cell proliferative zone analysis in AhR WT and KO (HGT) mice, presented as the distance from the crypt base to the highest EdU^{+} cell divided by total crypt length. Each symbol represents one crypt, n=3 mice per treatment, scale bar 20 μm. (F&G) AhR KO promoted cell proliferation 5 d post DSS treatment. AhR$^{f/f}$ X Villin-Cre (HV, n=4) and AhR$^{f/f}$ (H, n=4) mice were used. Data represent mean ± SE, quantified as the ratio of the EdU^{+} area relative to the DAPI^{+} area using Keyence^{TM} software. (H) Increased cell proliferation (EdU^{+} cells) observed in AhR KO vs WT organoids derived from HGC and GC mice, respectively (n=3 mice per group). (I) Effect of AhR KO on cell cycle S and G2-M phases (n=3 mice per group). (J). FoxM1 inhibition reduced cell proliferation. FoxM1 inhibitor Thiostrepton (50mg/kg) was intraperitoneally given to mice for 2 consecutive days. Scale bar, 200 μm.

2.3.5. AhR deletion increases stem cell proliferation

Considering the pivotal role of FoxM1 signaling in regulating cell proliferation and organoid size in AhR KO colonic stem and progenitor cells, we hypothesized that AhR KO directly modulates cell proliferation in vivo. To this end, inducible stem cell targeted AhR KO and WT mice were injected with 5-ethynyl-2'-deoxyuridine (EdU) 2 h prior to termination. We found that AhR KO significantly increased basal stem cell proliferation and the number of proliferating cells per crypt, compared with WT control (**Fig. 11A-C**). The crypt proliferative zone, defined as the ratio of the distance between crypt base and the uppermost EdU^+ cell relative to the crypt height, was also quantified (**Fig. 11D**). AhR KO promoted an extension of the crypt proliferation zone (**Fig. 11E**). In addition, cell proliferation following crypt wounding was examined in an intestine-specific constitutive AhR KO (Villin-Cre) model. Five days following DSS-induced injury, cell proliferation was increased in AhR KO mice (**Fig. 11F&G**).

To determine which cell cycle phases were altered in response to AhR KO, we cultured colonic organoids derived from AhR KO and WT mice in a growth factor-enriched medium. In this crypt culture system, AhR KO also promoted cell proliferation (**Fig. 11H**). Further analysis revealed that AhR KO reduced the percentage of cells in G1 phase, while increasing cell populations in S and G2-M phases (**Fig. 11I**). This is consistent with our RNAseq data where AhR KO upregulated the FoxM1 signaling pathway, which modulates various phases of the cell cycle, including G1/S and G2/M phases [179,180]. Moreover, FoxM1 inhibition robustly suppressed cell proliferation and rescued AhR KO mediated cell proliferation in vivo (**Fig. 11J**). Interestingly, the

observed increase in cell proliferation in AhR KO mice was not associated with any change in Wnt signaling or ERK1/2 status (**Fig. 12**).

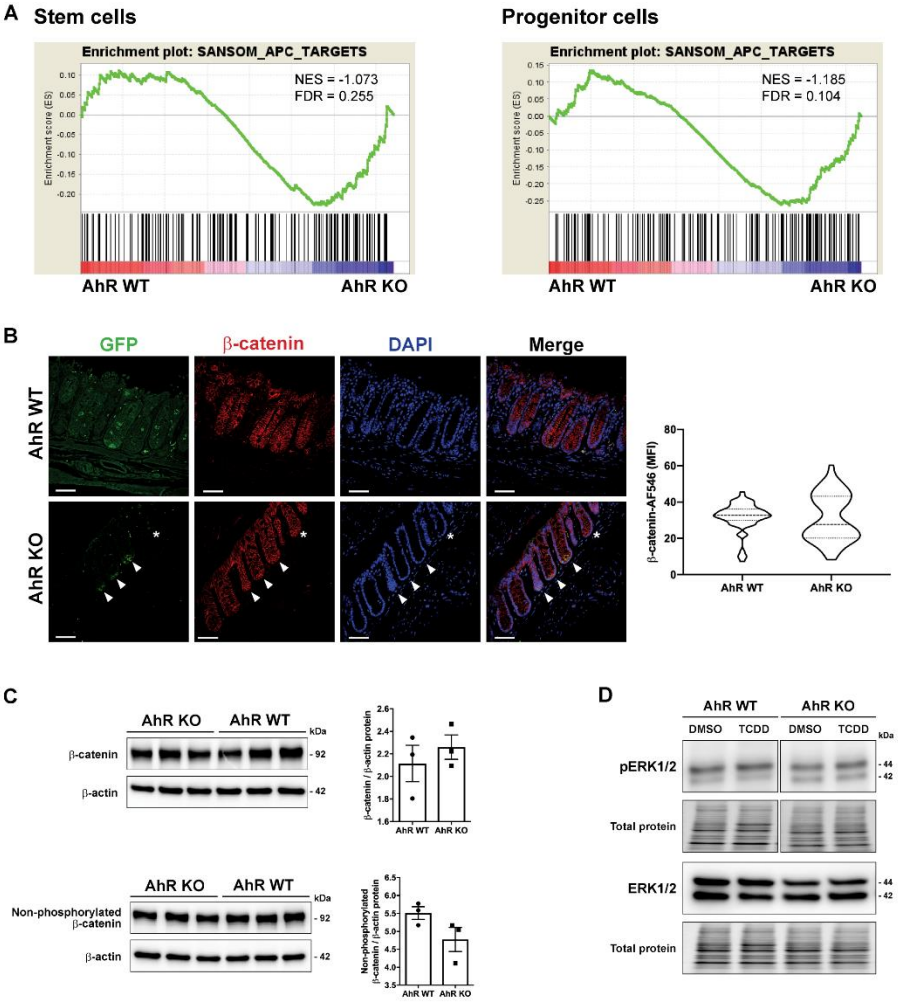

Figure 12. Wnt signaling and pERK1/2 are not altered by AhR signaling.
(A) GSEA using the KEGG Wnt Signaling Pathway gene set was examined with respect to sorted stem and progenitor cells from AhR KO (HGC) versus WT (GC) mice. No significant enrichment was observed in AhR KO stem or progenitor cells. (B) Representative immunohistochemisty for β-catenin in colon sections from AhR WT and KO mice. White arrows in GFP$^+$ crypts (KO group) indicate AhR KO crypts. Asterisk denotes WT crypt adjacent to KO crypts. Scale 50 µm. (C) Western blotting for β-catenin and non-phospho (active) β-catenin in AhR WT and KO organoids (n=3 independent observations per group). No significant difference was detected in AhR KO versus WT treatment. (D) Representative immunoblots for pERK1/2 and ERK1/2 from AhR WT and KO mouse colonic organoids treated with DMSO or TCDD from n>=3 independent samples. Total protein was used as a loading control.

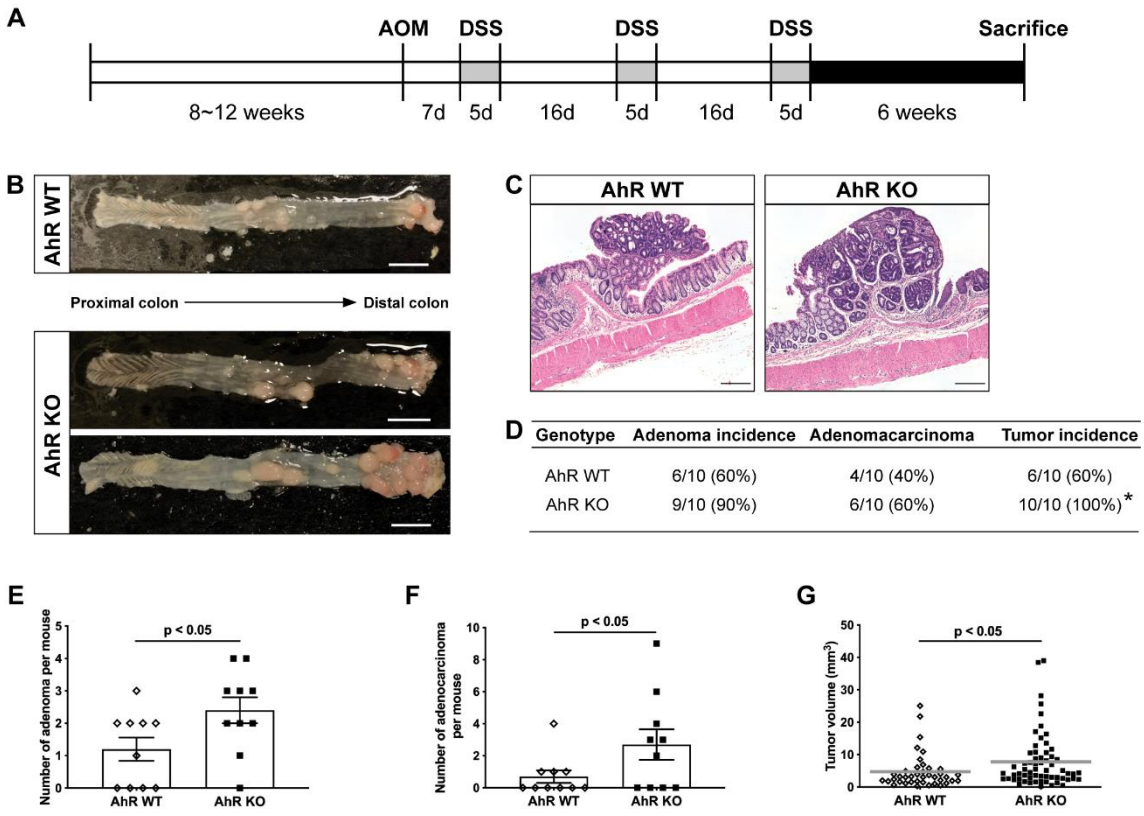

Figure 13. AhR KO promotes colorectal tumor growth in AOM/DSS treated mice.
(A) Schematic regimen for AOM/DSS-induction of colon tumorigenesis. At 8~12 wk of age, AhR WT (H, n=10) and KO (HV, n=10) mice were treated with a single dose of AOM (10 mg/kg) by s.c injection, followed by 3 cycles of 2% DSS in the drinking water for 5 d. Mice were terminated 6 wk after the third cycle of DSS. (B) Representative colon images from AhR WT and AhR KO mice following AOM/DSS treatment. Scale bar, 9 mm. (C) H&E staining of representative colon tumor sections from AhR WT and KO mice, scale bar 200 μm. (D) Incidence of colon adenomas, adenocarcinomas and both combined (tumor) in AhR WT and KO mice, *p<0.05. (E) Adenoma and (F) adenocarcinoma multiplicity in AhR WT and KO mice. One-tail student t-test. (G) Tumor volume in AhR KO and WT mice.

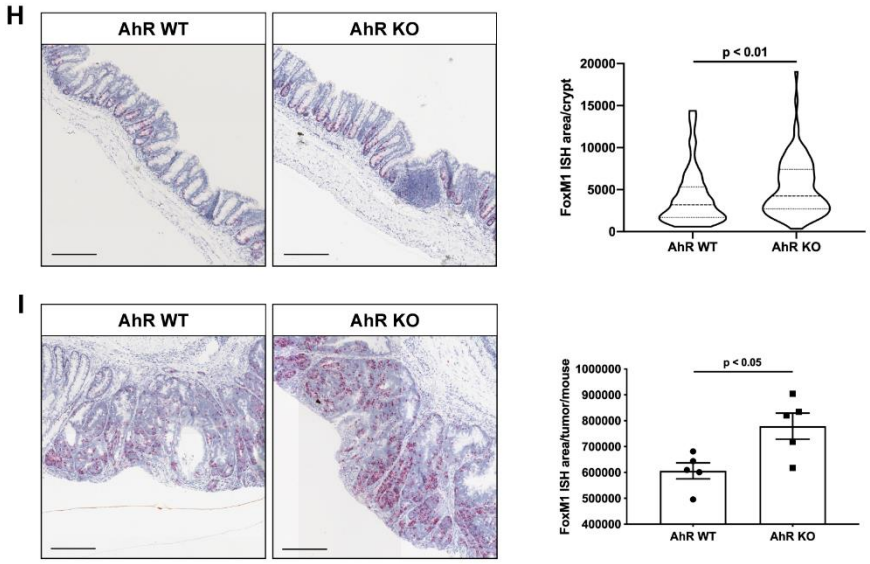

Figure 13. Continued.
(H) FoxM1 mRNA expression in normal (uninvolved) crypts adjacent to colonic tumors. Images were quantified and expressed as FoxM1 positive area per crypt (n=5 mice per group). Scale 200 µm. (I) FoxM1 mRNA expression in colon tumors. FoxM1 mRNA ISH area was averaged per tumor on each slide (n=5 mice per group). Scale 200 µm.

2.3.6. AhR KO promotes colonic tumor growth

Since the targeted loss of AhR in stem cells upregulated FoxM1 signaling and increased cell proliferation in intestinally-targeted AhR KO mice in response to DSS (**Fig. 11**), we subsequently investigated the ability of AhR KO to promote colitis-associated colorectal tumor growth (**Fig. 13A**). Consistent with a previous report that overexpression of FoxM1 promotes colitis associated colon cancer [181], we noted that AhR KO promoted the incidence of tumors in the AOM-DSS model (**Fig. 13B-D**). Moreover, AhR KO mice developed more adenomas and adenocarcinomas than WT mice (**Fig. 13E&F**). In addition, loss of AhR significantly promoted colorectal tumor growth: the average volume of colorectal tumors in AhR KO mice was 56% higher compared to WT mice (**Fig. 13G**). Since FoxM1 plays an important role in AOM/DSS-

induced colon tumorigenesis [181], we also examined FoxM1 mRNA expression in colon tumors and their adjacent normal crypts in AhR WT versus KO mice, and found that AhR KO promoted FoxM1 expression both in normal crypts and colon tumors (**Fig. 13H&I**). In addition, AhR activation by TCDD selectively downregulated FoxM1 expression in organoids derived from both mouse adenocarcinomas and polyps (**Fig. 14**).

Since Lgr5^{+} stem cells and cancer cells exhibit a Warburg-like metabolic profile [182,183], and the metabolic activity of the intestinal crypt supports stem cell function [184], we asked whether AhR signaling modulates the bioenergetic profiles of organoids derived from sorted stem cells. As shown in (**Fig. 15**), AhR KO vs WT organoids exhibited a reduced oxygen consumption rate (OCR) relative to the extracellular acidification rate (ECAR). In addition, AhR KO promoted the production of reactive oxygen species (**Table. 1**). These findings demonstrate that loss of AhR signaling drives metabolic activity toward a hyperproliferative tumor priming state.

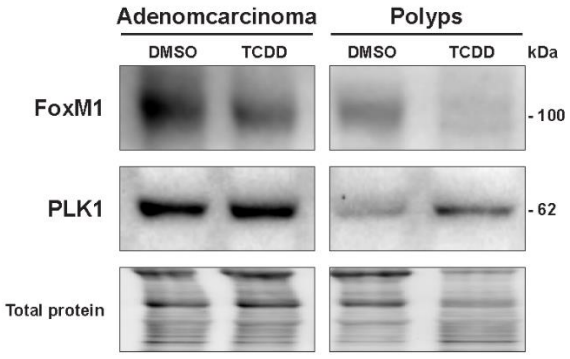

Figure 14. Representative immunoblots for FoxM1 and PLK1.
Organoids derived from mouse adenocarcinomas or polyp masses were treated with DMSO or TCDD. Total protein was used as a loading control.

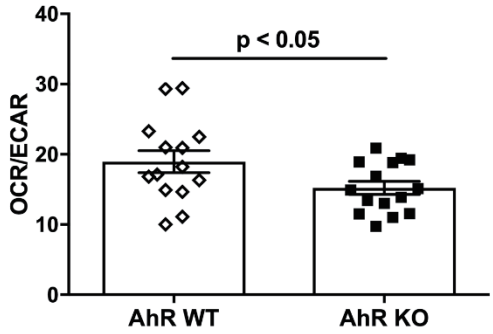

Figure 15. Effect of AhR KO on oxidative phosphorylation in colonocytes.
Organoids from AhR WT (GC) and KO (HGC) mice were cultured in stem/progenitor cell enriched WRN medium for 2 d after passage and subsequently seeded into a Seahorse XF24 cell culture microplate for measurement of OCR/ECAR. Data represent mean ± SE (n=14-16 replicates from 2 mice per group).

Table 1. Comparison of mitochondrial bioenergetic profiles in colonic organoids isolated from AhR WT (GC) and KO (HGC).

	AhR WT	AhR KO	P value
Basal respiration (pmol O_2/min)	651.2 ± 92.6	752.6 ± 123.7	n.s.
ATP turnover	278.5 ± 49.4	339.1 ± 61.68	n.s.
Proton leak	342.1 ± 48.6	303.0 ± 55.67	n.s.
ROS	136.2 ± 49.6	272.4 ± 19.63	0.0212
Maximal respiration capacity	1342 ± 180.2	1501 ± 273.6	n.s.
Reserved respiration capacity	691.2 ± 109.7	748.2 ± 154.9	n.s.

Refer to Figure 15 for additional details.

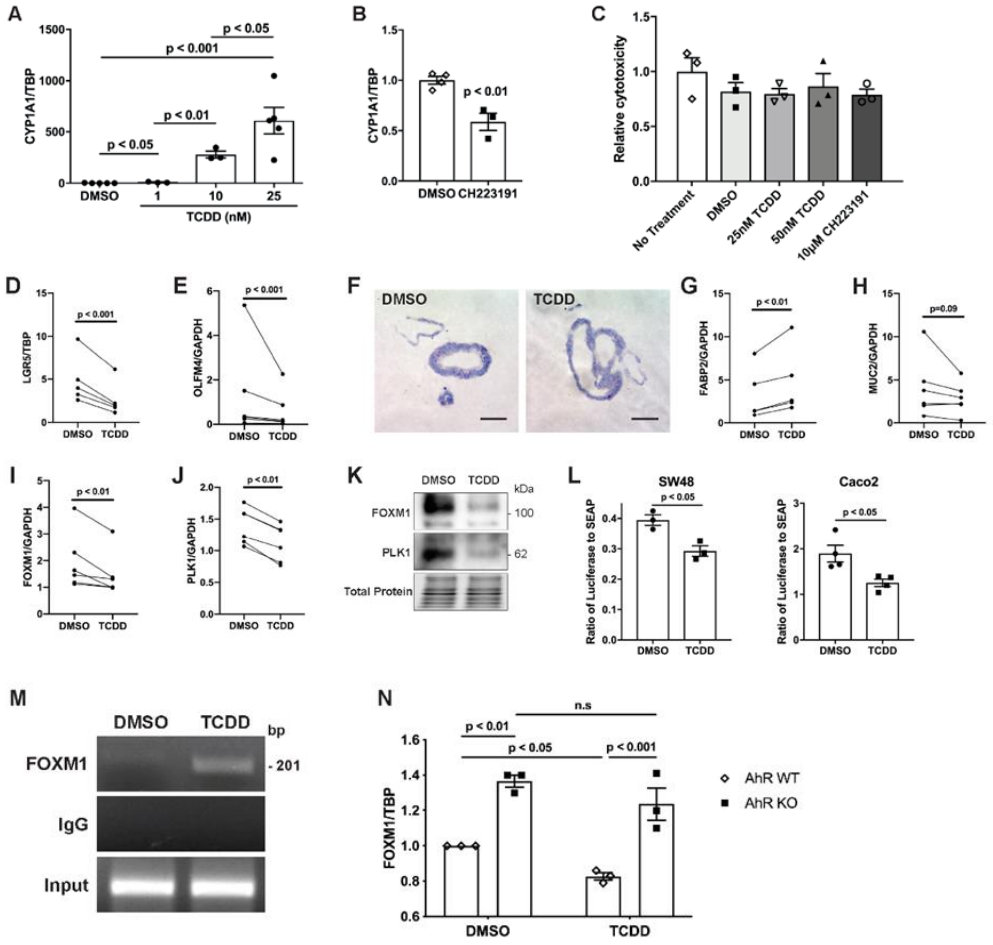

Figure 16. Assessment of AhR signaling in human colonic organoids.
(A)(B) As a measure of AhR activation status, CYP1A1 induction in human organoids treated with TCDD or CH223191 was assessed. Data represent mean ± SE, n=3. (C) TCDD or CH223191 cytotoxicity was assessed by measuring the release of lactate dehydrogenase into the culture medium. Data represent mean ± SE, n=3 per treatment. (D-E) mRNA expression of human colonic stem cell markers LGR5 and OLFM4, n=5 or 6 independent human samples. Paired student t-test. (F) Representative images of LGR5 ISH in human organoids treated with DMSO or TCDD. (G-J) mRNA expression of target genes, n=5 or 6 independent human samples. Paired student t-test. (K) Representative immunoblots for FoxM1 and PLK1 protein derived from organoids treated with DMSO or TCDD from n=6 independent samples. Total protein was used as a loading control. (L) Determination of luciferase reporter activity of human FoxM1 in SW48 and Caco2 cell lines treated with DMSO or TCDD. (M) Representative ChIP analysis of AhR binding to the FoxM1 promoter region in Caco2 cells. (N) FoxM1 mRNA expression in AhR WT and CRISPR KO Caco2 cell lines treated with DMSO or TCDD for 1 day.

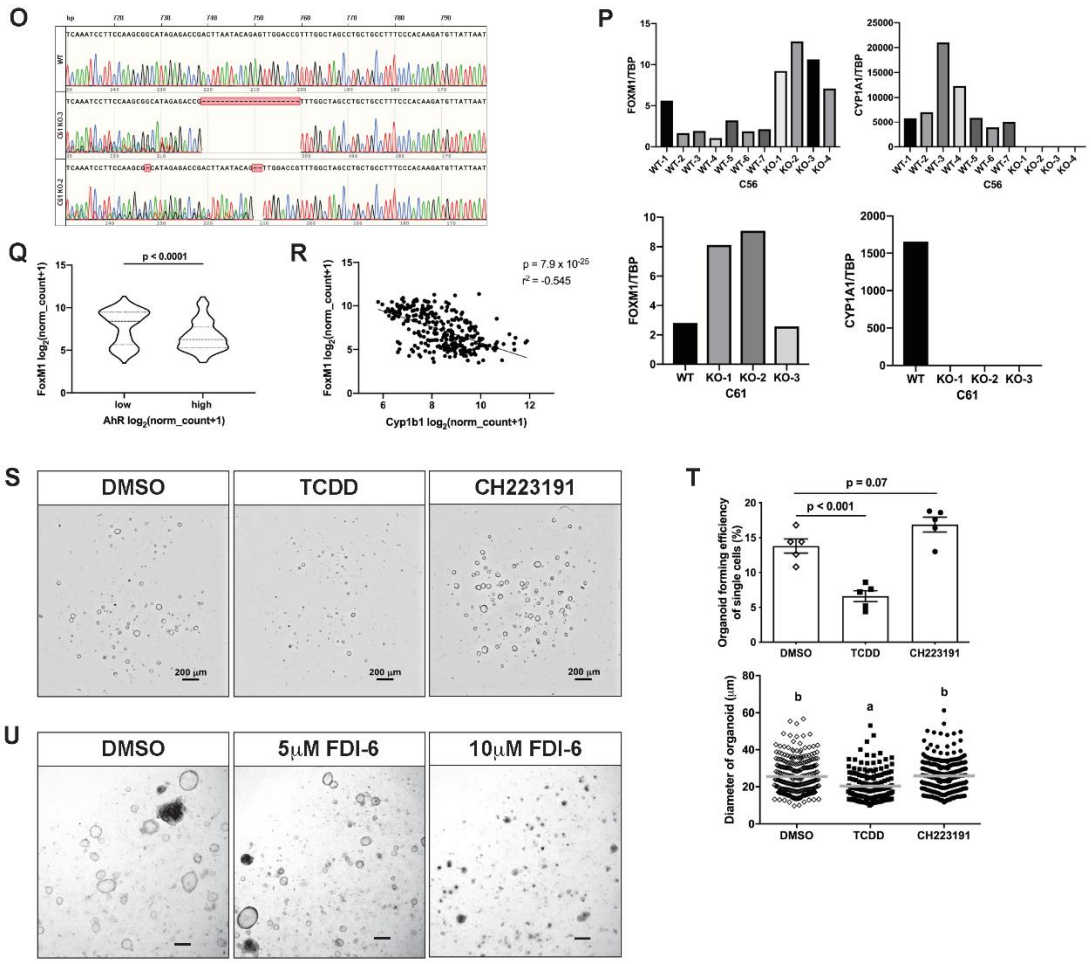

Figure 16. Continued.
(O) FOXM1 and CYP1A1 mRNA expression in different AhR WT and CRISPR KO clones treated with TCDD for 1 d. C56 and C61 designate different human subjects. (P) Validation of CRISPR KO clones was assessed by PCR amplification using primers flanking the targeted AhR exon. Subsequent sequencing revealed indels at the expected locations. (Q) The association of FoxM1 and AhR mRNA expression in human normal colon biopsies (n=304). AhR low (n=152) is defined as below its median expression; AhR high (n=152) is defined as above its median expression. (R) Correlation between FoxM1 and Cyp1b1 mRNA expression in human normal colon biopsies (n=303) analyzed by Spearman rank correlation. (S) Representative brightfield images of human colonic organoids from sorted live cells at day 6, scale bar 200 μm. (T) Human organoid forming efficiency, and organoid diameter from sorted individual cells from human colonic organoids in the presence of DMSO, TCDD and CH223191 (10 μM) for 6 d. 3 independent experiments. One-way ANOVA with Tukey's multiple comparisons. Treatments not sharing a common letter are significantly different, $p<0.05$. (U) Representative brightfield images of human colonic organoids treated with DMSO or FDI-6. FoxM1 inhibition suppressed human colonic organoid growth in a dose-dependent manner, scale bar 200 μm.

2.3.7. Suppression of FoxM1 signaling in human colonic organoids upon AhR activation

From a translational perspective, our novel findings in mouse colonic stem and progenitor cells directed us to investigate the effects of AhR status on the stemness of human colonic organoids. Since human AhR has a lower binding affinity for TCDD compared to mouse [185], we initially examined the AhR responsiveness of human colonic organoids to TCDD treatment. CYP1A1 was maximally induced by 25 nM of TCDD, while CH223191 inhibited basal AhR activity (**Fig. 16A&B**). The dosage of TCDD or CH223191 used did not cause any cytotoxicity (**Fig. 16C**), thus in complementary experiments, we used 25 nM TCDD to activate human organoid. TCDD significantly decreased expression of human colonic stem cell markers, Lgr5 and OLFM4 (**Fig. 16D&E**). Moreover, LGR5 ISH showed that TCDD treatment reduced the number of human $LGR5^+$ colonic stem cells (**Fig. 16F**). In addition, AhR activation by TCDD preferentially promoted the expression of FABP2 (**Fig. 16G**), an absorptive enterocyte marker, and slightly inhibited MUC2 expression (**Fig. 16H**), a goblet cell marker, implying that AhR activation directs colonic stem or progenitor cell differentiation toward absorptive enterocytes. Importantly, the expression of FoxM1 and PLK1 were robustly suppressed upon AhR activation, both at the mRNA and protein levels (**Fig 16I-K**). Further, human AhR was capable of binding to the FoxM1 promoter, reduced FoxM1 luciferase reporter activity (**Fig. 16L&M**), and inhibited its expression in Caco2 cell line (**Fig. 16N**). In complementary experiments, AhR KO in human colonic organoids, generated by CRISPR-Cas9, exhibited a significant increase in FoxM1 expression (**Fig. 16O&P**). In addition, we analyzed the association of FoxM1 and AhR, as well as CYP1B1 (AhR target gene) expression in normal human colon tissue, and found that

FoxM1 expression in subjects with a “high” AhR phenotype was much lower than those exhibiting “low” AhR expression (**Fig. 16Q**). In addition, FoxM1 expression was inversely correlated with CYP1B1 (**Fig. 16R**), suggesting that AhR activation leads to a reduction in FoxM1 expression in healthy subjects. Next, we interrogated the effects of AhR signaling on the organoid forming efficiency of human colonocytes. TCDD supplementation significantly suppressed organoid initiating capacity and organoid growth, while AhR inhibition by CH223191 enhanced organoid formation of human colonocytes, but had no effect on organoid growth (**Fig. 16S&T**). In a proof-of-concept experiment, FoxM1 inhibition significantly suppressed human colonic organoid growth (**Fig. 16U**). Collectively, these findings indicate that AhR signaling modulates the stemness of human colonocytes, in part by regulating the FoxM1 signaling pathway.

2.4. Discussion

In this study, we provide evidence demonstrating that loss of AhR signaling augments $Lgr5^{+}$ colonic stem cell and non-stem progenitor cell self-renewal and endows features of stemness (i.e., organoid forming capacity), at least partially by promoting FoxM1-mediated cell proliferation. Our findings indicate that AhR can specifically bind to the DRE motif in the FoxM1 promoter in vivo and in vitro and act as a transcriptional repressor of FoxM1. Furthermore, the elevated cell proliferation in colonic stem and progenitor cells due to ablation of AhR promoted tumor growth in a colitis-associated colorectal tumor model, without affecting immune response.

Previous studies have investigated the link between AhR signaling and stem cell regulation. For example, murine embryonic stem cells exhibit bidirectional regulation of

AhR and a pluripotency factor complex of OCT3/4-NANOG-SOX2 [8,186,187]. In addition, the AhR antagonist, SR-1, significantly increased the percentage of hematopoietic stem cells [168], suggesting that AhR activation suppresses stemness. Comparable results were obtained in our study using orthogonal pharmacological and genetic approaches, e.g., TCDD (AhR agonist), CH223191 (AhR antagonist) and targeted deletion of AhR in Lgr5-expressing intestinal stem cells. Our examination of the colonic epithelium revealed that AhR activation decreased the percentage of colonic stem cells both in mice and human organoids, while both AhR inhibition and stem cell targeted KO significantly increased the percentage of colonic stem cells and the number of proliferating colonic stem cells. This is noteworthy, because the life-time risk of cancer is strongly correlated with the total number of stem cell divisions [188].

Studies linking AhR signaling with cell proliferation have been widely investigated, and suggest that outcomes and mechanisms of action are highly cell context dependent. Of note, AhR activation has been reported to increase pERK1/2 level by interacting with Src in human colon cancer cell lines [189]. Interestingly, IPA upstream regulator analysis of our RNAseq data suggested that AhR modulates MAPK-dependent pathways. However, pERK1/2 levels and the activation status of key mediators associated with the EGFR-ERK1/2 axis were not altered upon AhR activation or deletion. This apparent discrepancy may result from the fact that many other pathways regulate the same ERK1/2-dependent downstream targets, thereby affecting upstream regulator predictions. It is also possible that AhR modulated pERK1/2 within a narrow time frame.

We show that AhR KO promoted intestinal stem cell proliferation and increased the proliferative zone in colonic crypts in part due to the upregulation of FoxM1-dependent signaling. We also demonstrated that AhR KO dramatically promoted cell proliferation in the transit amplifying region of the crypt following DSS injury. This is noteworthy because the accumulation of intestinal progenitor cells has been shown to drive tumorigenesis [190]. Thus, it is possible that AhR KO promotes the likelihood that progenitor cells acquire and fix DNA lesions in response to mutagens and inflammation. In addition, further analysis revealed that AhR KO decreased the crypt cell population in G1 phase, while it increased the percentage of cells in S and G2-M phases, which is in concordance with the elevated expression of FoxM1. Intriguingly, 3,3'-diindolylmethane, an AhR agonist [191], was found to effectively downregulate FoxM1 in various breast cancer cell lines and inhibit breast cancer cell growth [192]. In addition, FoxM1 upregulation was detected in various human cancer types, and increased FoxM1 expression in tumors correlated with poor prognosis [193]. Collectively, these findings are consistent with pharmaceutical interests to target FoxM1 in the treatment of pre-malignant lesions. In addition, it is possible that other signaling pathways may play a role in AhR KO mediated phenotypes in our models, which warrants additional characterization in future studies.

Globally AhR KO mice spontaneously developed cecal tumors, and the expression levels of β-catenin and c-myc were upregulated in AhR KO mice [131]. AhR was shown to bind to the promoter of c-myc and Znrf3 and suppressed c-myc expression in human tumor cells [9] and increased Znrf3 expression [194], which is a negative regulator of Wnt frizzled receptor. Interestingly, in a recent study using an intestinal AhR deletion mouse

model, a hyperproliferating stem cell phenotype was linked to dysregulated Wnt/β-catenin signaling [194]. In contrast, our global transcriptome analysis of both stem and progenitor cells did not detect altered expression of β-catenin, c-myc, Znrf3 and Wnt downstream targets, which was reported in a previous study [160]. Even though reduction of Lgr5 expression was detected upon AhR activation in mouse and human organoids, it is likely attributed to a decreased percentage of colonic stem cells, as opposed to a reduction in Wnt signaling.

Our study has shown that intestinal specific AhR KO significantly promoted tumor incidence and growth at least partly by upregulating FoxM1 signaling compared with WT mice in the AOM/DSS model. Interestingly, Rosa26 FoxM1b mice also exhibited an increase in the number and size of AOM-DSS induced colorectal tumors, compared with WT controls [181]. Although inflammatory status plays a pivotal role in modulating tumor growth in this model, e.g., IL22 effectively enhances DNA damage response against AOM exposure, reducing colon tumorigenesis in the AOM/DSS model [143], we did not detect an apparent difference in body weight, colon length, gut permeability, clinical pathology scores or proinflammatory cytokine expression, e.g., IL-1β, IL-6, IL-17α and IL-22, between WT and AhR KO mice, which is in contrast to previous reports [160,163,195]. This discrepancy may be explained by differences in the mouse models. Our study utilized intestinal specific AhR KO mice, while global AhR KO or AhR ligand supplementation were used in other studies. It is clear that AhR signaling plays a pivotal role in determining immune cell fate decision [152,196] . Hence, the use of either a global AhR KO mouse model or AhR ligand supplementation complicates the mechanistic interpretation of outcomes related to AhR mediated signaling in colon

cancer. Our results using knockout strategies targeting Lgr5^{+} CSCs and/or the intestinal epithelium demonstrate a protective role for AhR in mediating stem and progenitor cell homeostatic responses, including their capacity to initiate tumors.

To date, no loss of function-related AhR mutations have been reported in humans. Although a single nucleotide polymorphism rs1077773 risk loci has been linked to inflammatory bowel diseases (IBDs) [197], recent studies suggest that AhR ligand availability and its expression level contribute to chronic disease risk. Importantly, reduced AhR activation and production of AhR ligands were observed in patients with IBDs, obesity, Type 2 diabetes and high blood pressure [80-82]. The defect in AhR agonist production has been linked to the impaired capacity of gut microbiota to metabolize tryptophan into AhR agonists in mice and humans [81,82]. The regulation of AhR at the level of ligand availability is consistent with preclinical studies indicating that; (i) microbiota from caspase recruitment domain family member 9 (CARD9) knockout mice could not metabolize tryptophan into AhR ligands, resulting in defective AhR activation [81], and (ii) the constitutive overexpression of Cyp1a1 in mice depleted the reservoir of natural AhR ligands, subsequently increasing susceptibility to enteric infection [86].

In summary, we investigated the consequences of conditionally ablating AhR in the highly relevant Lgr5^{+} stem cell population to assess effects on stem cell plasticity in the colon. Our novel findings suggest that AhR plays a crucial role in colon cancer risk by modulating colonic stem/progenitor cell proliferation via regulation of FoxM1. Further experiments are warranted to determine whether AhR-FoxM1 can serve as a new potential target for cancer chemoprevention. From a translational perspective, AhR may be a critical dietary/gut microbial target for modulating stem cell biology in the gut

epithelium. This is consistent with studies showing that AhR agonists inhibit colon tumorigenesis[131,160,194].

3. LOSS OF ARYL HYDROCARBON RECEPTOR PROMOTES COLON TUMORIGENESIS IN $APC^{S580/+}$; $KRAS^{G12D/+}$ MICE

3.1. Introduction

Colorectal cancer (CRC) is the second leading cause of cancer death in men and women combined, affecting 6% of the U.S. population and followed by the progressive accumulation of several events, including chromosomal instability, microsatellite instability, and CpG island methylator phenotype. This results in transformation of normal epithelial cells to adenocarcinoma, of which, ~75% of CRC occur sporadically, and only 5-10% of patients results from hereditary genetic mutations[198]. Generally, in CRC, genetic alterations involve the inactivation of tumor suppressor genes and DNA mismatch repair genes, and/or activation of oncogenes. It is estimated 2~8 driver gene mutations are required to promote CRC development[199,200], even though the median number of nonsynonymous mutations in sporadic CRC is 66 mutations per tumor[201], in which Adenomatous polyposis coli (Apc) serves as an initiating event, accompanied by the mutations of other common genes, such as Kirsten RAS (Kras), Sma- and Mad-related protein 4 (SMAD4) and TP53.

Apc is a tumor suppressor gene encoding a 312 kDa protein that plays an important role in regulating the Wnt signaling pathway, cell migration and adhesion, transcriptional activation, apoptosis and DNA repair[202,203]. The multiple functions of Apc are achieved by binding to various protein partners, including β-catenin, axin, CtBP, Asefs, IQGAP1, EB1 and microtubes[204]. The most characterized consequence of Apc inactivation in CRC is assumed to be aberrant activation of the Wnt signaling pathway. In the absent

of Wnt ligands, the primary Wnt signaling effector β-catenin is sequestrated and targeted for proteasomal degradation in the cytosol by a multiprotein destruction complex, which contains the scaffold component axin, Apc, and GSK3β and CK1α/ϵ kinases. Inactivation of Apc, including mutations, deletions, and loss of heterozygotes, leads to an accumulation of β-catenin in the nucleus. Nucleus β-catenin then interacts with Tcf4 (transcription factor) to mediate the transcription of target genes, such as c-myc, cyclin D1, Ascl2 and EphB[205-208]. In human CRC, Apc point mutations occur primarily in a mutation cluster region (MCR, codons 1286~1513), generating premature stop codons or frameshift, resulting in the deletion of the C-terminal region of the Apc protein. Approximately 80% of sporadic CRC individuals harbor at least one inactivating Apc mutation[209], which serves as one of the earliest events driving normal-to-adenoma transition.

Kras is another common mutated driver gene involved in the progression of benign tumors (adenomas) or hyperplastic aberrant crypt focus (ACF). Mutations of this gene occur in approximately 30 to 50% of CRC and mutant Kras is also associated with poor prognosis and CRC metastasis[210,211]. This proto-oncogene encodes a small 21-kD guanosine triphosphatase (GTPase), serving as an effector mediating signal transduction from ligand-bound EGFR to the nucleus. When allosterically activated, Kras recruits downstream effectors typically usually containing a Ras-binding domain (RBD) or Ras association domain, ultimately promoting RACGEF-RAC1, RALGEFs-RAL, PI3K-AKT-mTOR and RAF-MEK-ERK dependent signaling networks[212]. Approximately 90% of Kras mutations occur at codons 12 or 13, rendering Kras

persistently GTP-bound and constitutively active regardless of extracellular stimuli. As a consequence, it is resistant to anti-EGFP antibody therapy.

In addition to these well-defined driver genes of CRC, the contribution of other genes capable of modifying the initiation and/or progression of cancer remains largely unknown. From this perspective, the aryl hydrocarbon receptor (AhR) is increasingly recognized as an important regulator of CRC[131-133]. AhR is a ligand activated bHLH transcription factor, capable of promiscuously recognizing diverse small molecules ranging from environmental pollutants, dietary and gut microbiota derived tryptophan metabolites, thus acting as an environmental sensor that integrates exogenous environmental stimuli and host response[213]. In the absence of ligands, AhR remains bound to several chaperon proteins in the cytoplasm including heat shock proteins 90, p23 and immunophilin related protein XAP2. Upon ligand binding, cytosolic AhR translocates to the nucleus and forms a heterodimer with the AhR nuclear translocator (ARNT) protein, which then interacts with AhR response elements (AREs) with the core sequence 5'-TNGCGTG-3' or 5'-CACGCNA-3' on the promoters of AhR target genes[6]. Our lab and others have previously showed that AhR KO promotes colitis-associated colon cancer[132]. However, the effect of AhR deletion targeted to the epithelium in a genetically susceptible colon tumorigenesis model has not previously been investigated. Therefore, we generated inducible and colon epithelial cell targeted ApcS580/+; KrasG12D/+ with or without AhRf/f compound mutant mice by crossing with CDX2P-CreERT2 mice. We found that additional AhR KO could potentiate Wnt signaling and promote colon tumorigenesis in this genetic model. Our findings provide further insights into targeting AhR as a promising strategy of CRC chemoprevention and/or treatment.

3.2. Materials and methods

3.2.1. Mice

Animals were housed under conventional conditions, adhering to the guidelines approved by the Institutional Animal Care and Use Committee at Texas A&M University. Lgr5-EGFP-IRES-Cre^{ERT2}, CDX2P-Cre^{ERT2}, AhR$^{f/f}$, Kras$^{LSL\ G12D/+}$, and Apc$^{S580/+}$ mouse strains have all been previously described. Specifically, Lgr5-EGFP-IRES-Cre^{ERT2} mice express EGFP and Cre^{ERT2} in crypt base columnar cells in the intestine under control of the *Lgr5* promoter[106]. CDX2P-CreERT2 mice express CreERT2 throughout the entire intestinal epithelium under the control of the CDX2 promoter[169,170]. AhR$^{f/f}$ mice carry loxP sites bordering exon 2 of the AhR gene, with recombination resulting in generation of a premature stop codon at codon 29[18]. Kras$^{LSL\ G12D/+}$ mice carry a latent point mutant *Kras* allele and Cre mediated recombination results in the expression of constitutively active KRas[214]. In addition, Apc$^{S580/+}$ mice carry loxP sites bordering exon 14 of the *Apc* gene, thus recombination results in an inactivating frame shift mutation at codon 580[215]. Mice were intraperitoneally injected with 2.5 mg of tamoxifen (Sigma, T5648) dissolved in corn oil (25 mg/ml) once a day for four consecutive days. Mice were maintained on an AIN-76A semi-purified diet (Research Diets, D12450B), fed *ad libitum* and housed on a 12 h light-dark cycle. For all experiments, littermate controls were cohoused with the knockout mice, unless specifically indicated.

For genotyping analyses, DNA was extracted from tails using DNeasy Blood and Tissue Kit (Qiagen, 69506). PCR was subsequently performed using the following primer sets: AhR (5'-CAGTGGGAATAAGGCAAGAGTGA-3' and 5'-GGTACAAGTGCACATGCCTGC-3'), CDX2P-Cre (5'-

GGACTTGAGCAGCTAGCTGTGCAACTT-3’ and 5’-TGTCTCGTGCCTGGAATGACCTT-3’), Lgr5-EGFP (5’-CACTGCATTCTAGTTGTGG-3’ and 5’- CGGTGCCCGCAGCGAG-3’), Kras-G12D (5’-TGTCTTTCCCCAGCACAGT-3’, 5’-CTGCATAGTACGCTATACCCTGT-3’, and 5’-GCAGGTCGAGGGACCTAATA-3’), and Apc (5’- GTTCTGTATCATGGAAAGATAGGTGGTC-3' and 5’-CACTCAAAACGCTTTTGAGGGTTGATTC-3').

3.2.2. Crypt and single cell isolation and cell sorting

Colons were removed, washed with cold PBS without calcium and magnesium (PBS-/-), everted on a disposable mouse gavage needle (Instech Laboratories), and incubated in 15 mM EDTA in PBS-/- at 37°C for 35 min as previously described[174]. Subsequently, following transfer to chilled PBS-/-, crypts were mechanically separated from the connective tissue by rigorous vortexing. Crypts were embedded in Matrigel and overlaid with crypt culture media as previously described[1]. For intestinal stem cell (ISC) isolation, crypt suspensions were dissociated to individual cells with 0.25% Trypsin-EDTA containing 200 U/ml DNase. Cell suspensions were then filtered through a 40-µm mesh and GFP-expressing cells were collected using a MoFlo Astrios Cell Sorter (Beckman Coulter) or Bio-Rad S3e Cell Sorter. Dead cells were excluded by staining with propidium iodide or 7-AAD. Sorted cells were collected in RNA lysis buffer (for RNA isolation) or crypt culture medium (for culturing).

3.2.3. Organoid culture

Isolated ISCs (GFF^{high}), progenitor cells (GFP^{low}) or bulk colonocytes were centrifuged for 3 min at 500xg, resuspended in the appropriate volume of crypt culture medium (100-250 cells μl^{-1}), then seeded (500 cells for ISC or progenitor cells, 1500 cells for bulk colonocytes) onto 30 µl Matrigel containing 1 µM Jagged-1 (Ana-Spec) in a flat bottom 24-well plate. Following Matrigel polymerization, cells were overlaid with 300 µl of crypt culture medium containing Advanced DMEM/F12 (Gibco) supplemented with 2 mM glutamax, penicillin/streptomycin, and 10 mM HEPES (ADF+), 50 ng ml^{-1} EGF (Life Technologies), 100 ng ml^{-1} Noggin (Peprotech), 10% R-spondin conditioned medium, 1 µM N-acetyl-l-cysteine (Sigma), 1X N2 (Life Technologies), 1X B27 (Life Technologies) and 50% Wnt conditioned medium as described previously[175] supplemented with 10 µM Y-27632 (Sigma Y0503), 1 µM Jagged-1 and 2.5 µM CHIR99021 (Stemgent, 04-0004). Y-27632, Jagged-1 and CHIR99021 were withdrawn from crypt culture medium 2 d after plating. The crypt media was changed every 2 d. Organoids were quantified on day 5 of culture, unless otherwise specified. For AhR-related treatments, DMSO or TCDD (10 nM) were added to cultures for 3 d. In some experiments, colonic organoids were cultured in 50% WRN conditioned medium derived from L-WRN cells (CRL-3276), and 10% FBS (WRN medium)[176]. To measure organoid viability, CellTiter-Blue reagent (Promega) was used according to manufacturer's instructions. Fluorescence was measured on a CLARIOstar microplate reader.

3.2.4. Gene combination characterization

For assessment of AhR recombination in vitro, mouse organoids derived from sorted colonic stem cells were incubated with 10nM TCDD for 1 day. Taqman assays were performed to examine the expression of AhR exon 2, and Cyp1a1 induction, a downstream readout of activated AhR. Recombination of Apc^{S580} and $Kras^{LSL\ G12D}$ was determined genetically by modifying a previously described multiplex PCR assay[216-218]. PCR was performed using Hot-Start-Taq Blue Mastermix (Denville Scientific, CB4040-8) according to manufacturer's instructions for 35 cycles using the Apc and Kras primer sets: Apc (5'-GTTCTGTATCATGGAAAGATAGGTGGTC-3′, 5'-CACTCAAAACGCTTTTGAGGGTTGATTC -3′, and 5'-GAGTACGGGGTCTCTGTCTCAGTGAA-3'), and Kras (5'-GTCTTTCCCCAGCACAGTGC-3', 5'- GCAGCGTTACCTCTATCGTA-3', and 5'-AGCTAGCCACCATGGCTTGAGTAAGTCTGCA-3′). The details are described in **Appendix B** and **C**.

3.2.5. Secondary murine organoid assay

For secondary organoid assays, organoids were pretreated DMSO or 10nM TCDD for 2 days and then were dissociated for 8 minutes in 0.25% Trypsin-EDTA at 37°C. Cell suspensions were then filtered through a 20-µm mesh, centrifuged for 3 minutes at 500*g, and then resuspended in cold ADF+ medium. Live cell density was counted. 2500 live cells were seeded into 30 µl Matrigel in a flat bottom 24-well plate. Following Matrigel polymerization, cells were overlaid with 300 µl of crypt culture medium supplemented with 10 µM Y-27632 (Sigma Y0503), 1 µM Jagged-1 and 2.5 µM

CHIR99021 (Stemgent, 04-0004). Y-27632, Jagged-1 and CHIR99021 were withdrawn from crypt culture medium 2 d after plating. The crypt media was changed every 2 d. Organoids were quantified on day 5 of culture, unless otherwise specified.

3.2.6. *Organoid supernatant transfer experiment*

HACKG colonic organoids were incubated with crypt culture medium (WREN) containing ADF+, EGF, LDN, R-Spondin, N2, B27, N-acetyl-l-cysteine, and Wnt conditioned medium or crypt culture medium without Wnt3a, R-Spondin1, and EGF (N) containing ADF+, LDN, N2, B27 and N-acetyl-l-cysteine for 1 day at 37°C. The concentration of each component was annotated above. The supernatants were then transferred to culture passaged ACKG organoids. Fresh N medium was also used as a control. Organoids were imaged on day 4 of culture.

3.2.7. Tumor study

At 8 to 12 weeks of age, male and female mice were administrated 100 mg/kg tamoxifen daily for 4 consecutive days. Mice were terminated 20 weeks post last tamoxifen injection. If the mice exhibited severely moribund or body weight decreased by 20% from highest body weight record during study, the mice were pre-terminated. EdU was injected 2 h prior to termination to examine cell proliferation. On the day of euthanasia, the cecum and colon were harvested, colon lesions were measured, mapped, excised, routinely processed and paraffin embedded. Hematoxylin and eosin (H&E) stained sections were examined using light microscopy by a board-certified

veterinary pathologist in a blinded manner. Histological lesions were categorized by predominant change. Tumor volume was calculated as length x width.

3.2.8. RNA isolation and quantitative real-time PCR

RNA from sorted cells or organoids was isolated using the Quick-RNA MicroPrep Kit (Zymo, R1050) and further processed using a DNA removal kit (DNA Free, Ambion, AM1906). RNA integrity was assessed on a Bioanalyzer 2100 (Agilent Technologies), quantified by Nanodrop and stored at -80°C. Real-time PCR was performed on a QuantStudio 3 System (Applied Biosystems) using TaqMan Universal PCR Master Mix (Applied Biosystems). Specific primer/probe mix for each gene was obtained from Applied Biosystems: AhR (Mm00478930_m1), Lgr5 (Mm00438890_m1), Cyp1a1 (Mm00487218_m1), Axin2 (Mm00443610_m1), FoxM1(Mm00514924_m1), Ccnd1 (Mm00432359_m1), and GAPDH (Mm99999915_g1).

3.2.9. Immunohistochemistry

In order to assess cell proliferation in the colon, mice were intraperitoneally injected with EdU 2 h prior to termination as previously described[177]. Colonic cell proliferation was measured using the Click-IT EdU kit (Life Technologies, C10340). Antigen retrieval was performed by sub-boiling in 10 mmol/L sodium citrate (pH 6.0) for 20 min. Antibodies used were: mouse polyclonal antibody to β-catenin (BD, 610153) followed by Alexa-568 donkey anti-mouse secondary antibody (Life Technologies, A-10037), FITC conjugated mouse anti-E-catenin (BD, 612130). Prolong Gold antifade with DAPI (Life Technologies, P36935) was used to coverslip the slides. Images of

colonic crypts were captured on a Leica DMi8 TCS SPE spectral confocal microscope. Images were processed using ImageJ software (ImageJ 1.51n version). For enumeration of immunohistochemical staining, about 40 crypts were assessed from at least three animals per treatment.

3.2.10. Cell cycle analysis

Colonic organoids were incubated with 10 μM EdU for 1 h and harvested from Matrigel, and a single cell suspension was obtained by trypsinization. Subsequently, the Click-IT EdU kit was used to determine the S-phase cell population, and nuclei were stained by FxCycle Violet (Life Technologies) according to the manufacturer's instructions. Cell cycle profiling was assessed using a FlowSight™ (Millipore) Imaging Flow Cytometer.

3.2.11. Western blotting

Organoids or colon tumor tissue were lysed in lysis buffer (50 mM Tris-HCl pH 7.2, 250 mM sucrose, 2 mM EDTA pH 7.6, 1 mM EGTA pH 7.5, 1% Triton X-100, 10 mM β-mercaptoethanol) supplemented with protease inhibitor cocktail (Sigma) and 1x phosphatase inhibitor (Life Technologies). Lysates were subjected to standard SDS-PAGE and Western blotting procedures using primary antibodies against β-catenin (1:2000, BD 610154), non-phospho β-catenin (1:2000, 8814S, Cell Signaling Technology), pERK1/2 (1:1000, 4370S, Cell Signaling Technology), and ERK1/2 (1:1000, ,9107S, Cell Signaling Technology). Secondary anti-mouse or rabbit conjugated to horseradish peroxidase or secondary StarBright Blue 700 goat anti-

mouse IgG (Bio-Rad, #12004159) were used to detect primary antibodies. Signal was detected using ECL substrate (Bio-Rad), imaged with the Bio-Rad Chemidoc System and protein bands quantified using Image Lab 6.0 (Bio-Rad).

3.2.12. Statistics

Two-tailed Student's t-tests were used to assess statistical significance of the differences between means across experimental groups. Paired student t-tests were used to examine the statistical significance of the differences between treatments within genotypes in organoids, unless otherwise specified. One-way ANOVA with Tukey's multiple comparisons test were used to compare more than 2 groups. Log-rank (Mantel-Cox) test was used for canparison of survival curves. All data are presented as mean ± SEM (standard error), and all analyses were conducted using Prism 8 statistical software (GraphPad Software, Inc.).

3.3. Results

3.3.1. Loss of AhR promotes the functionality of colonic stem and progenitor cells.

Our previous study showed that AhR signaling regulates the functionality of normal colonic stem and progenitor cells, however, it remains to determine if the effect can be phenocopied in colonic stem and progenitor cells harboring $Apc^{S580/+}$ and $Kras^{G12D/+}$ mutations. To study the role of AhR on a genetically induced CRC genetic background, we generated compound mutant mice carrying one floxed Apc allele ($Apc^{S580/+}$, abbreviated as A) and a floxed, latently oncogenic allele of Kras ($Kras^{LSL-G12D/+}$, abbreviated as K), with/without two alleles of AhR ($AhR^{f/f}$, abbreviated as H). By

crossing with CDX2P-Cre^{ERT2} (abbreviated as C) mice and upon injection of tamoxifen, the entire distal ileum, cecum and colonic epithelium becomes tumorigenic [216]. We found that additional AhR deletion promoted the organoid forming efficiency and growth of ACK unsorted (bulk) colonocytes (**Fig. 17A-C**). Since crypt stem cells are the cells-of-origin of intestinal cancer [122], we further characterized the effect of AhR KO on the ACK colonic stem and progenitor cell populations. For this purpose, Lgr5-GFP-IRES-Cre^{ERT2} (abbreviated as G) reporter mice were crossed with our compound mutant mice. Flow cytometry was used to sort colonic stem cells (defined as GFP^{hi}) and progenitor cells (defined as GFP^{low}) based on GFP fluorescence intensity. Interestingly, both ACKG colonic stem and progenitor cells exhibited enhanced stemness as compared with normal counterparts (**Fig. 17D-I**). In line with the results from sorted bulk colonocytes, AhR KO promoted organoid forming efficiency and organoid size of both sorted ACKG colonic stem and progenitor cells (**Fig. 17D-I**). We also validated the genetic mutations from organoids derived from sorted colonic stem cells derived from compound mutant mice (**Fig. 17J-M**).

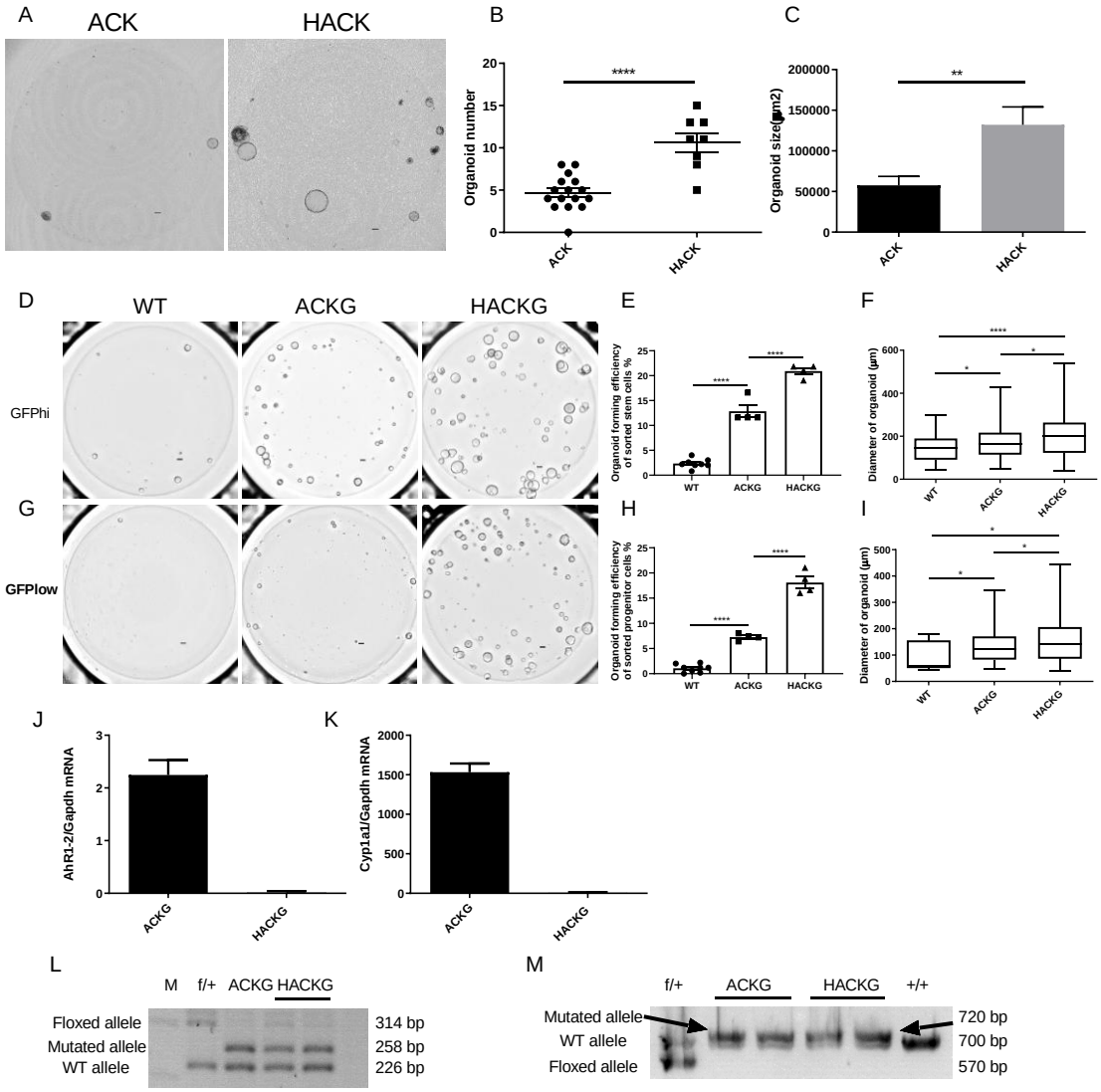

Figure 17. AhR KO promotes organoid growth derived from sorted colonic stem/progenitor cells expressing mutant Apc and Kras.

(A) Representative brightfield images of organoids generated from individual bulk colonocytes isolated from tamoxifen treated ACK mice ($Apc^{S580/+}$; $Kras^{G12D/+}$; CDX2P-Cre^{ERT2}) and HACK mice ($AhR^{f/f}$; $Apc^{S580/+}$; $Kras^{G12D/+}$; CDX2P-Cre^{ERT2}). Scale bar 200 µm. (B)(C) Quantification of organoid number and size at day 5 after plating, n=8 or 16 biological replicates per group from one or two mice, respectively. (D) Representative brightfield images of organoids generated from sorted GFPhi stem cells isolated from tamoxifen treated ACKG mice ($Apc^{S580/+}$; $Kras^{G12D/+}$; CDX2P-Cre^{ERT2}; Lgr5-GFP- Cre^{ERT2}) and HACKG mice ($AhR^{f/f}$; $Apc^{S580/+}$; $Kras^{G12D/+}$; CDX2P-Cre^{ERT2}; Lgr5-GFP-Cre^{ERT2}). Scale bar 200 µm. (E)(F) Quantification of organoid forming efficiency and size at day 5 after plating, n=4 or 8 biological replicates per group from one or two mice, 3 independent experiments. (G) Representative brightfield images of organoids generated from sorted GFPlow progenitor cells isolated from tamoxifen treated ACKG mice and HACKG mice. Scale bar 200 µm. (H)(I) Quantification of organoid forming efficiency and size at day 5 after plating, n=4 or 8 biological replicates per group from one or two mice, 3 independent experiments. (J-K) Expression of AhR and Cyp1a1 in organoids derived from sorted stem cells in ACKG and HACKG mice, n=2 per group. Data are presented as mean ± SEM. (L-M) PCR genotyping analysis of Apc (L) and Kras (M) in organoids derived from sorted stem cells in ACKG and HACKG mice. f: floxed allele; +: WT allele.

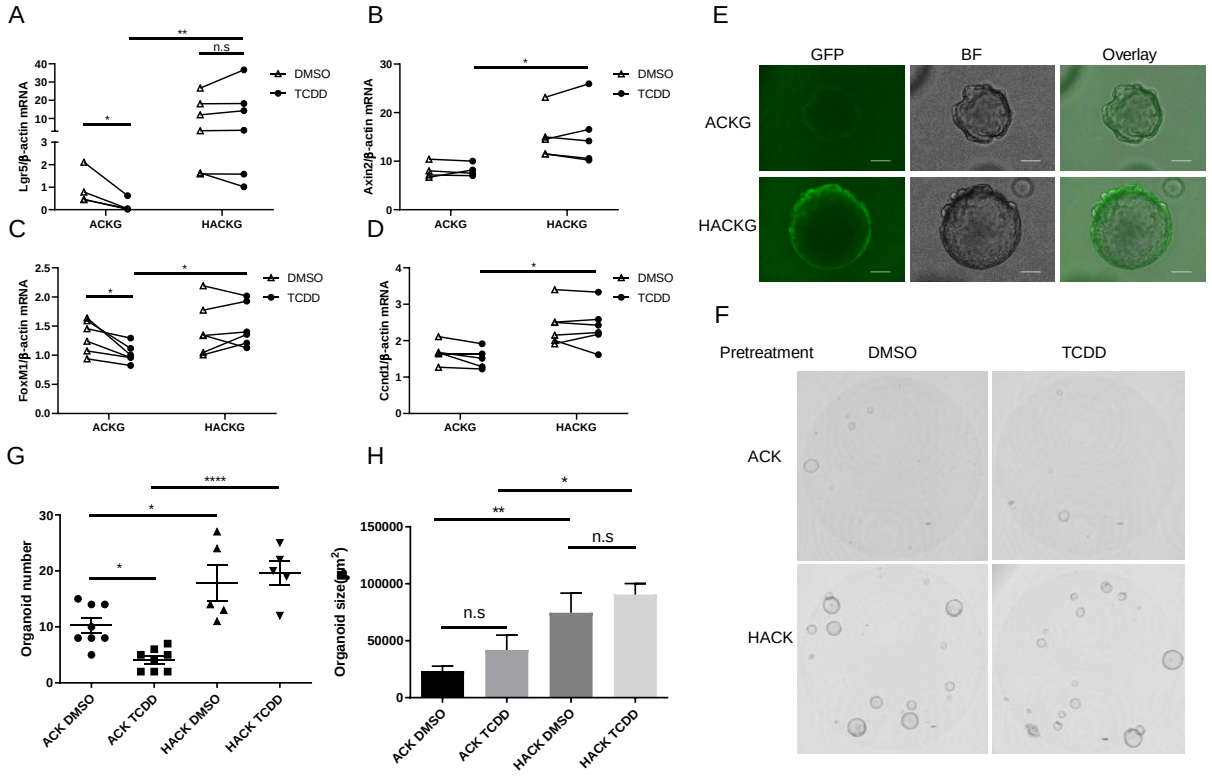

Figure 18. Deletion of AhR promotes colonic stem cell expansion.
(A-B) mRNA expression of mouse colonic stem cell markers Lgr5 and Axin2 following exposure to 10 nM TCDD (AhR agonist) or DMSO (control), n=5 - 6 independent organoids from 5~6 mice. (C-D) mRNA expression of FoxM1 and CCND1, n=5 - 6 independent organoids, see above for details. (E) Representative images of GFP+ organoids. Scale bar 50 μm. (F) Secondary organoid growth from ACK and HACK organoids pre-treated with DMSO or 10 nM AhR agonist TCDD. Scale bar 200 μm. (G-H) Quantification of secondary organoid number and size at day 5 after plating. n=5 or 8 biological replicates per group from one or two mice.

3.3.2. AhR signaling modulates the percentage of colonic stem cells.

Since deletion of AhR enhanced the growth of organoids derived from Apc and Kras mutant mice, we hypothesized that AhR signaling affects the percentage of colonic stem cells harboring the AK background. qPCR analysis of colonic stem cell markers, Lgr5 and Axin2, revealed that AhR KO increased the expression of Lgr5 and Axin2, and AhR activation by TCDD decreased the expression of Lgr5 (**Fig. 18A&B**). In addition, consistent with our previous findings, the expression of FoxM1, a pivotal regulator of cell proliferation, was decreased upon AhR activation (**Fig. 18C**), and AhR KO increased CCND1 expression (**Fig. 18D**). In addition, we consistently observed that AhR KO organoids expressed an enhanced GFP signal (**Fig. 18E**). Since GFP serves as a proxy of colonic stem cells, this indicates that AhR KO promoted the percentage of colonic stem cells. Moreover, we found that TCDD pretreatment decreased secondary organoid forming efficiency in the AK group, but not in the HAK group, compared to DMSO pretreatment (**Fig. 18F&G**). In addition, TCDD pretreatment had no effect on organoid size (**Fig. 18H**), suggesting that AhR activation effect was reversible. Collectively, AhR activation decreased the percentage of colonic stem cells carrying AK mutations, while AhR KO had the opposite effect.

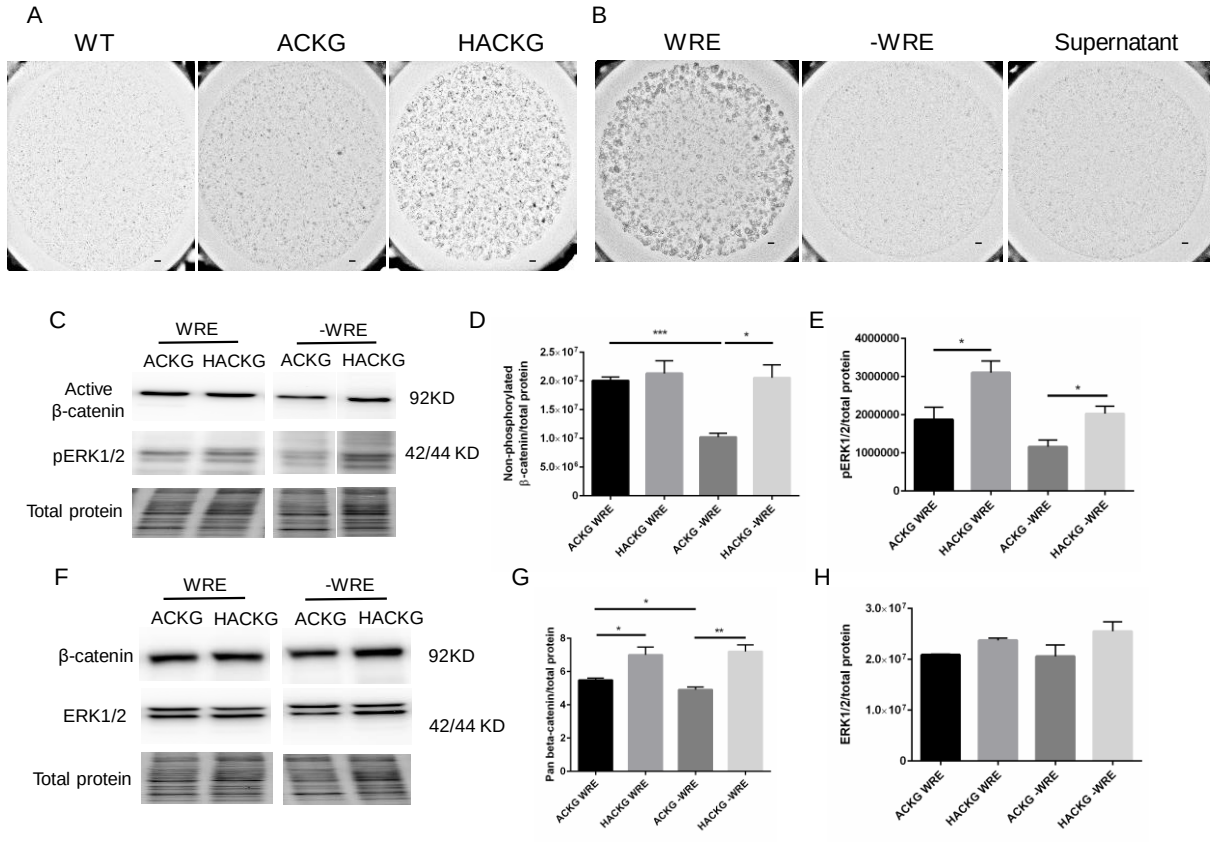

Figure 19. AhR loss enables compound mutant Apc and Kras organoids to grow independent of stem cell niche-derived factors.
(A) Representative brightfield images of organoids with indicated genotypes grown 4 days in medium without Wnt3a, R-spondin1, and EGF (-WRE). Scale bar 200 μm. (B) Representative brightfield images of ACKG organoids grown 4 days in the indicated medium. Scale bar 200 μm. (C-E) Immunoblot analysis for non-phosphorylated (active) β-catenin and pERK1/2 protein in organoids, n=3 per group. (F-H) Immunoblot analysis for total β-catenin and ERK1/2 protein in organoids, n=3 per group.

3.3.3. AhR deficiency enables compound mutant Apc and Kras organoids to maintain viability independent of stem cell niche growth factors.

Since Apc is a member of the core destruction complex of Wnt/β-catenin signaling, and oncogenic $Kras^{G12D}$ is constitutively activated, we assessed whether ACKG organoids could grow independently of exogenous Wnt3a, R-spondin 1 and EGF (WRE). By simply removing one or more of these niche factors, it is possible to determine whether intestinal epithelial cells and their growth dynamics are dependent on essential microenvironmental signals[219]. Interestingly, WT and ACKG organoids were not viable without WRE supplementation, while HACKG organoids exhibited normal growth independent of WRE (**Fig. 19A**). We hypothesized that HACKG organoids may condition the media by producing soluble WRE growth factors in order to sustain their growth. To this end, we performed a conditioned culture medium transfer experiment. Although ACKG organoids exhibited normal growth in whole medium (WRE), neither -WRE medium nor -WRE supernatant medium derived from HACKG organoids were capable of maintaining ACKG organoids, ruling out the contribution of a paracrine effect in HACKG organoids (**Fig. 19B**). Next, we assessed β-catenin and pERK1/2 levels in organoids with and without WRE after 2 days in culture. Consistent with the impact of AhR deletion on organoid growth, withdrawal of WRE decreased non-phosphorylated β-catenin (active β-catenin) and pERK1/2 levels in the ACKG group, while HACKG organoids were still able to maintain the activation status of β-catenin and pERK1/2 to a high level (**Fig. 19C-G**). Total ERK1/2 was not affect by WRE supplementation in the experimental groups (**Fig. 19H**). These data indicate that AhR

loss enables AK ($Apc^{S580/+}$; $Kras^{G12D/+}$) organoids to grow independently of stem cell niche-derived factors.

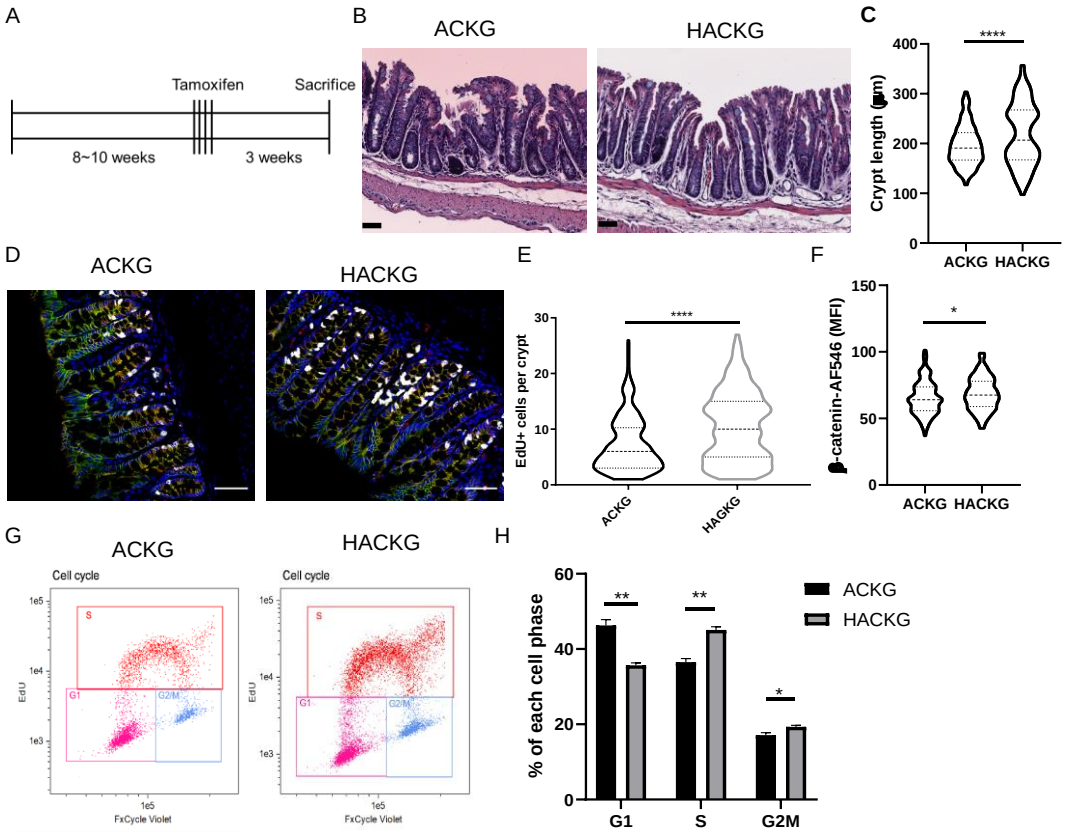

Figure 20. Effect of AhR deficiency on colonic crypt-related phenotypes.
(A) Schematic regimen for 3-week study examining cell proliferation. (B) H&E staining of representative colon sections from ACKG and HACKG mice. Scale bar, 50 μm. (C) Quantification of colon crypt length in ACKG and HACKG mice, n=4 mice per group. Asterisks indicate P<0.05 between groups. (D) Representative images of cell proliferation marked by EdU+ in the distal colon of ACKG and HACKG mice. Blue - DAPI, Green - E-cadherin, Red - β-catenin, and White - EdU. Scale bar 50 μm. (E) Quantification of EdU+ cells per crypt (F) and mean fluorescent intensity (MFI) of β-catenin per crypt, n=4 mice per group. (G-H) Cell cycle analysis between ACKG and HACKG organoids. n=3 per group.

3.3.4. AhR deletion promotes cell proliferation in vivo.

Since AhR KO potentiates Wnt and pERK1/2 signaling in organoids, we sought to determine whether AhR KO modulates cell proliferation in vivo. For this purpose, our compound mutant mice were sacrificed 3 weeks after tamoxifen administration (**Fig. 20A**). Strikingly, HACKG mice developed much longer colonic crypts (**Fig. 20B&C**). In addition, cell proliferation (marked by EdU+ cells) and β-catenin levels were elevated following the deletion of AhR (**Fig. 20D-F**). To further determine how AhR status affected cell cycle phases, ACKG and HACKG organoids were cultured in WREN medium, and pulsed with EdU 1 h prior to harvest. Flow cytometric cell cycle analysis revealed that AhR KO significantly reduced the percentage of cells in G1 phase and increased the percentage of cells in S and G2/M phases (**Fig. 20G-H**).

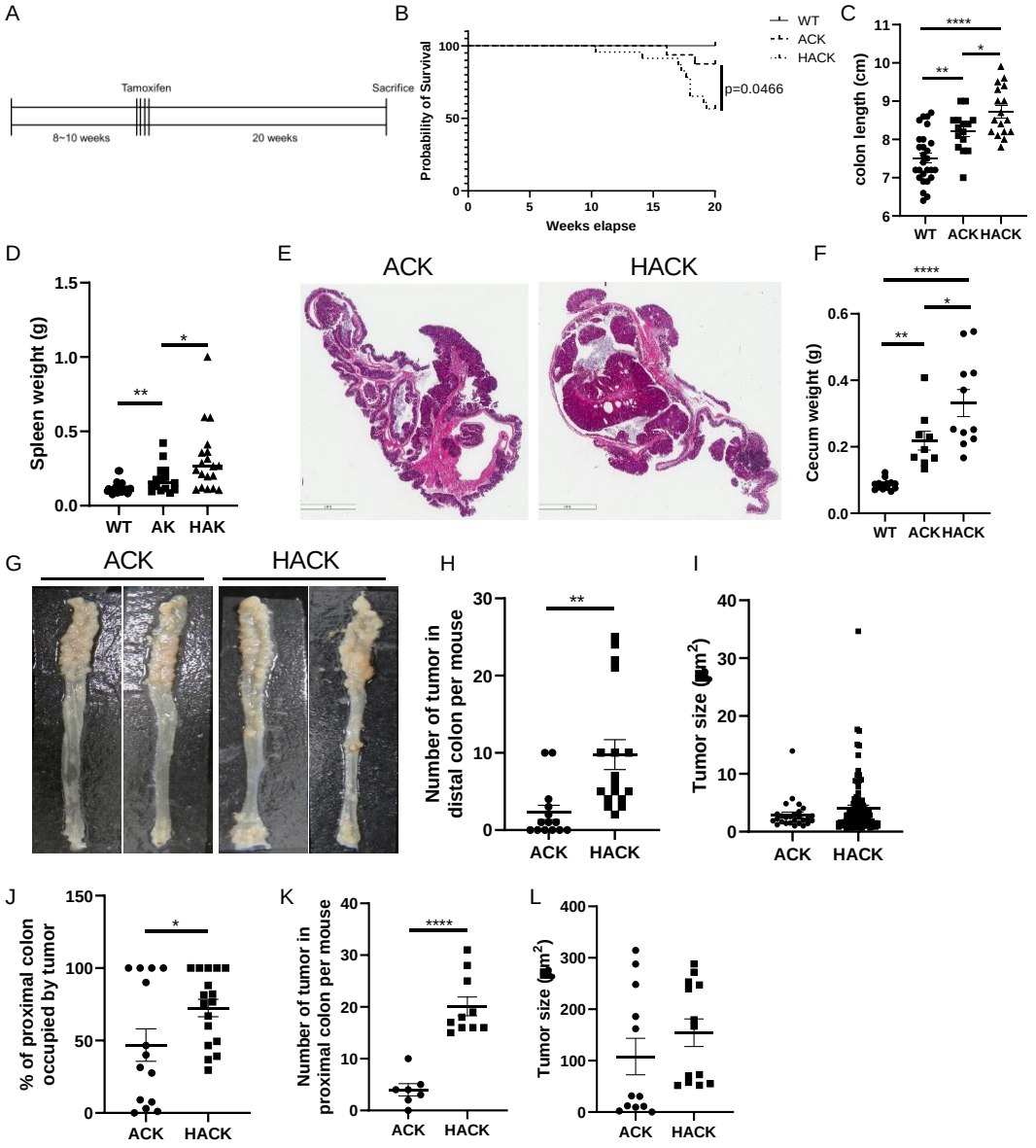

Figure 21. AhR KO promotes colorectal tumor growth in a mutant Kras and Apc mouse model. (A) Schematic regimen for colon tumorigenesis in a genetically susceptible model tumor. At 8~10 wk of age, inducible ACK (n=16) and HACK (n=23) mice were administrated with tamoxifen for 4 consecutive days to induce gene mutations. Mice were terminated 20 weeks after the final tamoxifen injection. (B) Kaplan-Meier survival plot indicating percentage survival over a 20 week period. (C) colon length. Asterisks indicate P<0.05 between groups. (D) Spleen weight. (E-F) Cecum tumor growth in ACK versus HACK mice. Scale bar 2 mm. (G) Representative colons from ACK and HACK mice 20 weeks post final tamoxifen injection. (H-I) Quantification of the number of (H) tumors and (I) tumor size in the distal colon. (J-L) Quantification of tumor growth in proximal colon.

3.3.5. AhR KO promotes colon tumorigenesis in compound mutant Apc and Kras mice.

Considering that AhR KO increased cell proliferation, Wnt and pERK1/2 signaling, we determined whether AhR modulates colon tumorigenesis in a genetic colon tumor model, carrying Apc^{S580} and $Kras^{G12D}$ mutations. Mice were terminated 20 wks after tamoxifen administration (**Fig. 21A**). We found that HACK mice had significantly lower survival rates, compared to ACK mice (**Fig. 21B**). In addition, colon length was elongated in compound mutant mice, compared with WT mice, and AhR KO further increased colon length (**Fig. 21C**), consistent with an increase in rates of cell proliferation. A similar trend was observed with respect to spleen weight (**Fig. 21D**), indicating enhanced tumor-associated inflammation. Since genetic mutations were targeted to the cecum and colon (CDX2P-Cre^{ERT2}), we monitored tumor development at these sites. AhR KO significantly increased cecum weights (**Fig. 21E&F**), reflecting an enhanced tumor load. In addition, the number of colonic tumors exhibited an obvious location-based distribution, with the preponderance of larger tumors occurring in the proximal colon. Specifically, AhR deletion robustly increased the number of tumors in distal colon, which was accompanied by a modest increase in tumor volume (**Fig. 21G,H&I**). Several mice (5/14 in ACK, and 10/17 in HACK) developed very severe tumors in the proximal colon, and it was not feasible to accurately quantify the number of tumors in all of the mice. Instead, we quantified the percentage of involved surface area in the proximal colon occupied by tumors. AhR KO significantly increased the percentage of proximal colon occupied by tumors (**Fig. 21J**). In addition, AhR KO remarkably elevated the number of tumors in the proximal colon per mouse (**Fig. 21K**), with no effect on tumor size (**Fig. 21L**). Similar to AhR deletion effects at 3 wks post-

tamoxifen injection (**Fig. 20C**), crypt length in the uninvolved colon was significantly longer in HACK mice, compared with ACK mice at 20 wks (**Fig. 22A&B**). β-catenin levels and cell proliferation were also enhanced in the uninvolved tumor region of HACK mice, compared with ACK mice (**Fig. 22C-E**). Moreover, β-catenin levels were also increased in tumors from HACK mice (**Fig. 22F&G**). In particular, the number of tumor cells with nuclear β-catenin was much higher in HACK mice, compared with ACK mice (**Fig. 22F**). However, cell proliferation was not altered in tumor tissues upon comparison between ACK and HACK mice (**Fig. 22H**). Interestingly, colonic cell proliferation (number of EdU^+ cells) was not correlated with β-catenin levels (**Fig. 22I**). We also analyzed levels of β-catenin and ERK1/2 protein in proximal colon tumors, and found that only non-phosphorylated β-catenin levels were significantly higher in HACK group (**Fig. 22J-L**). In addition, the growth of organoids derived from HACK proximal tumors was enhanced relative to ACK tumor organoids (**Fig. 22M**). Collectively, we observed that AhR KO promoted colon tumorigenesis and altered β-catenin levels in a genetic colon tumor model.

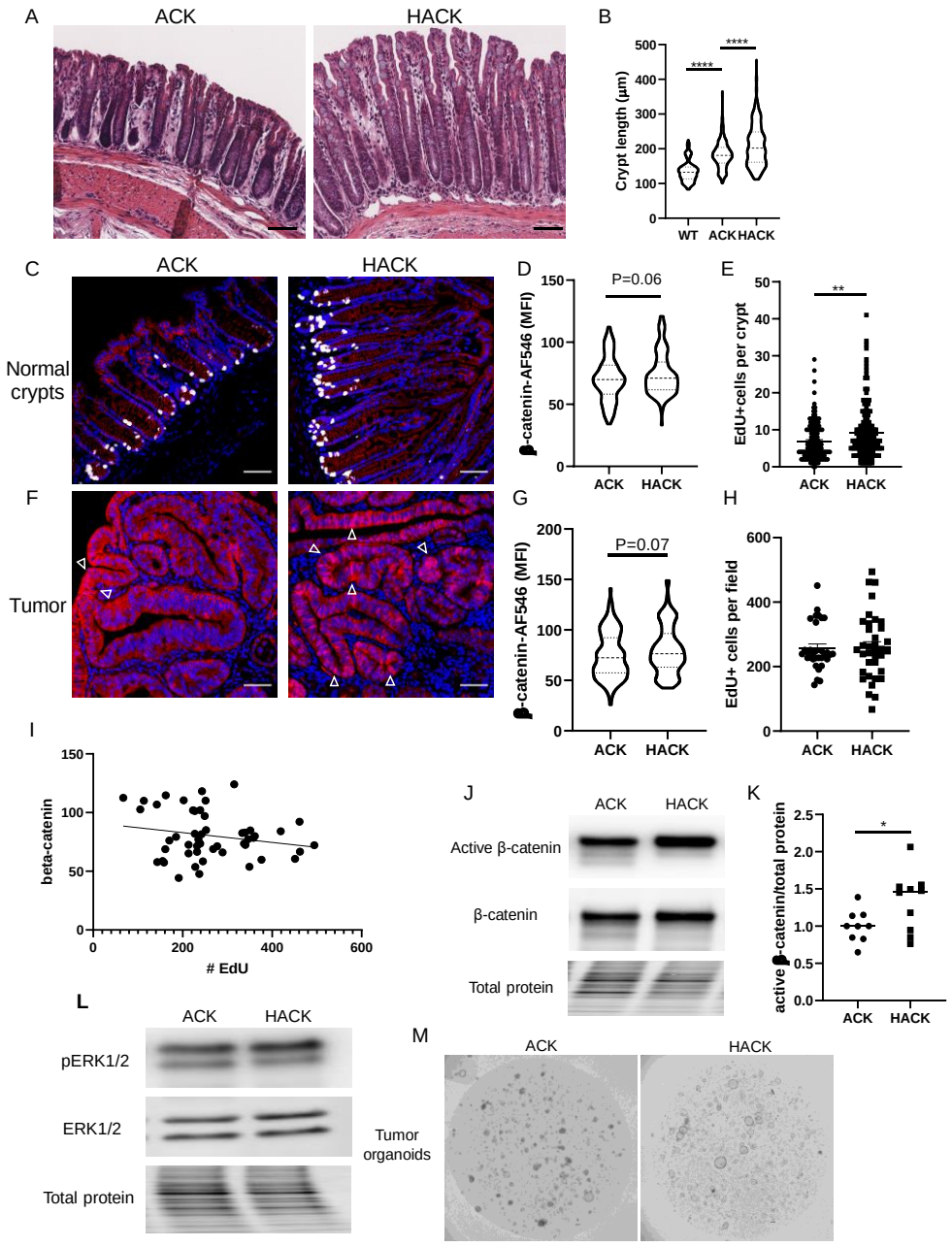

Figure 22. Loss of AhR potentiates Wnt signaling in colon tumors.
(A) H&E staining of representative colon sections from ACK and HACK mice. Scale bar, 50 μm. (B) Quantification of crypt length in colon, n=4 mice per group. Data are presented as mean ± SEM. Asterisks indicate P<0.05 between groups. (C) Cell proliferation marked by EdU+ in the uninvolved distal colon of ACK and HACK mice. Blue - DAPI, Red - β-catenin, and White - EdU. Scale bar 50 μm. (D) Quantification of MFI of β-catenin per crypt and (E) EdU+ cells per crypt, Each dot represents one crypt from n=4 mice per group. (F) Cell proliferation marked by EdU+ in the colon tumors from ACK and HACK mice. Blue - DAPI, Red - β-catenin, and White - EdU. Scale bar 50 μm. Quantification of MFI of (G) β-catenin per crypt and (H) EdU+ cells per crypt, n=4 mice per group. Arrow denotes accumulation of β-catenin in nucleus. (I) The association between MFI of β-catenin and EdU+ cells. Each dot represents different image fields from n=4 mice. (J-K) Representative immunoblots for β-catenin in proximal colon tumors from n=9-10 mice. (L) Representative immunoblots for ERK1/2 in proximal colon tumors from n=9-10 mice. (M) Representative brightfield images of organoids generated from proximal colon tumors. Scale bar 200 μm.

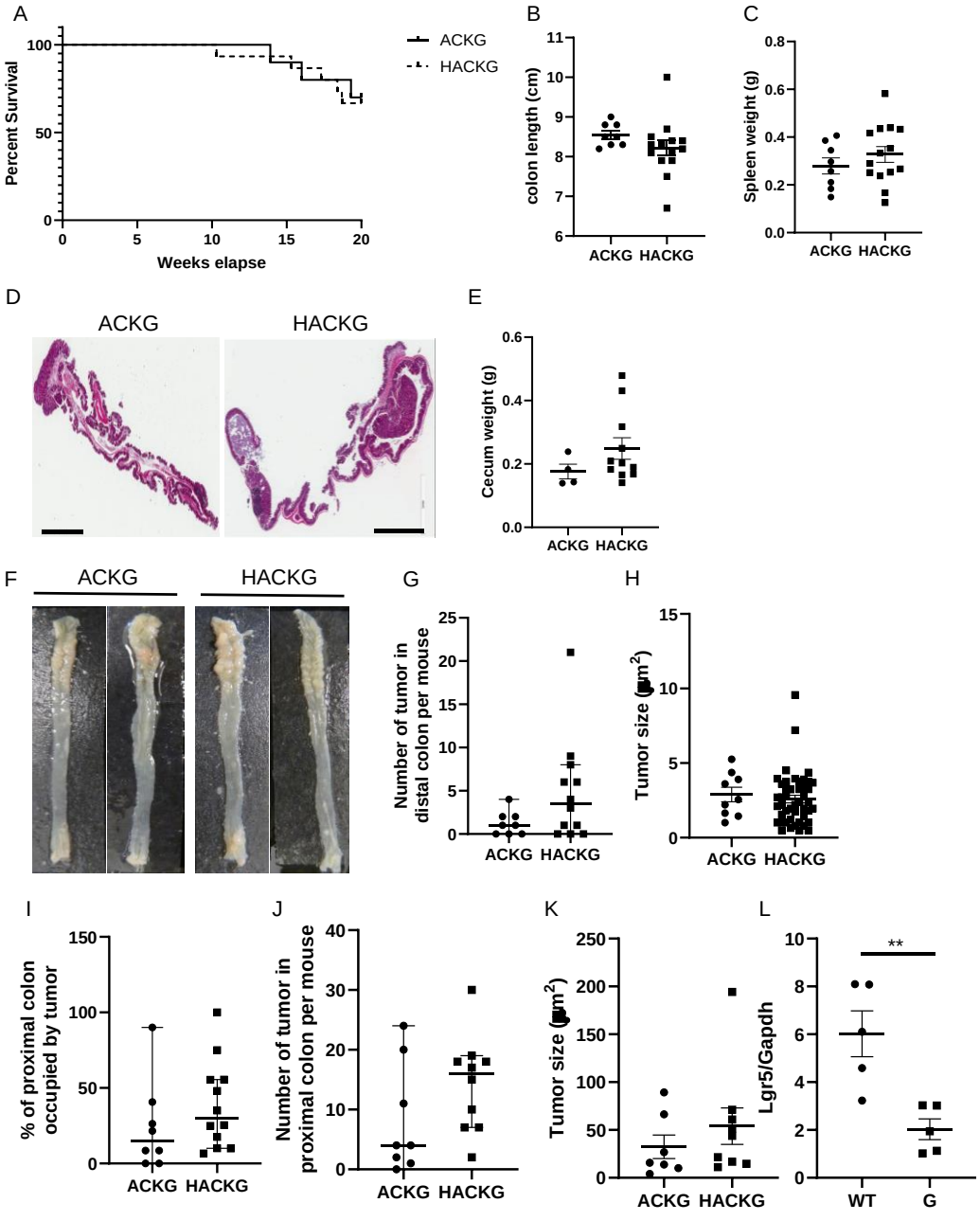

Figure 23. The deletion of one allele of Lgr5 attenuates the effect of AhR KO on colon tumorigenesis.

(A) Kaplan-Meier plot of percentage survival over a 20 week period. At 8~10 wk of age, inducible ACKG (n=10) and HACKG (n=15) mice were administrated tamoxifen for 4 consecutive days to induce gene mutations. Mice were terminated 20 weeks after the final tamoxifen injection. (B) colon length. Data are presented as mean ± SEM. (C) Spleen weight. (D-E) Cecum tumor growth from ACKG and HACKG mice. Scale bar 2 mm. (F) Representative colon images from ACKG and HACKG mice 20 weeks after the final tamoxifen injection. (G) Quantification of the number of tumors and (H) tumor size in the distal colon. (I-K) Quantification of tumor growth in the proximal colon. (L) Reduced Lgr5 expression in Lgr5-GFP reporter mice, compared with WT mice, n=5 per group. Asterisks indicate P<0.05 between groups.

3.3.6. Lgr5 haploinsufficiency attenuates AhR KO mediated colon tumorigenesis.

Since we have previously demonstrated that AhR signaling regulates colonic $Lgr5^{+}$ stem cell homeostasis, we examined whether targeted downregulation of intestinal stem cells can influence genetically-induced colon tumorigenesis. For this purpose, the Lgr5-EGFP-IRES-Cre^{ERT2} allele was introduced into ACK and HACK mice to generate Lgr5-haploinsufficient ACKG and HACKG mice carrying $Apc^{S580/+}$; $Kras^{G12D/+}$ mutations. Of note, we found that the knock-in of the Lgr5-GFP reporter remarkably reduced colon tumorigenesis in both mice and blunted the AhR KO phenotype with respect to colonic or cecum tumor growth (**Fig. 23A-K**). As expected, Lgr5-GFP reporter knockin reduced Lgr5 mRNA levels by 66% in Lgr5-GFP reporter mice, compared with WT mice (**Fig. 23L**). Considering the importance of Lgr5 receptor in Wnt signaling, our data suggest that reduced Wnt signaling accounted for the decreased tumor burden. Interestingly, Lgr5 haploinsufficiency had no effect on crypt length and AhR KO still promoted crypt elongation (**Fig. 24A&B**). Consistent with our expectation, Lgr5 haploinsufficiency reduced the expression of β-catenin but had no effect on cell proliferation (**Fig. 24C&D**). Interestingly, AhR KO still enhanced β-catenin levels and cell proliferation in the uninvolved tumor region but had no effect on colon tumor tissue (**Fig. 24E-J**). In addition, nuclear β-catenin was dramatically reduced in tumor tissue from either ACKG or HACKG mice (**Fig. 24H**). Collectively, these findings show that knockin of the Lgr5-GFP reporter allele remarkably reduced β-catenin stability, and attenuated AhR KO mediated colon tumorigenesis, while having no effect on cell proliferation.

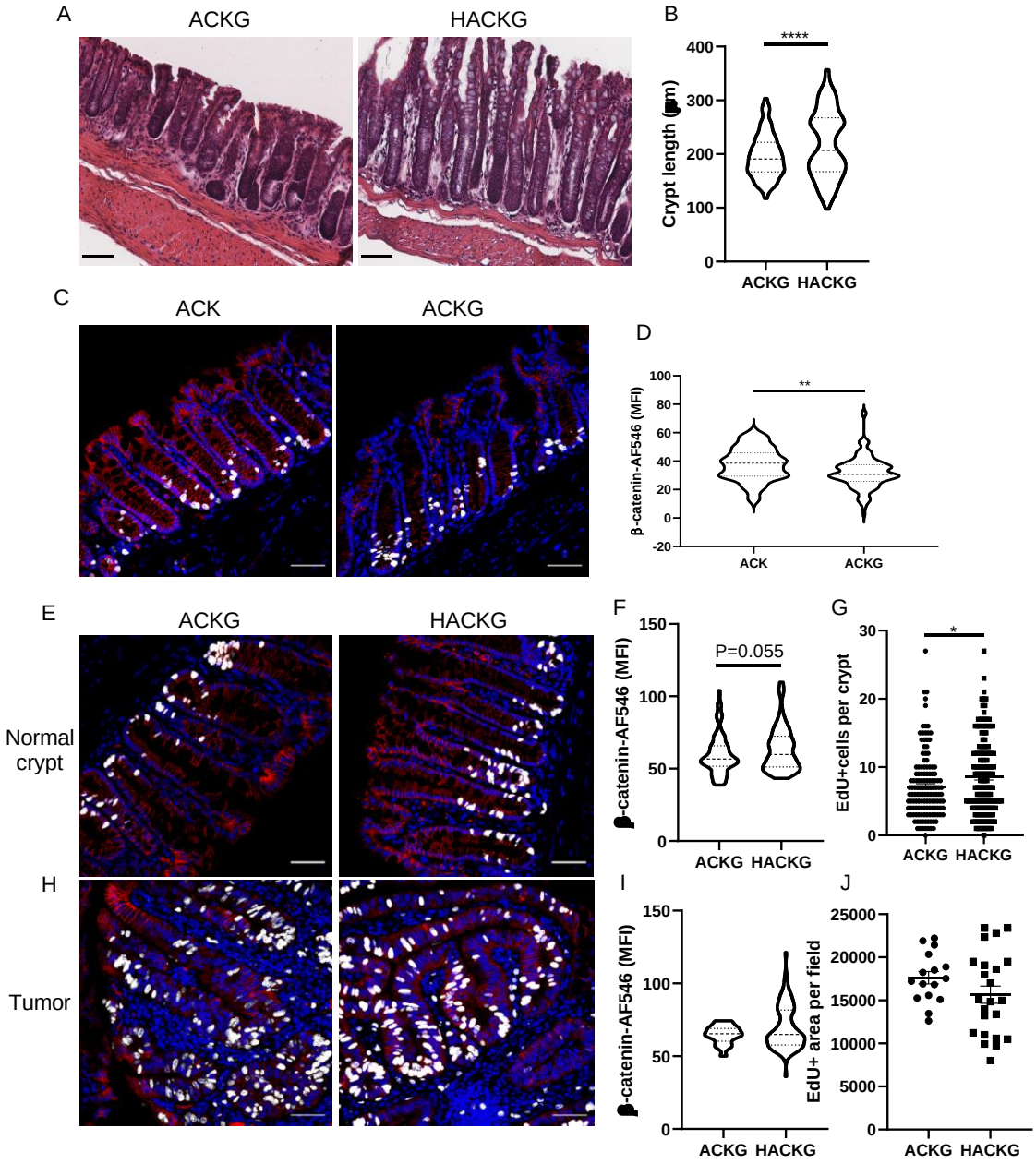

Figure 24. Lgr5 haploinsufficiency has no effect on cell proliferation.
(A) H&E staining of representative colon sections from ACKG and HACKG mice. Scale bar, 50 μm. (B) Quantification of crypt length in colon, n=4 mice per group. Data are presented as mean ± SEM. Asterisks indicate P<0.05 between groups. (C-D) Lgr5 haploinsufficiency reduced β-catenin level but has no effect on cell proliferation. Blue - DAPI, Red - β-catenin, and White - EdU. Scale bar 50 μm. (E) Cell proliferation marked by EdU+ in the uninvolved distal colon of ACKG and HACKG mice. Blue -DAPI, Red - β-catenin, and White - EdU. Scale bar 50 μm. (F) Quantification of MFI of β-catenin per crypt and (G) EdU+ cells per crypt, n=4 mice per group. (H) Cell proliferation in the colon tumors marked by EdU+ from ACKG and HACKG mice. Blue - DAPI, Red - β-catenin, and White - EdU. Scale bar 50 μm. (I) Quantification of MFI of β-catenin per crypt (J) and EdU+ cells per crypt, n=4 mice per group.

3.4. Discussion

The role of AhR signaling in regulating intestinal tumorigenesis is poorly understood. In this study, we provide evidence that the loss of AhR signaling promotes $Lgr5^{+}$ colonic stem cell and progenitor cell self-renewal and endows features of stemness (i.e., organoid forming capacity, cell proliferation) by potentiating Wnt signaling in mice expressing intestinally targeted $Apc^{S580/+}$ and $Kras^{G12D/+}$ mutations. This was associated with the enhancement of tumors in the cecum and colon.

Kawajiri et al reported that haploinsufficiency or knockout of AhR could cooperatively promote cecal and small intestinal carcinogenesis in ApcMin/+ mice, due to upregulated Wnt signaling. They noted that AhR acted as a ligand-dependent E3 ubiquitin ligase of β-catenin, and AhR activation by 3MC, β-naphthoflavone (βNF) or IAA could elevate the ubiquitylation and proteasomal degradation of β-catenin, thus downregulating Wnt signaling and suppressing intestinal tumorigenesis[131]. In addition, as a parallel pathway of Wnt signaling regulation, AhR was shown to bind to the promoter of Znrf3 and increase Znrf3 expression[194], which is a negative regulator of Wnt frizzled receptor. However, our lab and another group did not find any observable difference in terms of β-catenin expression and its downstream targets between WT and AhR KO colonocytes both in vivo and ex vivo[132]. Interestingly, in the genetically susceptible colon tumor model ($Apc^{S580/+}$; $Kras^{G12D/+}$), increased β-catenin levels were observed in AhR KO, compared with WT mice. This unexpected outcome might be due to two possibilities. One is the regulation of β-catenin by AhR is context dependent, including normal versus tumorigenic condition, in vivo versus in vitro, or mouse versus human AhR. This is consistent with a recent study using human colon cancer cell lines,

where AhR activation failed to recruit CUL4B or β-catenin to form the complex for subsequent β-catenin degradation[220]. The other possibility is that β-catenin is not a direct target of AhR. In addition, following tissue specific AhR KO, we did not observe enhanced β-catenin accumulation in the nucleus in normal crypts in vivo. Therefore, the association between AhR and β-catenin warrants future exploration.

Another important observation in our study is that Lgr5-GFP reporter mice significantly attenuated colon tumorigenesis, possibly due to the haploinsufficiency of Lgr5 in Lgr5-GFP reporter background. Lgr5 is an orphan G-protein coupled receptor and constitutes the receptor for R-spondin[221]. Upon R-spondin binding, Lgr5 interacts and forms a supercomplex with Rnf43/Znrf3, which antagonizes Wnt signaling by targeting Frizzled receptors for degradation and subsequent co-internalization[222]. Lgr5 expression level was decreased by ~60% in Lgr5-GFP reporter mice, compared with WT mice. Interestingly, Lgr5 haploinsufficiency did not result in any difference in crypt morphology and cell proliferation, but significantly reduced β-catenin levels and colon tumorigenesis. This observation is consistent with the “just right” theory of Wnt signaling in driving colon tumorigenesis, in which an optimal level of Wnt signaling is required for colon tumorigenesis[223]. Extensive studies have shown that haploinsufficient Apc and mutant Kras synergistically potentiate Wnt signaling in the intestine[224-227]. We present the first, to our knowledge, data demonstrating that additional ablation of AhR signaling in colonic epithelial cells further stabilized and increased β-catenin levels, thus increasing tumor burden. These data suggest that in mice carrying $Apc^{S580/+}$; $Kras^{G12D/+}$ mutations, that the additional loss of AhR can promote Wnt signaling to a threshold consistent with the promotion of colon tumor growth. To further explore this concept, we

also examined cecal tumor development in our mouse model. It has been previously reported that the Wnt signaling level is lowest in the cecum, compared with small intestine and colon, and Wnt signaling strength for the polyp initiation threshold is relatively low[223]. Thus, when Wnt signaling becomes a limiting factor to initiate adenoma growth, it should have the greatest impact on tumor burden in the cecum, which is exactly what we observed (**Fig. 21 and 23**). Consistent with this idea, we propose that Lgr5 haploinsufficiency titrates Wnt signaling below the threshold required for tumor growth.

Loss of AhR has been shown to promote cell proliferation both at basal homeostasis, following mucosal wounding and during carcinogen-induced colon tumor initiation. We recently demonstrated that the upregulation of FoxM1 signaling was at least partly responsible for the accelerated cell proliferation at basal and DSS-induced injury states, while Wnt signaling was not altered by AhR signaling under basal conditions. However, upregulated Wnt signaling, FoxM1 signaling and pERK1/2 may modulate cell proliferation following AhR deletion during the colon tumor initiation state. This suggests that under different cellular contexts, AhR signaling may impact different signaling nodes to regulate cell proliferation.

Currently no loss of function-related AhR mutations or causal effects of AhR SNPs alone have been linked to CRC risk. Instead, recent studies suggest that AhR ligand availability and AhR expression levels contribute to signaling strength and duration. The expression of AhR is upregulated in CRC, compared with normal tissue based on The Cancer Genome Atlas (TCGA) database. However, reduced CYP1A1 and CYP1B1 expression levels were detected in colon cancer, compared with normal tissue, implying

that AhR signaling is impaired in CRC patients. In addition, depletion of AhR ligand availability promoted carcinogen induced or colitis-associated colon tumorigenesis in mice[133]. It is increasingly appreciated that gut dysbiosis plays an important role in the pathogenesis of colorectal cancer[228]. It remains to be determined whether gut dysbiosis impairs the production of AhR ligands, and thus AhR activation in CRC individuals. Interestingly, impaired production of AhR ligands has been observed in patients with inflammatory bowel diseases[61,81,229], which is a risk factor for promoting CRC progression. Thus, it is possible that the increased AhR expression associated with colonic tumors represents a compensatory response to the diminished availability of AhR ligands. In future studies, it will be interesting to determine whether restoration of AhR ligand producing microbiota can attenuate CRC incidence and progression. In summary, emerging studies have shown that AhR signaling plays a protective role in carcinogen-induced colon cancer, colitis-associated colon tumorigenesis and $Apc^{Min/+}$ mouse models. Our data broaden and redefine the phenotypic features of colonic epithelial cell specific AhR deletion in mice carrying $Apc^{S580/+}$ and $Kras^{G12D/+}$ mutations, which are commonly mutated in humans during early phase adenoma development. Findings from the current study suggest that AhR signaling plays an important role in intestinal tumorigenesis, and could be a promising therapeutic target for colon cancer prevention and treatment.

4. LOSS OF ARYL HYDROCARBON RECEPTOR SUPPRESSES THE RESPONSE OF COLONIC EPITHELIAL CELLS TO IL22 SIGNALING

4.1. Introduction

Interleukin-22 (IL-22) is a member of the IL-10 family of cytokines that plays various roles in cell proliferation, host defense, inflammation and tissue repair[141]. Human IL-22, encoded by the *IL22* gene located on chromosome 12, contains 146 amino acids in its secreted form. IL-22 signals through a heterodimeric receptor consisting of two different subunits, IL-22R1 and IL-10R2. IL-22R1 is exclusively expressed in some subsets of tissues, such as skin, small intestine, liver, colon, lung, kidney and pancreas, but not in immune cells, thymus and spleen, while IL-10R2 is ubiquitously expressed [141,230]. Therefore, unlike most of interleukins, IL-22 signaling does not directly regulate the function of immune cells, but targets epithelial cells in the skin, gastrointestinal tract, respiratory system and other organs[141,230].

In the gastrointestinal tract, IL-22 signaling plays an important role in maintaining gut barrier function, resolution of inflammation, wound-associated regeneration and genotoxin induced DNA damage response (DDR)[143,145,231,232]. Many different types of immune cells, including innate lymphoid cells, NK T cells, γδ T cells, Th17 cells, neutrophils and $CD4^+$ T cells, are capable of producing IL-22 [143-149]. In patients with inflammatory bowel diseases, IL-22 mRNA expression was upregulated in the colon, which is similarly observed in murine dextran sulfate sodium-induced colitis[233,234]. Antagonism of IL-22 signaling worsens clinical disease scores and wound recovery in

DSS treated mice[145,234,235], implying that IL-22 signaling plays a protective role with regard to intestinal inflammation.

The IL-22 receptor is heterogeneously expressed across different intestinal cell types, and slightly enriched in transit amplifying (TA) progenitor cells in the small intestine[236]. IL-22 has a high binding affinity to the extracellular domain of IL-22R1[237]. Upon binding to IL-22R1, IL22 undergoes a conformational change which supports the interaction between the IL-22-IL-22R1 complex and IL-10R2. The intracellular moieties of IL-22R1 and IL-10R2 form a complex with the kinases Janus kinase 1 (JNK1) and tyrosine kinase 2 (TYK2), respectively. Generation of the tripartite complex induces the phosphorylation of JAK1 and TYK2, which further phosphorylate IL-22R1 in its cytoplasmic domain, thereby facilitating the docking of STAT3. Upon STAT3 recruitment to IL-22R1, JAK1 then phosphorylates STAT3 predominately at Tyr705. The phosphorylation of STAT3 enables its dimerization and translocation into the nucleus, where it regulates the expression of downstream targets[141,237]. In addition, IL-22 signaling can result in STAT1 and STAT5 phosphorylation [232,238].

Emerging studies have shown that aryl hydrocarbon receptor (AhR), a ligand activated basic helix-loop-helix transcription factor, plays a pivotal role in IL-22 production in immune cells. For example, it has been demonstrated that AhR can directly bind to the promoter of the IL-22 gene in mouse $CD4^+$ T cells and RORγt(+) innate lymphoid cells (ILCs), thereby promoting IL-22 transcription[87,154]. In addition, AhR signaling affects the immune cell fate programming, favoring IL22-induced ILCs and $FoxP3^+$ Treg cell differentiation[150,152]. Global AhR deficient mice exhibit reduced IL-22 expression and RORγt+ ILC3 development as well as increased intestinal Th17 cell

numbers[150]. In contrast AhR activation by FICZ treatment ameliorates TNBS-, DSS- and T-cell transfer-induced colitis in part by up-regulating IL-22 and downregulating the expression of pro-inflammatory cytokines, such as IFN-ɣ, IL-17α and TNF-α [80]. In addition, IL-22 signaling is required for the effective initiation of DNA damage-induced repair, and thus maintenance of genome integrity in ISCs[143]. However, the effect of AhR signaling on the response to IL-22 in intestinal stem cells (ISCs) is not fully understood. To this end, we utilized intestinal epithelial cell specific AhR KO mice to determine the response of colonic stem/progenitor cells to IL-22 signaling. We found that AhR KO impaired the response of colonic stem cells to IL-22 signaling by upregulating the expression of the suppressor of cytokine signaling 3 (SOCS3), a negative regulator of STAT3. These findings provide novel insight into the specific role of AhR signaling in mediating colonic epithelial cell responsiveness to IL-22.

4.2. Materials and methods

4.2.1. Mice

Animals were housed under conventional conditions, adhering to the guidelines approved by the Institutional Animal Care and Use Committee at Texas A&M University. Lgr5-EGFP-IRES-Cre^{ERT2}, CDX2P-Cre^{ERT2}, and AhR$^{f/f}$ mouse strains have all been previously described. Specifically, Lgr5-EGFP-IRES-Cre^{ERT2} mice express EGFP and Cre^{ERT2} in crypt base columnar cells in the intestine under control of the *Lgr5* promoter[106]. CDX2P-CreERT2 mice express CreERT2 throughout the entire intestinal epithelium under the control of the CDX2 promoter[169,170]. AhR$^{f/f}$ mice carry loxP sites bordering exon 2 of the AhR gene, with recombination resulting in generation of a

premature stop codon at codon 29[18]. Mice were intraperitoneally injected with 2.5 mg of tamoxifen (Sigma, T5648) dissolved in corn oil (25 mg/ml) once per day for 4 consecutive days. Mice were maintained on an AIN-76A semi-purified diet (Research Diets, D12450B), fed *ad libitum* and housed on a 12 h light-dark cycle. For all experiments, littermate controls were cohoused with the knockout mice, unless specifically indicated.

For genotyping analyses, DNA was extracted from tails using DNeasy Blood and Tissue Kit (Qiagen, 69506). PCR was subsequently performed using the following primer sets:
AhR (5'-CAGTGGGAATAAGGCAAGAGTGA-3' and 5'-GGTACAAGTGCACATGCCTGC-3'),
CDX2P-Cre (5'- GGACTTGAGCAGCTAGCTGTGCAACTT-3' and 5'-TGTCTCGTGCCTGGAATGACCTT-3'), Lgr5-EGFP (5'-CACTGCATTCTAGTTGTGG-3' and 5'- CGGTGCCCGCAGCGAG-3'). AhR recombination *in vivo* was previously prescribed and examined.

4.2.2. *Crypt single cell isolation and cell sorting*

Colons were removed, washed with cold PBS without calcium and magnesium (PBS-/-), everted on a disposable mouse gavage needle (Instech Laboratories), and incubated in 15 mM EDTA in PBS-/- at 37°C for 35 min as previously described[174]. Subsequently, following transfer to chilled PBS-/-, crypts were mechanically separated from the connective tissue by rigorous vortexing. Crypts were embedded in Matrigel and overlaid with crypt culture media as previously described[1]. For intestinal stem cell

(ISC) isolation, crypt suspensions were dissociated to individual cells with 0.25% Trypsin-EDTA containing 200 U/ml DNase. Cell suspensions were then filtered through a 40-µm mesh and GFP^{hi} and GFP^{low}-expressing cells were collected using a MoFlo Astrios Cell Sorter (Beckman Coulter) or Bio-Rad S3e Cell Sorter. Dead cells were excluded by staining with propidium iodide or 7-AAD. Sorted cells were collected in RNA lysis buffer (for RNA isolation).

4.2.3. Organoid culture

Mouse organoid cultures were maintained in crypt culture medium containing Advanced DMEM/F12 (Gibco) supplemented with 2 mM glutamax, penicillin/streptomycin, and 10 mM HEPES (ADF+), 50 ng ml^{-1} EGF (Life Technologies), 100 ng ml^{-1} Noggin (Peprotech), 10% R-spondin conditioned medium, 1 µM N-acetyl-l-cysteine (Sigma), 1X N2 (Life Technologies), 1X B27 (Life Technologies) and 50% Wnt conditioned medium as described previously[175]. The crypt media was changed every 2 d. Organoids were quantified on day 5 of culture, unless otherwise specified. For AhR-related treatments, DMSO or TCDD (10 nM) were added to cultures for 3 d. In some experiments, colonic organoids were cultured in 50% WRN conditioned medium derived from L-WRN cells (CRL-3276), and 10% FBS (WRN medium)[176].

To measure organoid viability, CellTiter-Blue reagent (Promega) was used according to manufacturer's instructions. Fluorescence was measured on a CLARIOstar microplate reader.

For experiments evaluating the effect of recombinant mouse IL-22 (BioLegend, 576202) on mouse organoid growth in the absence or presence of AhR, 1 or 5 ng ml^{-1}

IL-22 was added to the culture medium after passaging. To probe phosphorylated STAT3 in response to IL-22 treatment, organoids were harvested for protein extraction 30 min after the initiation of IL-22 treatment. To measure organoid growth in response to IL-22 treatment, organoids were cultured in medium containing IL-22 for 2 or 5 d. Images of organoids were captured using an upright AZ100 Nikon microscope or all-in-one BZ-X800 Keyence fluorescence microscope.

4.2.4. Secondary murine organoid assay

For secondary organoid assays, organoids were pretreated PBS or 5 ng ml^{-1} IL-22 for 2 d followed by dissociation for 8 min in 0.25% Trypsin-EDTA at 37°C. Cell suspensions were then filtered through a 20-µm mesh, centrifuged for 3 min at 500*g, and then resuspended in cold ADF+ medium. Live cell density was counted. Approximately, 5000 live cells were seeded into 30 µl Matrigel in flat bottomed 24-well plates. Following Matrigel polymerization, cells were overlaid with 300 µl of crypt culture medium supplemented with 10 µM Y-27632 (Sigma Y0503), 1 µM Jagged-1 and 2.5 µM CHIR99021 (Stemgent, 04-0004). Y-27632, Jagged-1 and CHIR99021 were withdrawn from crypt culture medium 2 d after plating. The crypt media was changed every 2 d and organoids were quantified on day 5 of culture, unless otherwise specified.

4.2.5. Gene editing

Organoid lipofection was performed as previously described[239]. Briefly, mouse organoids were dissociated into single or small cell clusters using 0.25% Trypsin- EDTA at 37 ºC, filtered through a 20 µm cell strainer, and washed twice with cold Advanced

DMEM/F12. Cells were then resuspended in 1.5 ml crypt culture medium containing 10 μM Y-27632 and plated in a 6-well plate at high density (80~90% confluent). Nucleic acid-Lipofectamine 3000 complexes were prepared according to the standard Lipofectamine 3000 Reagent protocol. For this purpose, 7.5 μl of Lipofectamine 3000 Reagent (Life Technologies, L3000008) was diluted in 125 μl Opti-MEM medium and mixed together. pSpCas9(BB)-2A-GFP (10 μg) with gRNA targeting Socs3 (TTCTACTGGAGCGCCGTGAC or CGAGCTGTCGCGGATAAGAA) was diluted into 125 μl Opti-MEM medium, and then mixed with 20 μl P3000 Reagent. Diluted DNA was then added into diluted Lipofectamine 3000 Reagent, mixed well, incubated for 15 min at room temperature, and added to the cells (250 μl per well). Plates were centrifuged at 600*g at 32°C for 1 h and incubated for 4 h at 37°C before single cells were re-plated in Matrigel. Cells were subsequently collected, centrifuged, resuspended with Matrigel and plated into the center of each well of prewarmed 24-well plates. Crypt culture medium supplemented with 1 μM Jagged-1, 5μM CHIR99021 and 10 μM Y-27632 was added after cell-Matrigel suspension drops had solidified. Two days after lipofection, cells were dissociated into single cells using 0.25% Trypsin-EDTA at 37 ºC and filtered through a 20 μm cell strainer. Dead cells were excluded by staining with 7-AAD. The top (highest) 30% GFP-expressing cells were collected using a Bio-Rad S3e Cell Sorter. Sorted GFP-expressing cells were mixed with an appropriate volume of Matrigel (~30 cells per 30 ul Matrigel) and seeded into the center of each well of prewarmed 24-well plates. Subsequently, 10~14 d after plating, single organoids were picked and trypsinized into small cell clusters. Cells were resuspended with Matrigel and plated as described above.

4.2.6. *RNA isolation and quantitative real-time PCR*

RNA from sorted cells or organoids was isolated using the Quick-RNA MicroPrep Kit (Zymo, R1050) and further processed using a DNA removal kit (DNA Free, Ambion, AM1906). RNA integrity was assessed using a Bioanalyzer 2100 (Agilent Technologies), quantified by Nanodrop and stored at -80°C. Real-time PCR was performed on a QuantStudio 3 System (Applied Biosystems) using TaqMan Universal PCR Master Mix (Applied Biosystems). Specific primer/probe mix for each gene was obtained from Applied Biosystems: Reg3b (Mm00440616_g1), Reg3g (Mm00441127_m1), Lgr5 (Mm00438890_m1), Ascl2 (Mm01268891_g1), Atm(Mm01177457_m1), p21 (Mm04205640_g1), Puma (Mm00519268_m1), Socs3 (Mm00545913_s1) and GAPDH (Mm99999915_g1).

4.2.7. Immunohistochemistry

In order to assess cell proliferation in the colon, mice were intraperitoneally injected with EdU 2 h prior to termination as previously described[177]. Colonic cell proliferation was measured using the Click-IT EdU kit (Life Technologies, C10340). Antigen retrieval was performed by sub-boiling in 10 mmol/L sodium citrate (pH 6.0) for 20 min. Antibodies used were: rabbit polyclonal antibody to SOCS3 (Abcam, ab16030) followed by Alexa-568 donkey anti-rabbit secondary antibody (Life Technologies, A-10042). Prolong Gold antifade with DAPI (Life Technologies, P36935) was used to coverslip the slides. Images of colonic crypts were captured on a Leica DMi8 TCS SPE spectral confocal microscope. Images were processed using ImageJ software (ImageJ 1.51n

version). For enumeration of immunohistochemical staining, approximately 35 crypts were assessed from at least 3 animals per treatment.

4.2.8. Western blotting

Organoids were lysed in lysis buffer (50 mM Tris-HCl pH 7.2, 250 mM sucrose, 2 mM EDTA pH 7.6, 1 mM EGTA pH 7.5, 1% Triton X-100, 10 mM β-mercaptoethanol) supplemented with protease inhibitor cocktail (Sigma) and 1x phosphatase inhibitor (Life Technologies). Lysates were subjected to standard SDS-PAGE and Western blotting procedures using primary antibodies against STAT3 (1:2000, 4904S, Cell Signaling Technology), STAT3 (1:1000, Abcam 119352), phospho STAT3 (Tyr705) (1:2000, 9145S, Cell Signaling Technology), β-actin (1:5000, Abcam ab8227) and SOCS3 (1:1000, Abcam, ab16030). Secondary anti-mouse or rabbit conjugated to horseradish peroxidase or secondary StarBright Blue 700 goat anti-mouse IgG (Bio-Rad, #12004159) were used to detect primary antibodies. Signal was detected using ECL substrate (Bio-Rad), imaged with the Bio-Rad Chemidoc System and protein bands quantified using Image Lab 6.0 (Bio-Rad).

4.2.9. Statistics

Two-tailed Student's t-tests were used to assess statistical significance of the differences between means across experimental groups. Paired student t-tests were used to examine the statistical significance of the differences between treatments within genotypes in organoids, unless otherwise specified. One-way ANOVA with Tukey's multiple comparisons test were used to compare more than 2 groups. All data are

presented as mean ± SEM (standard error), and all analyses were conducted using Prism 8 statistical software (GraphPad Software, Inc.).

4.3. Results

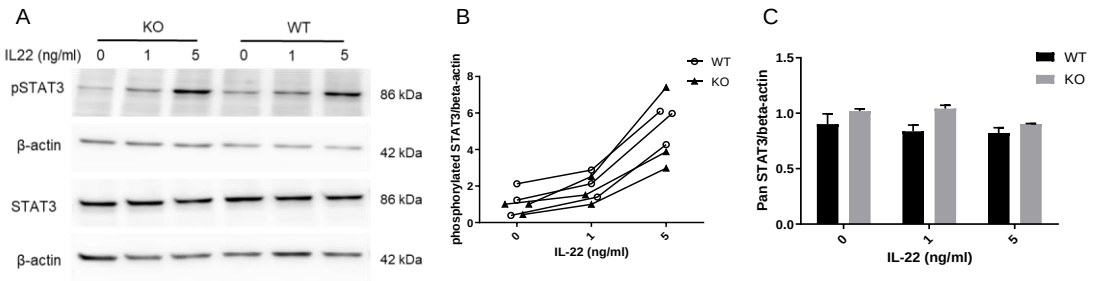

Figure 25. Dose response of IL22 in organoids.
(A) Representative immunoblots for pSTAT3 Tyr705 and STAT3 in AhR WT and KO organoids from n=3 mice. Organoids were harvested 30 min after IL22 treatment. (B-C) Quantification of pSTAT3 Tyr705 and STAT3 protein levels following IL22 exposure.

4.3.1. *IL-22 responsiveness is impaired in AhR KO colonic organoids.*

Since IL-22 modulates ISC renewal and expansion[232,236], we initially assessed the dose responsiveness of colonic organoids to exogenous IL-22 treatment in the presence or absence of AhR (WT vs KO). For this purpose, colonic GFP^{hi} $Lgr5^{+}$ stem cells were sorted from isolated from mouse colonic crypts. We found that IL-22 treatment robustly boosted the phosphorylation of STAT3 within 30 min in a dose dependent manner, and AhR KO had no effect on STAT3 phosphorylation (**Fig. 25A&B**). The total protein level of STAT3 remained unchanged in response to IL-22 treatment (**Fig. 25A&C**). Since AhR KO did not affect acute IL-22 signal transduction,

we determined the effect of AhR KO on ISC-dependent organoid growth in response to IL-22 treatment. Surprisingly, IL-22 supplementation decreased the number of organoids and organoid size in a dose-dependent manner in the WT group, which differs from previous reports indicating that IL-22 treatment promotes intestinal organoid growth[232,236]. In contrast, AhR KO abrogated the inhibitory effects of IL-22 on organoid growth (**Fig. 26A-C**). Immunoblot analysis also revealed that the phosphorylation of STAT3 was attenuated by AhR depletion 5 d after IL-22 treatment, and the total protein level of STAT3 was not affected either by AhR status or IL-22 treatment (**Fig. 26D-F**). One of the most notable effects of IL-22 signaling was the induction of anti-microbial Reg3g and Reg3b gene expression, and its subsequent repression following AhR KO (**Fig. 26G&H**). Since IL-22 inhibited colonic organoid growth, we hypothesized that IL-22 signaling had an impact on colonic stem cells. Interestingly, IL-22 treatment suppressed the expression of colonic stem cell markers, Lgr5 and Ascl2, and reduced secondary organoid growth in WT organoids, while AhR KO reduced the effect of IL-22 signaling on colonic stem cells (**Fig. 26I-K**). Collectively, IL-22 treatment suppressed colonic ISC-dependent organoid growth and AhR KO desensitized colonic organoid responsiveness to IL-22 signaling.

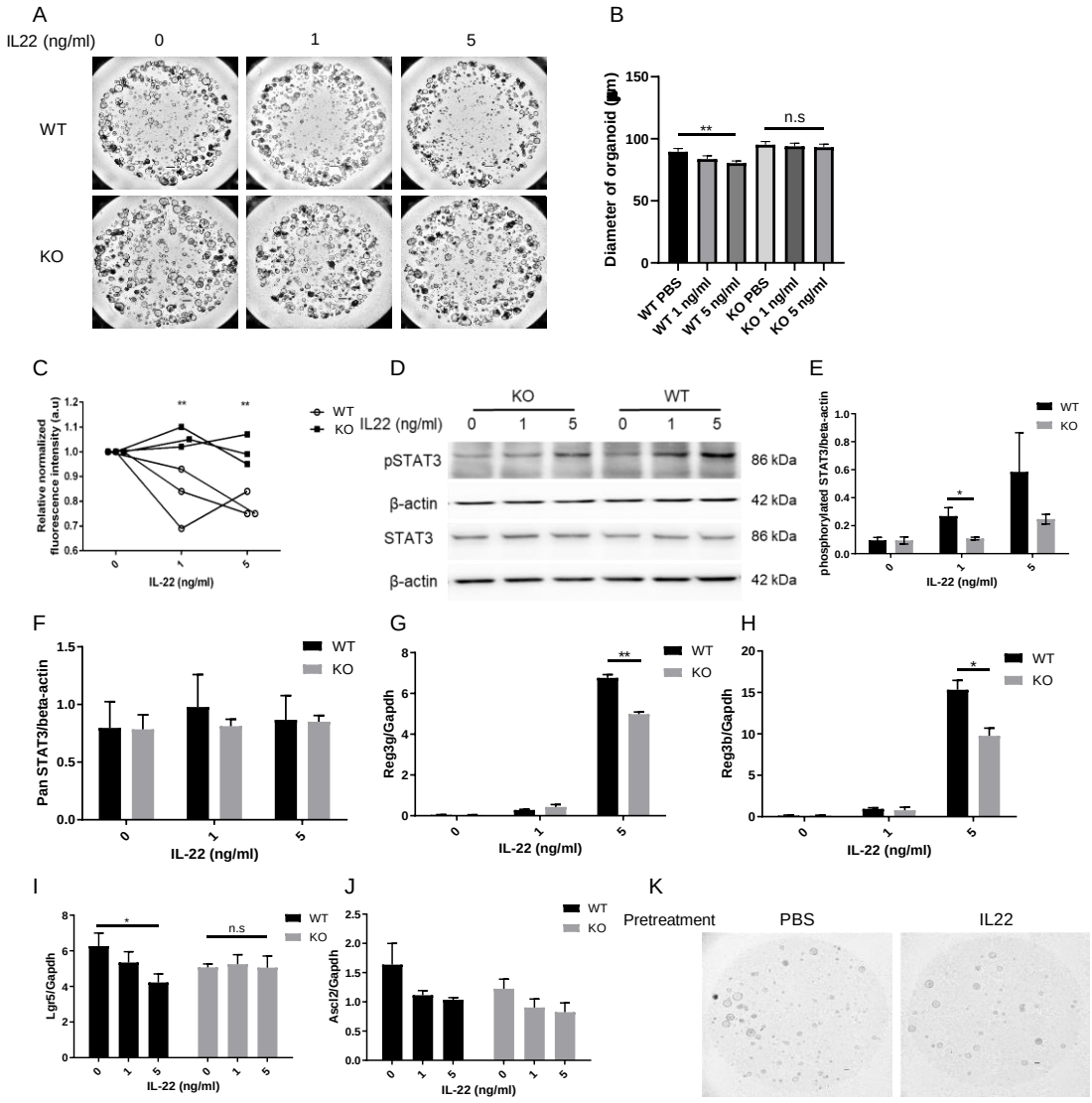

Figure 26. The response to IL22 signaling is impaired in AhR KO organoids.
(A) Representative brightfield images of organoids treated with IL22 for 5 d. Scale bar 200 μm. (B) Organoid diameter. The organoid diameter greater than 50 μm was quantified. (C) The number of viable cells assessed by CellTiter Blue assay. (D) Representative immunoblots for pSTAT3 Tyr705 and STAT3 in AhR WT and KO organoids treated with IL22 for 5 d from n=3 mice. (E-F) Quantification of pSTAT3 Tyr705 and STAT3 protein levels. (G-H) Expression of antimicrobial peptides Reg3g and Reg3b in response to IL22 treatment, n=3 mice. (I-J) Expression of colonic stem cell markers, Lgr5 and Ascl2, in response to IL22, n=3 mice. (K) Representative images of secondary organoid growth from WT organoids pre-treated with IL22 for 2 d. Scale bar 200 μm.

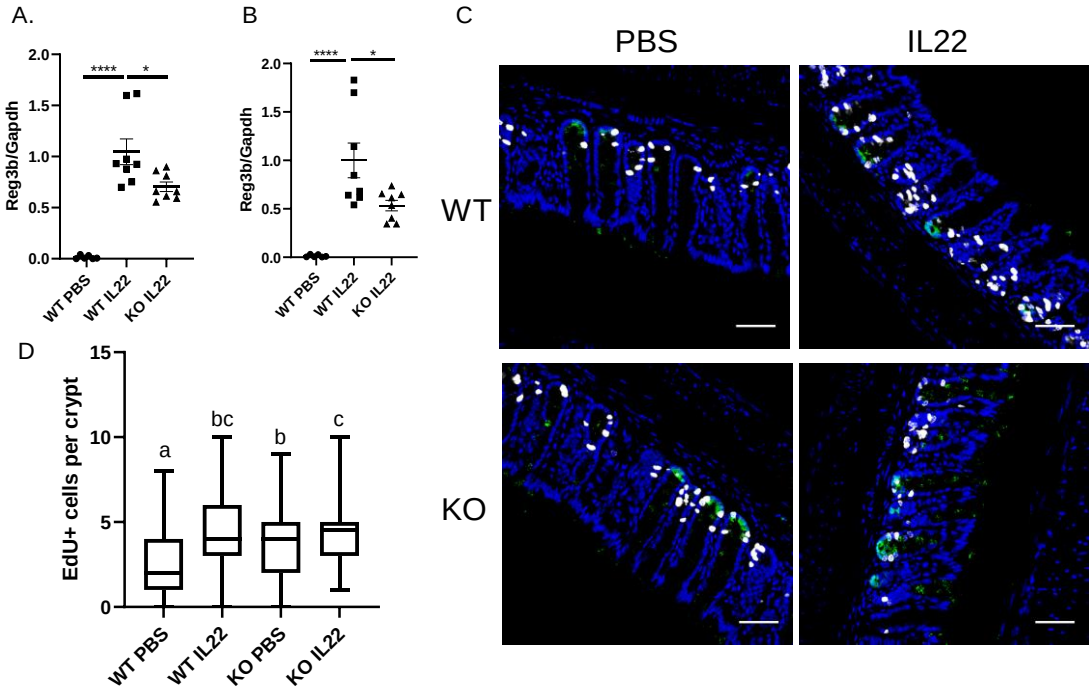

Figure 27. AhR KO attenuates IL22-induced cell proliferation in vivo.
(A) Expression of Reg3b in sorted colonic stem cells, n=6-8 mice per group. (B) Expression of Reg3b in sorted colonic progenitor cells, n=6-8 mice per group(C) Representative images of cell proliferation marked by EdU$^+$ in the distal colon of n=3-4 mice treated with IL22 or vehicle (control) for 2 d. GFP$^+$ crypts were quantified; Green – GFP, Blue – DAPI, Gray – EdU. Scale bar 50 μm. (D) Quantification of EdU$^+$ cells per crypt using1-way ANOVA without Fisher's LSD correction. Treatments not sharing a common letter are significantly different, $p<0.05$.

4.3.2. *Loss of AhR inhibits IL-22-induced cell proliferation in vivo.*

To further investigate the link between IL-22 signaling, AhR and GI cell proliferation[232,236,240], mice were i.p administrated PBS or 4 μg IL-22 per day for 2 consecutive days, and cell proliferation was assessed *in vivo*. In addition, Lgr5-GFP-IRES-CreERT2 reporter mice were used to mark colonic GFP^+ stem cells. In this context, IL-22 treatment robustly induced the expression of Reg3b and AhR KO inhibited its expression in colonic stem cells (**Fig. 27A&B**). In addition, IL-22 treatment dramatically increased cell proliferation in AhR WT group, while only slightly promoted cell proliferation in AhR KO group (**Fig. 27C&D**), implying that AhR KO attenuated IL-22 induced cell proliferation *in vivo*.

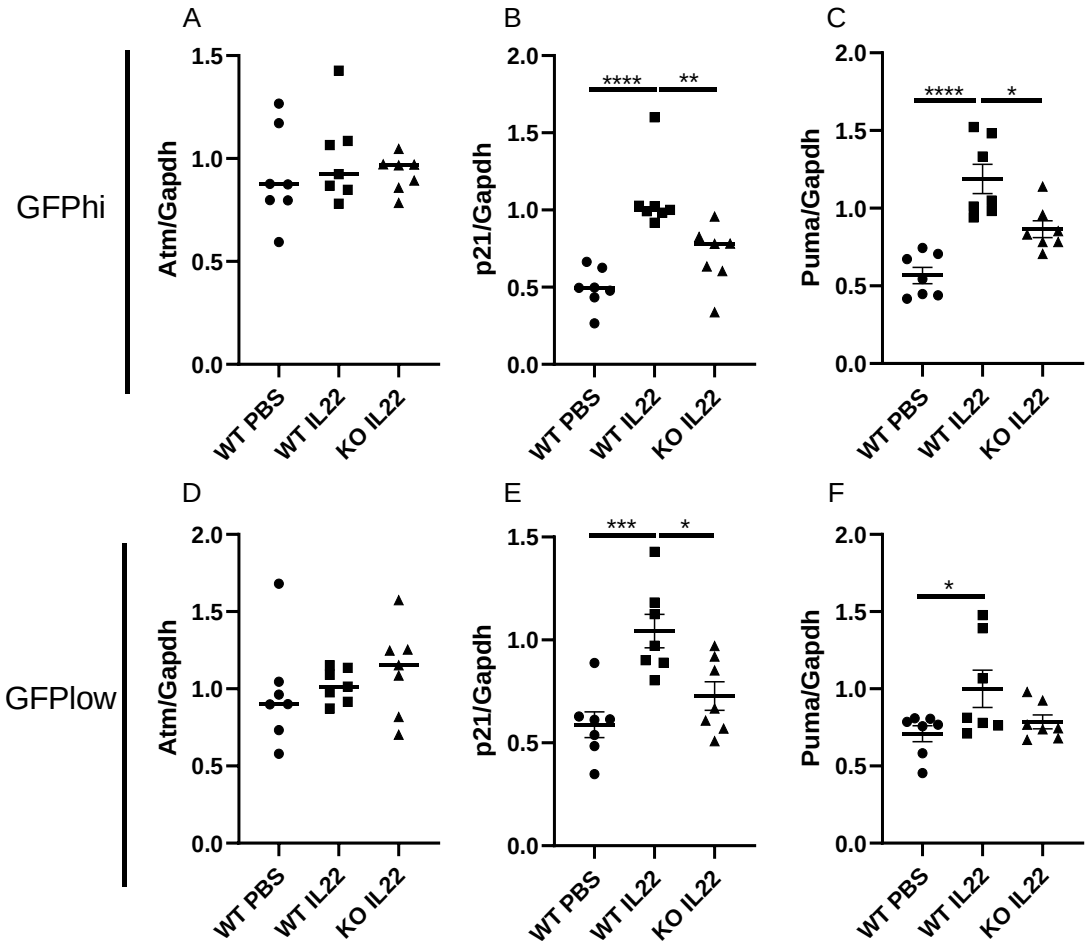

Figure 28. AhR KO compromises DNA damage response induced by AOM exposure.
(A-C) Expression of DNA damage response genes, Atm, p21, and Puma in sorted colonic stem cells, n=7 mice per group. (D-F) The expression of DNA damage response genes, Atm, p21, and Puma in sorted colonic progenitor cells, n=7 mice per group.

4.3.3. Loss of AhR suppresses carcinogen-induced DNA damage response (DDR).

It has been recently demonstrated that IL-22 is required to initiate efficient DNA damage repair after genotoxic stress following exposure to carcinogen, e.g., azoxymethane (AOM), in order to maintain ISC genome integrity[143]. Thus, we determined the effect of AhR KO on AOM-induced DNA damage repair in response to IL-22. Lgr5-GFP-IRES-CreERT2 reporter mice were administrated PBS or 4 μg IL-22 for 1.5 d prior to AOM injection and terminated 12 h following AOM injection. IL-22 treatment upregulated the expression of p21 and Puma, but not Atm, in sorted colonic GFP^{hi} stem or GFP^{low} progenitor cells, while AhR KO dampened the expression of p21 and Puma, compared with IL-22 treated counterparts (**Fig. 28**). This suggests that AhR KO compromised the ability colonic stem or progenitor cells to repair damaged cells, potentially leading to the accumulation of DNA lesions. Thus, there is an association between AhR and colonic stem/progenitor cell responsiveness to IL-22 *in vivo*. This extends to the expression of genes involved in DDR following exposure to AOM.

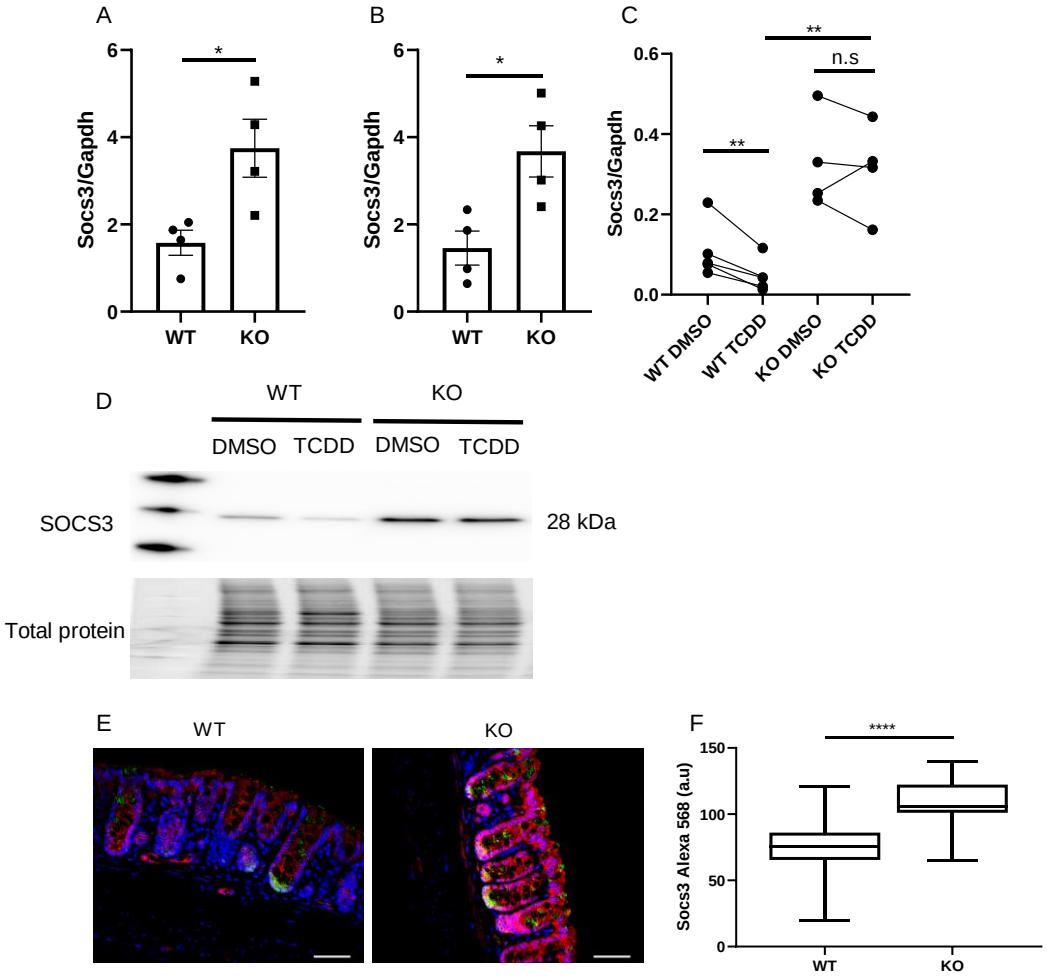

Figure 29. SOCS3 expression is upregulated in AhR deficient organoids.
(A) mRNA expression of Socs3 in sorted GFP^{hi} colonic stem cells, n=4 mice per group. (B) mRNA expression of Socs3 in sorted GFP^{low} colonic progenitor cells, n=4 mice per group. (C) mRNA expression of Socs3 in organoids treated with DMSO or 10nM TCDD, n=4 mice per group. (D) Representative immunoblots for SOCS3 in AhR WT and KO organoids treated with DMSO or TCDD, n=3 mice per group. (E) Representative images of SOCS3 expression in colonic crypts. GFP+ crypts were quantified; Magenta – SOCS3, Green – GFP, Blue – DAPI. Scale bar 50 μm. (F) Quantification of mean fluorescence intensity of SOCS3 per crypt, n=3 mice per group.

4.3.4. *AhR KO enhances the expression of SOCS3.*

We further investigated the mechanism by which AhR KO decreased the response of colonic epithelial cells to IL-22, by examining the expression of each member of the canonical IL-22 signaling pathway. Assessment of RNAseq data from sorted colonic GFP^{hi} stem and GFP^{low} progenitor cells, revealed that Socs3 expression was upregulated in AhR KO mice, while the expression of other members remained unaltered. qPCR was performed to confirm the expression of Socs3 expression in sorted colonic stem/progenitor cells. We found that Socs3 expression was upregulated in AhR KO mouse colonic stem and progenitor cells, respectively (**Fig. 29A&B**). In addition, AhR activation by TCDD decreased the expression of Socs3 in AhR WT organoids, while AhR KO organoids increased the expression of Socs3. TCDD had no effect on Socs3 expression in AhR KO organoids (**Fig. 29C**). Effects on the protein level of SOCS3 were consistent with mRNA expression in organoids (**Fig. 29D**). Immunostaining of SOCS3 revealed that SOCS3 was widely expressed in all colonic epithelial cells, and AhR KO upregulated SOCS3 expression *in vivo* (**Fig. 29E&F**).

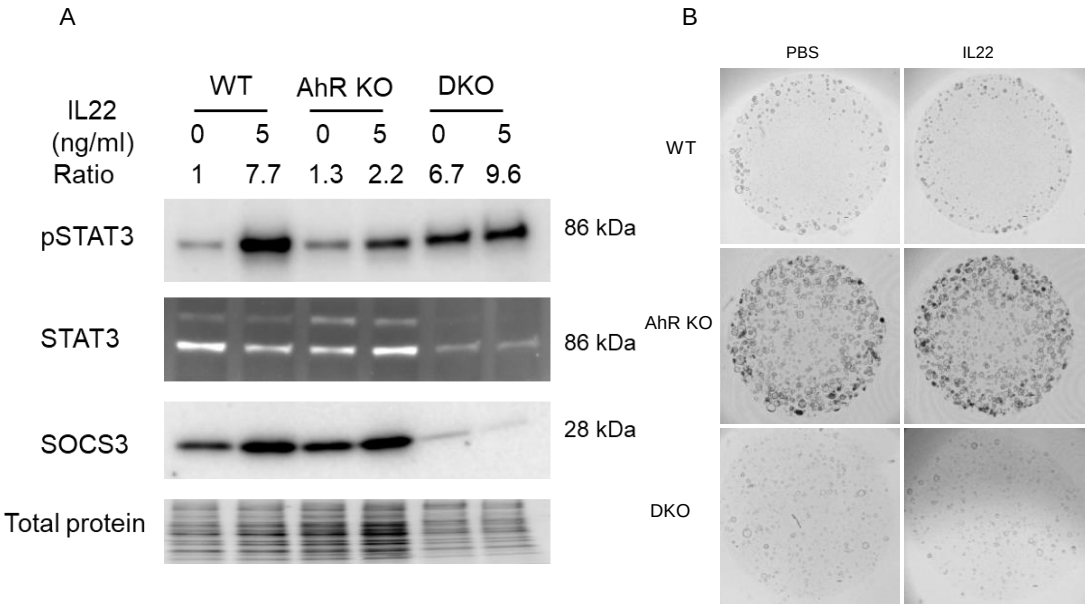

Figure 30. SOCS3 deletion constitutively activates STAT3 and reduces organoid growth.
(A) Representative immunoblot for pSTAT3 at Tyr705, STAT3 and SOCS3. STAT3 was constitutively activated upon SOCS3 deletion. The ratio represents normalized fold change of pSTAT3 to total protein. DKO: AhR and SOCS3 double KO. (B) Representative brightfield images of organoid growth. Activated STAT3 reduced organoid growth. Scale bar 200 μm.

4.3.5. Loss of SOCS3 potentiates pSTAT3 level and inhibits organoid growth.

Next, we determined whether the enhanced expression of SOCS3 was attributed to diminished IL-22 responsiveness in the AhR KO cells. For this purpose, CRISPR-Cas9 was utilized to delete SOCS3 expression in AhR KO organoids. SOCS3 and AhR double KO (DKO) clones were validated by immunoblotting (**Fig. 30A**). SOCS3 KO dramatically enhanced the basal phosphorylation of STAT3 (without IL-22 treatment), which was comparable with WT and DKO organoids treated with IL-22 (**Fig. 30A**). SOCS3 deletion or IL-22 treatment did not affect the protein level of total STAT3 (**Fig. 30A**). Since DKO organoids restored pSTAT3 to a level comparable to IL-22 treated WT organoids, we also assessed the effects of SOCS3 KO on organoid growth in the presence or absence of IL-22 treatment. As expected, IL-22 treatment decreased WT organoid growth, but had no obvious effect on AhR KO organoids (**Fig. 30B**). Importantly, SOCS3 KO remarkably inhibited AhR KO organoid growth, including organoid number and size, and additional IL-22 treatment did not cause notable changes in DKO organoids (**Fig. 30B**). Finally, pSTAT3 was similar between PBS and IL-22 treatment in DKO organoids. Overall, this underscores that SOCS3 plays an important role in suppressing the phosphorylation of STAT3, and enhanced SOCS3 expression contributed to the diminished response to IL-22 in AhR KO organoids.

4.4. Discussion

Previous studies have focused on the ability of AhR signaling to regulate IL-22 production in intestinal immune cells, e.g., innate lymphocytes[87,143,148,150]. This supports the hypothesis that AhR signaling ensures the on-demand production of IL-22 by

immune cells, thereby indirectly affecting IECs, the ultimate effector cells of IL-22 signaling[241,242]. In this study, we provide evidence demonstrating that loss of mucosal epithelial AhR signaling leads to an impaired response of colonic stem/progenitor cells to IL-22 signaling. The impaired response by IECs to IL-22 was in part mediated via upregulation of SOCS3 expression, an important negative regulator of IL-22 receptor-mediated STAT3 activation[243,244]. These data reveal a novel homeostatic control circuit by which AhR signaling regulates the response of colonic stem cells to IL-22.

IL-22 along with IL-10, can act as anti-inflammatory cytokines, and play an important role in mitigating inflammation, pathogen defense and promoting tissue regeneration. One of the hallmarks of IL-22 signaling is to induce the expression of anti-microbial peptides, such as Reg3b, Reg3g, β-defensin, and serum amyloid A, to enable the host to defend against pathogen invasion[245,246]. Interestingly, intestinal specific AhR KO mice exhibit increased susceptibility to C. rodentium infection[133], and IL-22 plays a crucial role in the early phase of host defense against C. rodentium[247], which is consistent with our findings that intestinal-specific AhR KO suppresses IEC responsiveness to IL-22 signaling. However, in a previous study, IL-22 and Reg3g levels were elevated in intestinal specific AhR KO mice[133], suggesting the contribution of a secondary response to impaired IL-22 signaling due to increased bacterial loads in the host. In addition, IL-22 signaling can also serve a protective role in some pathological conditions. For example, neutralizing IL-22 signaling by anti-IL22 antibody suppressed recovery from dextran sodium sulphate (DSS)-induced colitis, while IL-22 delivery promoted crypt regeneration and recovery from DSS[234,248,249]. Since IL-22R1 is not expressed in

immune cells, IL-22 treatment does not affect immune cell activity and therefore might be an ideal therapeutic strategy for acute inflammatory diseases[250,251].

IL-22 signaling promotes ISC recovery in graft vs. host disease (GVHD) mediated tissue damage[232,252,253], and loss of ISCs in IL-22 deficient recipient mice with GVHD exacerbates disease progression relative to WT mice due to increased ISC apoptosis[253]. In addition, Lindemans et al. reported that IL-22 directly promoted ISC expansion and epithelial regeneration after allogeneic bone marrow transplantation or GVHD[232]. They found that IL-22 induced STAT3 phosphorylation in ISCs and promoted cell proliferation and organoid growth *in vitro*. Collectively, these reports suggest that IL-22 is an intestinal stem cell growth factor[252]. In contrast, our results in healthy mice suggest that in certain contexts, IL-22 treatment decreases colonic stem cells and secondary organoid formation and inhibits organoid growth in a dose-dependent manner. These findings are consistent with recent studies that IL-22 treatment downregulated Wnt and Notch signaling pathways, and consequently decreased the intestinal stem cell pools[236,240]. Thus, the effect of IL-22 may be dependent on organoid culture medium and organoid source. Zha et al. found that IL-22 promoted jejunal- and ileal-derived organoids in medium without Wnt3a, while suppressing jejunal derived organoid growth in medium containing Wnt3a[240], which was utilized to culture colonic organoids in our study. In addition, emerging studies indicate that IL-22 does not promote ISC proliferation but spares progenitor cell proliferation[236,240]. Further work is still needed to clarify the selective effect of IL-22 on different cell types. Several

mechanisms are proposed to account for IL-22 mediated cell proliferation, including pERK1/2, pSTAT1/3/5, and Reg3b[232,238,241,254].

IL-22 was recently implicated in the initiation of the DDR induced by genotoxic stress, such as radiation and carcinogen[143]. Since global AhR KO mice exhibit an increase in DNA adducts and colitis-associated colon tumorigenesis after exposure to carcinogen AOM[132], we hypothesized that this enhanced susceptibility may be explained by the impairment of IL-22 signaling following the loss of AhR KO. Indeed, we found that intestinal specific AhR KO desensitized the response of colonic epithelial cells to IL-22 signaling, thereby leading to unwanted accumulation of damaged cells due to defective DNA damage response. In addition, our lab and another group showed that intestinal specific AhR KO also promoted carcinogen or colitis associated colon tumor growth, even though the immune system was not affected. Interestingly, loss of Apc function can also render intestinal epithelial cells resistant to IL-22 signaling[255]. In addition, Gronke et al found that ATM serine/threonine kinase (ATM) was the main downstream target of IL-22-pSTAT3 following radiation or carcinogen exposure[143]. However, we did not detect a change in the expression of Atm in response to IL-22 signaling. These findings lay the foundation for future studies aiming to determine how AhR status, biological context and cell type shape the response to IL-22.

In summary, our study identified a new mechanism linking the AhR-SOCS3-pSTAT3 signaling axis in colonic Lgr5^{+} stem cells. SOCS3 constitutes one of the most important negative feedback pathways to regulate IL-22 signaling strength and duration. SOCS3

itself is a STAT3 downstream target, and thus provides transcription-dependent negative feedback regulation. In addition, a N-terminal kinase inhibitory region (KIR) in SOCS3 resembles a JAK substrate, and can directly bind to JAK, resulting in inhibition of JAK's catalytic activity[256,257]. In line with previous studies that increased pSTAT3 levels are detected in the colonic epithelium of intestinal cell specific SOCS3 KO mice[258], while SOCS3 overexpression decreased pSTAT3[259,260], we found that loss of SOCS3 increased pSTAT3 level even in the absence of exogenous IL-22 in AhR KO organoids. In addition, restoring pSTAT3 levels in AhR KO organoids by deleting SOCS3 rescued AhR KO mediated organoid growth. The regulation of the AhR-SOCS3-pSTAT3 axis has also been identified in other tissues, such as liver and kidney[261,262]. Interestingly, SOCS3 is a direct transcriptional target of AhR in the liver[262]. In addition to inhibition of pSTAT3, SOCS3 is also involved in other signaling pathways, including inhibition of pSTAT1, degradation of indoleamine dioxygenase, NF-κB, insulin receptor, insulin receptor substrate-1, and inhibition of Smad3 nucleus translocation[244,263]. It is therefore possible that AhR signaling could affect multiple SOCS3-regulated signaling pathways. In addition to IL-22, several other cytokines can induce the phosphorylation of STAT3, including IL-6, IL-11, gp130, IL-27, and LIF[244]. Whether AhR KO decreases the response of colonic epithelial cells to those cytokines via the upregulation of SOCS3 expression remains to be determined. This is noteworthy, because an array of cytokines, such as IL-6, IL-10, IL-17, IL-22, and TNF-α, are elevated in subjects with IBD[142]. In conclusion, our findings suggest that AhR signaling modulates the response of colonic epithelial cells to IL-22, providing rationale for targeting AhR as a means of ameliorating IBD and reducing colon cancer risk.

5. CONCLUSIONS

5.1. Summary

The AhR, an ancestral transcription factor, is evolutionarily conserved in metazoans. In the past several decades, advances in studies on AhR biology have extended its initially identified function in response to toxic polychlorinated aromatic hydrocarbons to its roles in the development of chemosensory and neural systems, immunity regulation and beyond. Recently, major progress has been made in linking AhR signaling to the self-renewal and differentiation of stem cells, including embryonic stem cells, hematopoietic stem cells, neural progenitor cells, and intestinal stem cells, implying that AhR signaling plays an important role in maintaining tissue homeostasis, regeneration post injury and tumorigenesis.

Previous studies have demonstrated that global AhR KO promotes colon tumorigenesis in $Apc^{Min/+}$ or AOM/DSS treated mice[131,132]. However, AhR signaling is required for the development of many immune cells, and AhR null mice exhibit impaired immune responses[95,264]. Hence, it is unknown as to whether the increased colon tumorigenesis observed in AhR null mice is due to globally dysregulated immune and metabolic systems, or direct effects on intestinal epithelial cells. Importantly, dysregulated intestinal stem cells are highly susceptible to colon tumorigenesis[122]. Even though Metidji et al reported that intestinal epithelial cell specific AhR KO increases intestinal stem cell proliferation possibly by transcriptional regulation of Rnf43 and Znrf3, negative regulators of the Wnt-β-catenin pathway, and increased colon tumorigenesis[133], the mechanistic insights regarding how AhR signaling regulates

intestinal stem cells still remains ill-defined. By using intestinal stem cell or intestinal epithelial cell specific AhR KO mouse models, we demonstrate for the first time that AhR signaling plays a crucial role in regulating the dynamics and functionality of colonic stem/progenitor cells and consequently colonic tumorigenesis via multiple mechanisms.

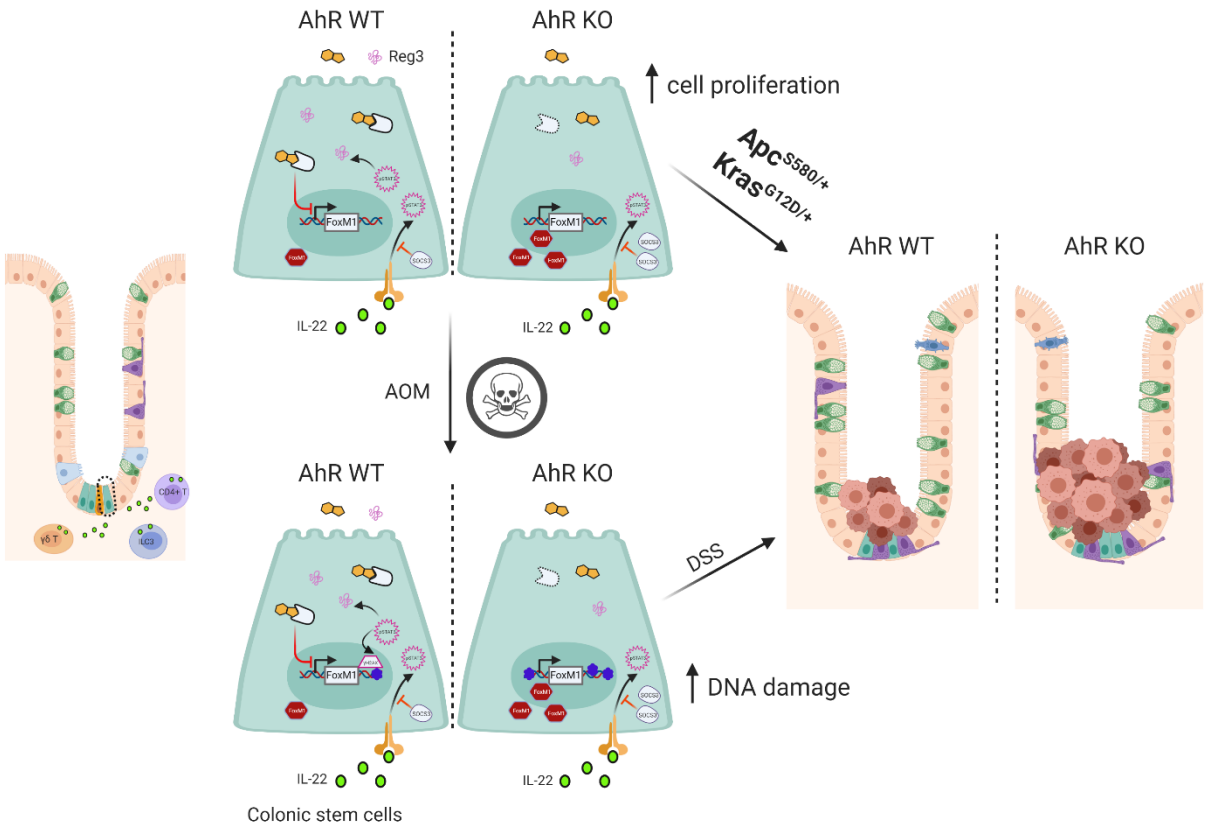

Figure 31. Illustrative summary of the regulation of AhR signaling in relation to colon tumorigenesis.
Colonic stem or progenitor cells reside in the lower basal region of crypts. Upon diet or gut microbiota derived AhR ligand binding, AhR shuttles into the nucleus from the cytosol, and associates with the FoxM1 promoter, inhibiting its expression. Consequently, AhR knockout promotes the expression of FoxM1, and increases colonic stem cell proliferation. In addition, AhR activation inhibits the expression of SOCS3, a negative regulator of IL-22 signaling, resulting in the induction of pSTAT3. Following exposure to genotoxic stress induced by a carcinogen (azoxymethane, AOM), pSTAT3 is required to effectively initiate DNA damage repair response and induces the formation of γH2AX, resulting in clearance of DNA adducts. Hence, increased cell proliferation and accumulated DNA damage collectively contribute to increased colitis-associated colon tumorigenesis in AhR KO mice. Moreover, AhR deletion also promotes colon tumorigenesis in mice carrying $Apc^{S580/+}$; $Kras^{G12D/+}$ mutations, which are the most common genetic mutations in sporadic and hereditary colorectal cancer. Created with BioRender.com.

The inducible deletion of AhR in Lgr5^{+} stem cells increased the percentage of colonic stem cells and enhanced organoid initiating capacity and growth of sorted stem and progenitor cells, while AhR activation had the opposite effect. Moreover, intestine-specific AhR knockout increased basal stem cell and crypt injury-induced cell proliferation and promoted AOM/DSS-induced colon tumor growth. RNAseq data from sorted stem and progenitor cells revealed that AhR KO increased the expression level of FoxM1 signaling pathway genes, which drive cell cycle progression and cell proliferation. Further analysis revealed that AhR transcriptionally suppressed FoxM1 expression. Importantly, activation of AhR in human organoids recapitulated the phenotypes observed in mice, e.g., reduction in the percentage of colonic stem cells, promotion of stem cell differentiation, and attenuation of FoxM1 signaling. This is noteworthy, because FoxM1 expression is upregulated and associated with poor prognosis in various different cancer types[265]. Interestingly, only 12 FoxM1 somatic mutations were detected in 13 out of 400 individuals with CRC, and 19 AhR mutations were detected in 14 out of 400 CRC patients (https://portal.gdc.cancer.gov/). Therefore, it is unlikely that FoxM1 or AhR somatic mutations are associated with colon tumorigenesis. Collectively, these findings suggest that AhR expression levels and/or ligand availablity modulate colon tumorigenesis risk.

Recent elegant work indicates that IL-22 signaling is required to efficiently initiate carcinogen (AOM) induced DNA damage response, and IL-22 receptor deficient mice develop more AOM/DSS induced colon tumors[143]. In addition, AhR whole body null mice exhibit a reduction in IL-22 levels along with increased DNA adducts in response

to AOM[132,150]. Numerous studies have focused on the ability of AhR signaling to regulate IL-22 production in intestinal immune cells, e.g., innate lymphocytes[266], however, the colonic epithelial cell specific role of AhR signaling on IL-22-dependent responses remains poorly defined. Our study provides evidence demonstrating that AhR KO suppresses DNA damage repair resulting in the accumulation of DNA mutations in colonic stem cells in response to carcinogen (AOM), which contributes to the promotion of AOM/DSS-induced colon tumorigenesis. We also found that AhR KO impairs the responsiveness of colonic stem cells to IL-22 signaling, reducing pSTAT3 levels, the induction of anti-microbial peptides Reg3b/g, and attenuating IL-22 mediated stem cell loss and cell proliferation. Moreover, deletion of AhR decreased the expression of p21 and Puma, which are critical mediators regulating stem cell cycle arrest and apoptosis and the accumulation of DNA mutations. From a mechanistic perspective, AhR KO results in the upregulation of SOCS3 expression, which is a negative regulator of IL-22 signaling, and deletion of SOCS3 robustly increases the phosphorylation of STAT3, and reduces organoid growth in AhR KO organoids, which phenocopies IL-22 treatment in WT counterparts. Therefore, the increased stem cell proliferation induced via upregulation of FoxM1 signaling and defective DNA damage repair in combination with the elevation of SOCS3 expression, contribute to the increased risk of colon tumorigenesis in intestinal epithelial cell specific AhR KO mice.

Following CRC progression, several driver genes are sequentially mutated. Tumor suppressor gene Apc and oncogenic Kras are the most frequently mutated genes, in which approximately 80% of sporadic CRC patients harbor at least one inactivating Apc mutation[209], and 30~50% of CRC have oncogenic Kras mutation[14]. Therefore, in

contrast to the AOM/DSS-induced tumor model in which a battery of genes are randomly mutated, a genetic tumor model provides precise insight into the role of AhR signaling during human CRC progression. To this end, intestinal targeted $Apc^{S580/+}$; $Kras^{G12D/+}$ mice in the presence (double mutants) or absence (triple mutants) of AhR were utilized in our study. Our findings reveal that triple mutants further promote the organoid forming efficiency and growth of colonic stem and progenitor cells, and increase cell proliferation *in vivo*, compared with double mutant controls (AhR WT). Importantly, triple mutant organoids are capable of growing independently of Wnt3a, R-spondin1, and EGF growth factors, which were required for WT or double mutant organoids. In addition, AhR KO potentiated Wnt and EGF signaling in organoids, compared with double mutants. Consequently, triple mutant compound mice promoted cecum and colon tumorigenesis. In addition, suppression of Wnt signaling by inactivating one allele of Lgr5 dramatically reduced colon tumorigenesis and attenuated AhR KO effects. Hence, to our knowledge, this is the first report indicating that loss of AhR promotes cecum and colon tumorigenesis in mice carrying $Apc^{S580/+}$; $Kras^{G12D/+}$ mutations in part by upregulating Wnt signaling. This is noteworthy, because the composition of microbiota following colorectal cancer progression is altered, and reduced AhR ligands are observed in IBD patients[61,81,229], which represents a high risk CRC population. Therefore, it is possible that impaired AhR signaling during CRC progression might provide a positive loop to drive colon tumor growth. Collectively, our study provides rationale for targeting AhR as a new therapeutic strategy for colon cancer prevention and treatment.

5.2. Future work

The research presented defines the role of AhR signaling in terms of effects on the homeostasis of colonic stem/progenitor cells in relation to colonic tumorigenesis. AhR is ubiquitously expressed across different tissues and has been shown to affect the self-renewal and differentiation of stem cells in various target tissues, e.g., embryonic stem cells, hematopoietic stem cells, neuronal stem cells and intestinal stem cells. In future studies, it will be interesting to determine whether the regulation of FoxM1 expression by AhR is a universal principle to govern stem cell proliferation. If not, what is the underlying mechanism by which AhR signaling is capable of interacting with different signaling pathways in different stem cells? This is a very challenging scientific question, to determine what confers AhR functionality in a cellular context dependent way. It is also intriguing to explore the mechanisms by which AhR activation can either promote or suppress the expression of downstream targets, which essentially is a common characteristic of a transcription factor. An inibitory DRE was identified in the promoter region of select AhR targets, such as cathepsin D and Hsp27[267,268]. It will be interesting to determine whether inhibitory DREs exsist in the promoter region of AhR suppressive downstream targets, such as FoxM1 and SOCS3, even though the core requirement for inhibitory DREs is still not clear. In addition, previous studies indicate that AhR activation reduces Wnt signaling[131,133], and suppresses carcinogen AOM or AOM/DSS induced colon tumorigenesis and intestinal tumorigenesis in $Apc^{Min/+}$ mice[131-133]. Two mechanisms have been proposed regarding the attenuation of Wnt signaling. First, AhR acts as a ligand activated E3 ligase and could ubiquitinate β-catenin, the main effector of Wnt signaling, for subsequent proteasomal degradation[14,131]. However, it is

controversial regarding β-catenin degradation, since a recent study showed that the complex of AhR, Arnt, β-catenin, CUL4B and DDB1 could not be confirmed, and AhR activation did not increase β-catenin ubiquitination and degradation[220]. Secondly, AhR directly controls the expression of Wnt- β-catenin negative regulator, Rnf43, and AhR activation increases Rnf43 expression, leading to dampened Wnt signaling[133]. In our lab, we found that AhR KO did not alter Wnt signaling homeostasis under basal conditions, but upregulated Wnt signaling in organoids or mice carrying $Apc^{S580/+}$; $Kras^{G12D/+}$ mutations. Therefore, the investigation into the relationship between AhR and Wnt signaling warrants further investigation. In addition, we found that HACKG organoids can grow independently of growth factors Wnt3a, R-spondin1, and EGF, while ACKG organoids did not survive in the absence of growth factors. It is therefore worthwhile to determine the molecular mechanisms by which additional AhR KO allows colonocytes to bypass the need for select growth factors in an $Apc^{S580/+}$; $Kras^{G12D/+}$ background. Finally, we found that AhR KO reduced the phosphorylation of STAT3 upon IL-22 treatment by upregulating the expression of SOCS3. However, several cytokines, including IL-6 and IL-11 are also able to induce pSTAT3[244]. Hence, it is important to determine whether AhR signaling can affect the response of colonic stem cells to cytokines capable of inducing pSTAT3. These proposed studies will continue to probe the role of AhR signaling in the colon tumorigenesis field.

REFERENCES

1 Poland., A. & Glover, E. Stereospecific, high affinity binding of 2,3,7,8-tetrachlorodibenzo-p-dioxin by hepatic cytosol. Evidence that the binding species is receptor for induction of aryl hydrocarbon hydroxylase. *J Biol Chem* **251**, 4936-4946 (1976).

2 Lucier, G. W. *et al.* TCDD-induced changes in rat liver microsomal enzymes. *Environmental health perspectives* **5**, 199-209, doi:10.1289/ehp.7305199 (1973).

3 Petrulis, J. R., Kusnadi, A., Ramadoss, P., Hollingshead, B. & Perdew, G. H. The hsp90 Co-chaperone XAP2 alters importin beta recognition of the bipartite nuclear localization signal of the Ah receptor and represses transcriptional activity. *J Biol Chem* **278**, 2677-2685, doi:10.1074/jbc.M209331200 (2003).

4 Soshilov, A. & Denison, M. S. Role of the Per/Arnt/Sim domains in ligand-dependent transformation of the aryl hydrocarbon receptor. *The Journal of biological chemistry* **283**, 32995-33005, doi:10.1074/jbc.M802414200 (2008).

5 Denison, M. S., Soshilov, A. A., He, G., DeGroot, D. E. & Zhao, B. Exactly the Same but Different: Promiscuity and Diversity in the Molecular Mechanisms of Action of the Aryl Hydrocarbon (Dioxin) Receptor. *Toxicological Sciences* **124**, 1-22, doi:10.1093/toxsci/kfr218 (2011).

6 Li, S., Pei, X., Zhang, W., Xie, H. Q. & Zhao, B. Functional analysis of the dioxin response elements (DREs) of the murine CYP1A1 gene promoter: beyond the core DRE sequence. *Int J Mol Sci* **15**, 6475-6487, doi:10.3390/ijms15046475 (2014).

7 Matikainen, T. *et al.* Aromatic hydrocarbon receptor-driven Bax gene expression is required for premature ovarian failure caused by biohazardous environmental chemicals. *Nat Genet* **28**, 355-360, doi:10.1038/ng575 (2001).

8 Cheng, J. *et al.* Tryptophan derivatives regulate the transcription of Oct4 in stem-like cancer cells. *Nat Commun* **6**, 7209, doi:10.1038/ncomms8209 (2015).

9 Yang, X. *et al.* The aryl hydrocarbon receptor constitutively represses c-myc transcription in human mammary tumor cells. *Oncogene* **24**, 7869-7881, doi:10.1038/sj.onc.1208938 (2005).

10 Stanford, E. A. *et al.* The role of the aryl hydrocarbon receptor in the development of cells with the molecular and functional characteristics of cancer stem-like cells. *BMC Biol* **14**, 20, doi:10.1186/s12915-016-0240-y (2016).

11 Davarinos, N. A. & Pollenz, R. S. Aryl Hydrocarbon Receptor Imported into the Nucleus following Ligand Binding Is Rapidly Degraded via the Cytosplasmic Proteasome following Nuclear Export. *Journal of Biological Chemistry* **274**, 28708-28715, doi:10.1074/jbc.274.40.28708 (1999).

12 Huang, G. & Elferink, C. J. A novel nonconsensus xenobiotic response element capable of mediating aryl hydrocarbon receptor-dependent gene expression. *Mol Pharmacol* **81**, 338-347, doi:10.1124/mol.111.075952 (2012).

13 Wilson, S. R., Joshi, A. D. & Elferink, C. J. The tumor suppressor Kruppel-like factor 6 is a novel aryl hydrocarbon receptor DNA binding partner. *J Pharmacol Exp Ther* **345**, 419-429, doi:10.1124/jpet.113.203786 (2013).

14 Ohtake, F. *et al.* Dioxin receptor is a ligand-dependent E3 ubiquitin ligase. *Nature* **446**, 562-566, doi:10.1038/nature05683 (2007).

15 Xie, G., Peng, Z. & Raufman, J. P. Src-mediated aryl hydrocarbon and epidermal growth factor receptor cross talk stimulates colon cancer cell proliferation. *Am J Physiol Gastrointest Liver Physiol* **302**, G1006-1015, doi:10.1152/ajpgi.00427.2011 (2012).

16 Huang, N. *et al.* Crystal structure of the heterodimeric CLOCK:BMAL1 transcriptional activator complex. *Science* **337**, 189-194, doi:10.1126/science.1222804 (2012).

17 Lahvis, G. P. *et al.* The aryl hydrocarbon receptor is required for developmental closure of the ductus venosus in the neonatal mouse. *Mol Pharmacol* **67**, 714-720, doi:10.1124/mol.104.008888 (2005).

18 Walisser, J. A., Glover, E., Pande, K., Liss, A. L. & Bradfield, C. A. Aryl hydrocarbon receptor-dependent liver development and hepatotoxicity are mediated by different cell types. *Proc Natl Acad Sci U S A* **102**, 17858-17863, doi:10.1073/pnas.0504757102 (2005).

19 Huffman, J. L., Mokashi, A., Bächinger, H. P. & Brennan, R. G. The Basic Helix-Loop-Helix Domain of the Aryl Hydrocarbon Receptor Nuclear Transporter (ARNT) Can Oligomerize and Bind E-box DNA Specifically. *Journal of Biological Chemistry* **276**, 40537-40544, doi:10.1074/jbc.M105675200 (2001).

20 Seok, S.-H. *et al.* Structural hierarchy controlling dimerization and target DNA recognition in the AHR transcriptional complex. *Proceedings of the National Academy of Sciences* **114**, 5431-5436, doi:10.1073/pnas.1617035114 (2017).

21 Wu, D., Potluri, N., Kim, Y. & Rastinejad, F. Structure and dimerization properties of the aryl hydrocarbon receptor PAS-A domain. *Molecular and cellular biology* **33**, 4346-4356, doi:10.1128/MCB.00698-13 (2013).

22 Schulte, K. W., Green, E., Wilz, A., Platten, M. & Daumke, O. Structural Basis for Aryl Hydrocarbon Receptor-Mediated Gene Activation. *Structure* **25**, 1025-1033.e1023, doi:https://doi.org/10.1016/j.str.2017.05.008 (2017).

23 Emmons, R. B. *et al.* The spineless-aristapedia and tango bHLH-PAS proteins interact to control antennal and tarsal development in Drosophila. *Development* **126**, 3937-3945 (1999).

24 Powell-Coffman, J. A., Bradfield, C. A. & Wood, W. B. Caenorhabditis elegans orthologs of the aryl hydrocarbon receptor and its heterodimerization partner the aryl hydrocarbon receptor nuclear translocator. *Proc Natl Acad Sci U S A* **95**, 2844-2849, doi:10.1073/pnas.95.6.2844 (1998).

25 Kumar, M. B., Ramadoss, P., Reen, R. K., Vanden Heuvel, J. P. & Perdew, G. H. The Q-rich Subdomain of the Human AhReceptor Transactivation Domain Is Required for Dioxin-mediated Transcriptional Activity. *Journal of Biological Chemistry* **276**, 42302-42310, doi:10.1074/jbc.M104798200 (2001).

26 Tkachenko, A. *et al.* The Q-rich/PST domain of the AHR regulates both ligand-induced nuclear transport and nucleocytoplasmic shuttling. *Sci Rep* **6**, 32009, doi:10.1038/srep32009 (2016).

27 Flaveny, C., Reen, R. K., Kusnadi, A. & Perdew, G. H. The mouse and human Ah receptor differ in recognition of LXXLL motifs. *Arch Biochem Biophys* **471**, 215-223, doi:10.1016/j.abb.2008.01.014 (2008).

28 Flaveny, C. A., Murray, I. A. & Perdew, G. H. Differential gene regulation by the human and mouse aryl hydrocarbon receptor. *Toxicol Sci* **114**, 217-225, doi:10.1093/toxsci/kfp308 (2010).

29 Jackson, D. P., Joshi, A. D. & Elferink, C. J. Ah Receptor Pathway Intricacies; Signaling Through Diverse Protein Partners and DNA-Motifs. *Toxicology research* **4**, 1143-1158, doi:10.1039/c4tx00236a (2015).

30 Safe, S. Polychlorinated biphenyls (PCBs), dibenzo-p-dioxins (PCDDs), dibenzofurans (PCDFs), and related compounds: environmental and mechanistic considerations which support the development of toxic equivalency factors (TEFs). *Critical reviews in toxicology* **21**, 51-88, doi:10.3109/10408449009089873 (1990).

31 Bradfield, C. A. & Poland, A. A competitive binding assay for 2,3,7,8-tetrachlorodibenzo-p-dioxin and related ligands of the Ah receptor. *Mol Pharmacol* **34**, 682-688 (1988).

32 Denison, M. S. & Faber, S. C. And Now for Something Completely Different: Diversity in Ligand-Dependent Activation of Ah Receptor Responses. *Curr Opin Toxicol* **2**, 124-131, doi:10.1016/j.cotox.2017.01.006 (2017).

33 Zhao, B., Degroot, D. E., Hayashi, A., He, G. & Denison, M. S. CH223191 is a ligand-selective antagonist of the Ah (Dioxin) receptor. *Toxicol Sci* **117**, 393-403, doi:10.1093/toxsci/kfq217 (2010).

34 Soshilov, A. A. & Denison, M. S. Ligand promiscuity of aryl hydrocarbon receptor agonists and antagonists revealed by site-directed mutagenesis. *Molecular and cellular biology* **34**, 1707-1719, doi:10.1128/mcb.01183-13 (2014).

35 Flaveny, C. A., Murray, I. A., Chiaro, C. R. & Perdew, G. H. Ligand selectivity and gene regulation by the human aryl hydrocarbon receptor in transgenic mice. *Mol Pharmacol* **75**, 1412-1420, doi:10.1124/mol.109.054825 (2009).

36 McDougal, A., Wormke, M., Calvin, J. & Safe, S. Tamoxifen-induced antitumorigenic/antiestrogenic action synergized by a selective aryl hydrocarbon receptor modulator. *Cancer Res* **61**, 3902-3907 (2001).

37 Safe, S., Han, H., Goldsby, J., Mohankumar, K. & Chapkin, R. S. Aryl hydrocarbon receptor (AhR) ligands as selective AhR modulators: Genomic studies. *Curr Opin Toxicol* **11-12**, 10-20, doi:https://doi.org/10.1016/j.cotox.2018.11.005 (2018).

38 Katzenellenbogen, J. A., O'Malley, B. W. & Katzenellenbogen, B. S. Tripartite steroid hormone receptor pharmacology: interaction with multiple effector sites as a basis for the cell- and promoter-specific action of these hormones. *Mol Endocrinol* **10**, 119-131, doi:10.1210/mend.10.2.8825552 (1996).

39 Hahn, M. E., Karchner, S. I. & Merson, R. R. Diversity as Opportunity: Insights from 600 Million Years of AHR Evolution. *Curr Opin Toxicol* **2**, 58-71, doi:10.1016/j.cotox.2017.02.003 (2017).

40 Butler, R. A., Kelley, M. L., Powell, W. H., Hahn, M. E. & Van Beneden, R. J. An aryl hydrocarbon receptor (AHR) homologue from the soft-shell clam, Mya arenaria: evidence that invertebrate AHR homologues lack 2,3,7,8-tetrachlorodibenzo-p-dioxin and beta-naphthoflavone binding. *Gene* **278**, 223-234 (2001).

41 Huang, X., Powell-Coffman, J. A. & Jin, Y. The AHR-1 aryl hydrocarbon receptor and its co-factor the AHA-1 aryl hydrocarbon receptor nuclear translocator specify GABAergic neuron cell fate in C. elegans. *Development* **131**, 819-828, doi:10.1242/dev.00959 (2004).

42 Qin, H. & Powell-Coffman, J. A. The Caenorhabditis elegans aryl hydrocarbon receptor, AHR-1, regulates neuronal development. *Developmental Biology* **270**, 64-75, doi:https://doi.org/10.1016/j.ydbio.2004.02.004 (2004).

43 Wernet, M. F. *et al.* Stochastic spineless expression creates the retinal mosaic for colour vision. *Nature* **440**, 174-180, doi:10.1038/nature04615 (2006).

44 Duncan, D. M., Burgess, E. A. & Duncan, I. Control of distal antennal identity and tarsal development inDrosophila by spineless–aristapedia, a homolog of the mammalian dioxin receptor. *Genes & Development* **12**, 1290-1303 (1998).

45 Kim, M. D., Jan, L. Y. & Jan, Y. N. The bHLH-PAS protein Spineless is necessary for the diversification of dendrite morphology of Drosophila dendritic arborization neurons. *Genes Dev* **20**, 2806-2819, doi:10.1101/gad.1459706 (2006).

46 Busbee, P. B., Rouse, M., Nagarkatti, M. & Nagarkatti, P. S. Use of natural AhR ligands as potential therapeutic modalities against inflammatory disorders. *Nutrition reviews* **71**, 353-369, doi:10.1111/nure.12024 (2013).

47 Hubbard, T. D., Murray, I. A. & Perdew, G. H. Indole and Tryptophan Metabolism: Endogenous and Dietary Routes to Ah Receptor Activation. *Drug Metab Dispos* **43**, 1522-1535, doi:10.1124/dmd.115.064246 (2015).

48 Jin, U. H. *et al.* Structure-Dependent Modulation of Aryl Hydrocarbon Receptor-Mediated Activities by Flavonoids. *Toxicol Sci* **164**, 205-217, doi:10.1093/toxsci/kfy075 (2018).

49 Zhang, S., Qin, C. & Safe, S. H. Flavonoids as aryl hydrocarbon receptor agonists/antagonists: effects of structure and cell context. *Environ Health Perspect* **111**, 1877-1882, doi:10.1289/ehp.6322 (2003).

50 Chevolleau, S., Gasc, N., Rollin, P. & Tulliez, J. Enzymatic, Chemical, and Thermal Breakdown of 3H-Labeled Glucobrassicin, the Parent Indole Glucosinolate. *Journal of Agricultural and Food Chemistry* **45**, 4290-4296, doi:10.1021/jf970449k (1997).

51 Barba, F. J. *et al.* Bioavailability of Glucosinolates and Their Breakdown Products: Impact of Processing. *Frontiers in nutrition* **3**, 24, doi:10.3389/fnut.2016.00024 (2016).

52 Wang, S. Q., Cheng, L. S., Liu, Y., Wang, J. Y. & Jiang, W. Indole-3-Carbinol (I3C) and its Major Derivatives: Their Pharmacokinetics and Important Roles in Hepatic Protection. *Current drug metabolism* **17**, 401-409, doi:10.2174/1389200217666151210125105 (2016).

53 Jellinck, P. H. *et al.* Ah receptor binding properties of indole carbinols and induction of hepatic estradiol hydroxylation. *Biochem Pharmacol* **45**, 1129-1136, doi:10.1016/0006-2952(93)90258-x (1993).

54 Denison, M. S. & Nagy, S. R. Activation of the aryl hydrocarbon receptor by structurally diverse exogenous and endogenous chemicals. *Annu Rev Pharmacol Toxicol* **43**, 309-334, doi:10.1146/annurev.pharmtox.43.100901.135828 (2003).

55 Sugihara, K. *et al.* Aryl hydrocarbon receptor-mediated induction of microsomal drug-metabolizing enzyme activity by indirubin and indigo. *Biochemical and biophysical research communications* **318**, 571-578, doi:https://doi.org/10.1016/j.bbrc.2004.04.066 (2004).

56 Sender, R., Fuchs, S. & Milo, R. Revised Estimates for the Number of Human and Bacteria Cells in the Body. *PLOS Biology* **14**, e1002533, doi:10.1371/journal.pbio.1002533 (2016).

57 Paliy, O., Kenche, H., Abernathy, F. & Michail, S. High-Throughput Quantitative Analysis of the Human Intestinal Microbiota with a Phylogenetic Microarray. *Applied and Environmental Microbiology* **75**, 3572-3579, doi:10.1128/aem.02764-08 (2009).

58 Wang, B., Yao, M., Lv, L., Ling, Z. & Li, L. The Human Microbiota in Health and Disease. *Engineering* **3**, 71-82, doi:https://doi.org/10.1016/J.ENG.2017.01.008 (2017).

59 Zhang, Y.-J. *et al.* Impacts of gut bacteria on human health and diseases. *International journal of molecular sciences* **16**, 7493-7519, doi:10.3390/ijms16047493 (2015).

60 Sekirov, I., Russell, S. L., Antunes, L. C. M. & Finlay, B. B. Gut Microbiota in Health and Disease. *Physiological Reviews* **90**, 859-904, doi:10.1152/physrev.00045.2009 (2010).

61 Agus, A., Planchais, J. & Sokol, H. Gut Microbiota Regulation of Tryptophan Metabolism in Health and Disease. *Cell Host Microbe* **23**, 716-724, doi:10.1016/j.chom.2018.05.003 (2018).

62 Geisler, S. *et al.* in *Pteridines* Vol. 26 31 (2015).

63 Wikoff, W. R. *et al.* Metabolomics analysis reveals large effects of gut microflora on mammalian blood metabolites. *Proceedings of the National Academy of Sciences* **106**, 3698-3703, doi:10.1073/pnas.0812874106 (2009).

64 Roager, H. M. & Licht, T. R. Microbial tryptophan catabolites in health and disease. *Nature Communications* **9**, 3294, doi:10.1038/s41467-018-05470-4 (2018).

65 Lee, J. H., Wood, T. K. & Lee, J. Roles of indole as an interspecies and interkingdom signaling molecule. *Trends Microbiol* **23**, 707-718, doi:10.1016/j.tim.2015.08.001 (2015).

66 Karlin, D. A., Mastromarino, A. J., Jones, R. D., Stroehlein, J. R. & Lorentz, O. Fecal skatole and indole and breath methane and hydrogen in patients with large bowel polyps or cancer. *Journal of Cancer Research and Clinical Oncology* **109**, 135-141, doi:10.1007/BF00391888 (1985).

67 Hubbard, T. D. *et al.* Adaptation of the human aryl hydrocarbon receptor to sense microbiota-derived indoles. *Sci Rep* **5**, 12689, doi:10.1038/srep12689 (2015).

68 Lee, J. H. & Lee, J. Indole as an intercellular signal in microbial communities. *FEMS microbiology reviews* **34**, 426-444, doi:10.1111/j.1574-6976.2009.00204.x (2010).

69 Elsden, S. R., Hilton, M. G. & Waller, J. M. The end products of the metabolism of aromatic amino acids by Clostridia. *Archives of microbiology* **107**, 283-288 (1976).

70 Li, G. & Young, K. D. Indole production by the tryptophanase TnaA in Escherichia coli is determined by the amount of exogenous tryptophan. *Microbiology (Reading, England)* **159**, 402-410, doi:10.1099/mic.0.064139-0 (2013).

71 Devlin, A. S. *et al.* Modulation of a Circulating Uremic Solute via Rational Genetic Manipulation of the Gut Microbiota. *Cell Host Microbe* **20**, 709-715, doi:10.1016/j.chom.2016.10.021 (2016).

72 Rui, L., Reardon, K. F. & Wood, T. K. Protein engineering of toluene ortho-monooxygenase of Burkholderia cepacia G4 for regiospecific hydroxylation of indole to form various indigoid compounds. *Applied microbiology and biotechnology* **66**, 422-429, doi:10.1007/s00253-004-1698-z (2005).

73 Williams, Brianna B. *et al.* Discovery and Characterization of Gut Microbiota Decarboxylases that Can Produce the Neurotransmitter Tryptamine. *Cell Host & Microbe* **16**, 495-503, doi:https://doi.org/10.1016/j.chom.2014.09.001 (2014).

74 Zelante, T. *et al.* Tryptophan catabolites from microbiota engage aryl hydrocarbon receptor and balance mucosal reactivity via interleukin-22. *Immunity* **39**, 372-385, doi:10.1016/j.immuni.2013.08.003 (2013).

75 Dodd, D. *et al.* A gut bacterial pathway metabolizes aromatic amino acids into nine circulating metabolites. *Nature* **551**, 648, doi:10.1038/nature24661 (2017).

76 Wlodarska, M. *et al.* Indoleacrylic Acid Produced by Commensal Peptostreptococcus Species Suppresses Inflammation. *Cell Host & Microbe* **22**, 25-37.e26, doi:https://doi.org/10.1016/j.chom.2017.06.007 (2017).

77 Spaepen, S., Vanderleyden, J. & Remans, R. Indole-3-acetic acid in microbial and microorganism-plant signaling. *FEMS microbiology reviews* **31**, 425-448, doi:10.1111/j.1574-6976.2007.00072.x (2007).

78 Zhang, P. *et al.* The Distribution of Tryptophan-Dependent Indole-3-Acetic Acid Synthesis Pathways in Bacteria Unraveled by Large-Scale Genomic Analysis. *Molecules (Basel, Switzerland)* **24**, doi:10.3390/molecules24071411 (2019).

79 Gaweska, H. M., Taylor, A. B., Hart, P. J. & Fitzpatrick, P. F. Structure of the flavoprotein tryptophan 2-monooxygenase, a key enzyme in the formation of galls in plants. *Biochemistry* **52**, 2620-2626, doi:10.1021/bi4001563 (2013).

80 Monteleone, I. *et al.* Aryl hydrocarbon receptor-induced signals up-regulate IL-22 production and inhibit inflammation in the gastrointestinal tract. *Gastroenterology* **141**, 237-248, 248 e231, doi:10.1053/j.gastro.2011.04.007 (2011).

81 Lamas, B. *et al.* CARD9 impacts colitis by altering gut microbiota metabolism of tryptophan into aryl hydrocarbon receptor ligands. *Nat Med*, doi:10.1038/nm.4102 (2016).

82 Natividad, J. M. *et al.* Impaired Aryl Hydrocarbon Receptor Ligand Production by the Gut Microbiota Is a Key Factor in Metabolic Syndrome. *Cell Metab* **28**, 737-749 e734, doi:10.1016/j.cmet.2018.07.001 (2018).

83 Celiberto, L. S. *et al.* Inflammatory bowel disease and immunonutrition: novel therapeutic approaches through modulation of diet and the gut microbiome. *Immunology* **155**, 36-52, doi:10.1111/imm.12939 (2018).

84 Korecka, A. *et al.* Bidirectional communication between the Aryl hydrocarbon Receptor (AhR) and the microbiome tunes host metabolism. *npj Biofilms and Microbiomes* **2**, 16014, doi:10.1038/npjbiofilms.2016.14 (2016).

85 Li, Y. *et al.* Exogenous Stimuli Maintain Intraepithelial Lymphocytes via Aryl Hydrocarbon Receptor Activation. *Cell* **147**, 629-640, doi:10.1016/j.cell.2011.09.025 (2011).

86 Schiering, C. *et al.* Feedback control of AHR signalling regulates intestinal immunity. *Nature* **542**, 242, doi:10.1038/nature21080 (2017).

87 Qiu, J. *et al.* The aryl hydrocarbon receptor regulates gut immunity through modulation of innate lymphoid cells. *Immunity* **36**, 92-104, doi:10.1016/j.immuni.2011.11.011 (2012).

88 Zhang, L. *et al.* Persistent Organic Pollutants Modify Gut Microbiota-Host Metabolic Homeostasis in Mice Through Aryl Hydrocarbon Receptor Activation. *Environ Health Perspect* **123**, 679-688, doi:10.1289/ehp.1409055 (2015).

89 Sun, Y. *et al.* Activation of aryl hydrocarbon receptor by dioxin directly shifts gut microbiota in zebrafish. *Environmental Pollution* **255**, 113357, doi:https://doi.org/10.1016/j.envpol.2019.113357 (2019).

90 Petriello, M. C., Hoffman, J. B., Vsevolozhskaya, O., Morris, A. J. & Hennig, B. Dioxin-like PCB 126 increases intestinal inflammation and disrupts gut microbiota and metabolic homeostasis. *Environmental pollution (Barking, Essex : 1987)* **242**, 1022-1032, doi:10.1016/j.envpol.2018.07.039 (2018).

91 Stedtfeld, R. D. *et al.* TCDD influences reservoir of antibiotic resistance genes in murine gut microbiome. *FEMS microbiology ecology* **93**, doi:10.1093/femsec/fix058 (2017).

92 Busbee, P. B., Nagarkatti, M. & Nagarkatti, P. Indole-3-carbinol ameliorates murine colitis symptoms through alterations in gut microbial composition and metabolomic pathways, particularly through decreasing disease-associated Bacteroides acidifaciens species. *The Journal of Immunology* **198**, 218.218 (2017).

93 Brawner, K. M. *et al.* Depletion of dietary aryl hydrocarbon receptor ligands alters microbiota composition and function. *Scientific Reports* **9**, 14724, doi:10.1038/s41598-019-51194-w (2019).

94 Murray, I. A., Nichols, R. G., Zhang, L., Patterson, A. D. & Perdew, G. H. Expression of the aryl hydrocarbon receptor contributes to the establishment of intestinal microbial community structure in mice. *Scientific Reports* **6**, 33969, doi:10.1038/srep33969 (2016).

95 Gutierrez-Vazquez, C. & Quintana, F. J. Regulation of the Immune Response by the Aryl Hydrocarbon Receptor. *Immunity* **48**, 19-33, doi:10.1016/j.immuni.2017.12.012 (2018).

96 Opitz, C. A. *et al.* An endogenous tumour-promoting ligand of the human aryl hydrocarbon receptor. *Nature* **478**, 197-203, doi:10.1038/nature10491 (2011).

97 Simon, G. *et al.* Serum tryptophan, kynurenine, phenylalanine, tyrosine and neopterin concentrations in 100 healthy blood donors. *Pteridines* **26**, 31-36, doi:https://doi.org/10.1515/pterid-2014-0015 (2015).

98 Novikov, O. *et al.* An Aryl Hydrocarbon Receptor-Mediated Amplification Loop That Enforces Cell Migration in ER-/PR-/Her2- Human Breast Cancer Cells. *Mol Pharmacol* **90**, 674-688, doi:10.1124/mol.116.105361 (2016).

99 Lowe, M. M. *et al.* Identification of cinnabarinic acid as a novel endogenous aryl hydrocarbon receptor ligand that drives IL-22 production. *PLoS One* **9**, e87877, doi:10.1371/journal.pone.0087877 (2014).

100 Fritsche, E. *et al.* Lightening up the UV response by identification of the arylhydrocarbon receptor as a cytoplasmatic target for ultraviolet B radiation. *Proc Natl Acad Sci U S A* **104**, 8851-8856, doi:10.1073/pnas.0701764104 (2007).

101 Banoglu, E., Jha, G. G. & King, R. S. Hepatic microsomal metabolism of indole to indoxyl, a precursor of indoxyl sulfate. *European journal of drug metabolism and pharmacokinetics* **26**, 235-240, doi:10.1007/bf03226377 (2001).

102 Banoglu, E. & King, R. S. Sulfation of indoxyl by human and rat aryl (phenol) sulfotransferases to form indoxyl sulfate. *European journal of drug metabolism and pharmacokinetics* **27**, 135-140, doi:10.1007/bf03190428 (2002).

103 Schroeder, J. C. *et al.* The Uremic Toxin 3-Indoxyl Sulfate Is a Potent Endogenous Agonist for the Human Aryl Hydrocarbon Receptor. *Biochemistry* **49**, 393-400, doi:10.1021/bi901786x (2010).

104 SANDLE, G. I. Salt and water absorption in the human colon: a modern appraisal. *Gut* **43**, 294-299, doi:10.1136/gut.43.2.294 (1998).

105 Barker, N., van Oudenaarden, A. & Clevers, H. Identifying the stem cell of the intestinal crypt: strategies and pitfalls. *Cell Stem Cell* **11**, 452-460, doi:10.1016/j.stem.2012.09.009 (2012).

106 Barker, N. *et al.* Identification of stem cells in small intestine and colon by marker gene Lgr5. *Nature* **449**, 1003-1007, doi:10.1038/nature06196 (2007).

107 Sasaki, N. *et al.* Reg4+ deep crypt secretory cells function as epithelial niche for Lgr5+ stem cells in colon. *Proc Natl Acad Sci U S A*, doi:10.1073/pnas.1607327113 (2016).

108 Gehart, H. & Clevers, H. Tales from the crypt: new insights into intestinal stem cells. *Nature Reviews Gastroenterology & Hepatology* **16**, 19-34, doi:10.1038/s41575-018-0081-y (2019).

109 Snippert, H. J. *et al.* Intestinal crypt homeostasis results from neutral competition between symmetrically dividing Lgr5 stem cells. *Cell* **143**, 134-144, doi:10.1016/j.cell.2010.09.016 (2010).

110 Barker, N., van de Wetering, M. & Clevers, H. The intestinal stem cell. *Genes Dev* **22**, 1856-1864, doi:10.1101/gad.1674008 (2008).

111 van Es, J. H. *et al.* Dll1+ secretory progenitor cells revert to stem cells upon crypt damage. *Nat Cell Biol* **14**, 1099-1104, doi:10.1038/ncb2581 (2012).

112 Tetteh, P. W. *et al.* Replacement of Lost Lgr5-Positive Stem Cells through Plasticity of Their Enterocyte-Lineage Daughters. *Cell Stem Cell* **18**, 203-213, doi:10.1016/j.stem.2016.01.001 (2016).

113 Tetteh, P. W., Farin, H. F. & Clevers, H. Plasticity within stem cell hierarchies in mammalian epithelia. *Trends in Cell Biology* **25**, 100-108, doi:10.1016/j.tcb.2014.09.003 (2015).

114 Bankaitis, E. D., Ha, A., Kuo, C. J. & Magness, S. T. Reserve Stem Cells in Intestinal Homeostasis and Injury. *Gastroenterology* **155**, 1348-1361, doi:10.1053/j.gastro.2018.08.016 (2018).

115 Carlone, D. L. & Breault, D. T. Tales from the crypt: the expanding role of slow cycling intestinal stem cells. *Cell stem cell* **10**, 2-4, doi:10.1016/j.stem.2011.12.012 (2012).

116 Schonhoff, S. E., Giel-Moloney, M. & Leiter, A. B. Minireview: Development and Differentiation of Gut Endocrine Cells. *Endocrinology* **145**, 2639-2644, doi:10.1210/en.2004-0051 (2004).

117 Ueo, T. *et al.* The role of Hes genes in intestinal development, homeostasis and tumor formation. *Development* **139**, 1071-1082, doi:10.1242/dev.069070 (2012).

118 Yang, Q., Bermingham, N. A., Finegold, M. J. & Zoghbi, H. Y. Requirement of Math1 for secretory cell lineage commitment in the mouse intestine. *Science* **294**, 2155-2158, doi:10.1126/science.1065718 (2001).

119 Allaire, J. M. *et al.* Frontline defenders: goblet cell mediators dictate host-microbe interactions in the intestinal tract during health and disease. *American journal of physiology. Gastrointestinal and liver physiology* **314**, G360-G377, doi:10.1152/ajpgi.00181.2017 (2018).

120 Worthington, J. J., Reimann, F. & Gribble, F. M. Enteroendocrine cells-sensory sentinels of the intestinal environment and orchestrators of mucosal immunity. *Mucosal Immunology* **11**, 3-20, doi:10.1038/mi.2017.73 (2018).

121 Kim, E. *et al.* Homeostatic responses of colonic LGR5+ stem cells following acute in vivo exposure to a genotoxic carcinogen. *Carcinogenesis*, doi:10.1093/carcin/bgv250 (2015).

122 Barker, N. *et al.* Crypt stem cells as the cells-of-origin of intestinal cancer. *Nature* **457**, 608-611, doi:10.1038/nature07602 (2009).

123 Knerr, S. & Schrenk, D. Carcinogenicity of 2,3,7,8-tetrachlorodibenzo-p-dioxin in experimental models. *Molecular Nutrition & Food Research* **50**, 897-907, doi:10.1002/mnfr.200600006 (2006).

124 Yi, S. W. & Ohrr, H. Agent Orange exposure and cancer incidence in Korean Vietnam veterans: a prospective cohort study. *Cancer* **120**, 3699-3706, doi:10.1002/cncr.28961 (2014).

125 Pesatori, A. C., Consonni, D., Rubagotti, M., Grillo, P. & Bertazzi, P. A. Cancer incidence in the population exposed to dioxin after the "Seveso accident": twenty years of follow-up. *Environmental health : a global access science source* **8**, 39-39, doi:10.1186/1476-069X-8-39 (2009).

126 Xu, J. *et al.* Association between dioxin and cancer incidence and mortality: a meta-analysis. *Scientific reports* **6**, 38012-38012, doi:10.1038/srep38012 (2016).

127 Warner, M. *et al.* Dioxin exposure and cancer risk in the Seveso Women's Health Study. *Environmental health perspectives* **119**, 1700-1705, doi:10.1289/ehp.1103720 (2011).

128 Baan, R. *et al.* A review of human carcinogens--Part F: chemical agents and related occupations. *The Lancet. Oncology* **10**, 1143-1144 (2009).

129 Safe, S., Lee, S. O. & Jin, U. H. Role of the aryl hydrocarbon receptor in carcinogenesis and potential as a drug target. *Toxicol Sci* **135**, 1-16, doi:10.1093/toxsci/kft128 (2013).

130 Kolluri, S. K., Jin, U. H. & Safe, S. Role of the aryl hydrocarbon receptor in carcinogenesis and potential as an anti-cancer drug target. *Archives of toxicology* **91**, 2497-2513, doi:10.1007/s00204-017-1981-2 (2017).

131 Kawajiri, K. *et al.* Aryl hydrocarbon receptor suppresses intestinal carcinogenesis in ApcMin/+ mice with natural ligands. *Proc Natl Acad Sci U S A* **106**, 13481-13486, doi:10.1073/pnas.0902132106 (2009).

132 Diaz-Diaz, C. J. *et al.* The Aryl Hydrocarbon Receptor is a Repressor of Inflammation-associated Colorectal Tumorigenesis in Mouse. *Ann Surg*, doi:10.1097/SLA.0000000000001874 (2016).

133 Metidji, A. *et al.* The Environmental Sensor AHR Protects from Inflammatory Damage by Maintaining Intestinal Stem Cell Homeostasis and Barrier Integrity. *Immunity*, doi:https://doi.org/10.1016/j.immuni.2018.07.010 (2018).

134 Ikuta, T. *et al.* ASC-associated inflammation promotes cecal tumorigenesis in aryl hydrocarbon receptor-deficient mice. *Carcinogenesis* **34**, 1620-1627, doi:10.1093/carcin/bgt083 (2013).

135 Haggar, F. A. & Boushey, R. P. Colorectal cancer epidemiology: incidence, mortality, survival, and risk factors. *Clin Colon Rectal Surg* **22**, 191-197, doi:10.1055/s-0029-1242458 (2009).

136 Armaghany, T., Wilson, J. D., Chu, Q. & Mills, G. Genetic alterations in colorectal cancer. *Gastrointest Cancer Res* **5**, 19-27 (2012).

137 Ikuta, T., Kurosumi, M., Yatsuoka, T. & Nishimura, Y. Tissue distribution of aryl hydrocarbon receptor in the intestine: Implication of putative roles in tumor suppression. *Exp Cell Res* **343**, 126-134, doi:10.1016/j.yexcr.2016.03.012 (2016).

138 Megna, B. W. *et al.* The aryl hydrocarbon receptor as an antitumor target of synthetic curcuminoids in colorectal cancer. *Journal of Surgical Research* **213**, 16-24, doi:10.1016/j.jss.2017.02.010 (2017).

139 Yin, J. *et al.* The AhR is involved in the regulation of LoVo cell proliferation through cell cycle-associated proteins. *Cell Biol Int* **40**, 560-568, doi:10.1002/cbin.10592 (2016).

140 Yamaguchi, M. & Hankinson, O. 2,3,7,8tetrachlorodibenzopdioxin suppresses the growth of human colorectal cancer cells in vitro: Implication of the aryl hydrocarbon receptor signaling. *Int J Oncol* **54**, 1422-1432, doi:10.3892/ijo.2019.4703 (2019).

141 Sabat, R., Ouyang, W. & Wolk, K. Therapeutic opportunities of the IL-22-IL-22R1 system. *Nat Rev Drug Discov* **13**, 21-38, doi:10.1038/nrd4176 (2014).

142 Strober, W. & Fuss, I. J. Proinflammatory cytokines in the pathogenesis of inflammatory bowel diseases. *Gastroenterology* **140**, 1756-1767, doi:10.1053/j.gastro.2011.02.016 (2011).

143 Gronke, K. *et al.* Interleukin-22 protects intestinal stem cells against genotoxic stress. *Nature* **566**, 249-253, doi:10.1038/s41586-019-0899-7 (2019).

144 Colonna, M. Interleukin-22-producing natural killer cells and lymphoid tissue inducer-like cells in mucosal immunity. *Immunity* **31**, 15-23, doi:10.1016/j.immuni.2009.06.008 (2009).

145 Zindl, C. L. *et al.* IL-22–producing neutrophils contribute to antimicrobial defense and restitution of colonic epithelial integrity during colitis. *Proceedings of the National Academy of Sciences* **110**, 12768, doi:10.1073/pnas.1300318110 (2013).

146 Sonnenberg, G. F. *et al.* Innate lymphoid cells promote anatomical containment of lymphoid-resident commensal bacteria. *Science* **336**, 1321-1325, doi:10.1126/science.1222551 (2012).

147 Esser, C., Rannug, A. & Stockinger, B. The aryl hydrocarbon receptor in immunity. *Trends Immunol* **30**, 447-454, doi:10.1016/j.it.2009.06.005 (2009).

148 Lee, J. S. *et al.* AHR drives the development of gut ILC22 cells and postnatal lymphoid tissues via pathways dependent on and independent of Notch. *Nat Immunol* **13**, 144-151, doi:10.1038/ni.2187 (2012).

149 Mielke, L. A. *et al.* Retinoic acid expression associates with enhanced IL-22 production by γδ T cells and innate lymphoid cells and attenuation of intestinal inflammation. *The Journal of Experimental Medicine* **210**, 1117-1124, doi:10.1084/jem.20121588 (2013).

150 Qiu, J. *et al.* Group 3 innate lymphoid cells inhibit T-cell-mediated intestinal inflammation through aryl hydrocarbon receptor signaling and regulation of microflora. *Immunity* **39**, 386-399, doi:10.1016/j.immuni.2013.08.002 (2013).

151 Singh, N. P. *et al.* Activation of Aryl Hydrocarbon Receptor (AhR) Leads to Reciprocal Epigenetic Regulation of FoxP3 and IL-17 Expression and Amelioration of Experimental Colitis. *PLOS ONE* **6**, e23522, doi:10.1371/journal.pone.0023522 (2011).

152 Quintana, F. J. *et al.* Control of T(reg) and T(H)17 cell differentiation by the aryl hydrocarbon receptor. *Nature* **453**, 65-71, doi:10.1038/nature06880 (2008).

153 Lu, Z. *et al.* MicroRNA 15a/16-1 suppresses aryl hydrocarbon receptor–dependent interleukin-22 secretion in CD4+ T cells and contributes to immune-mediated organ injury. *Hepatology* **67**, 1027-1040, doi:10.1002/hep.29573 (2018).

154 Yeste, A. *et al.* IL-21 induces IL-22 production in CD4+ T cells. *Nature Communications* **5**, 3753, doi:10.1038/ncomms4753 (2014).

155 Hubbard, T. D., Murray, I. A. & Perdew, G. H. Indole and Tryptophan Metabolism: Endogenous and Dietary Routes to Ah Receptor Activation. *Drug Metabolism and Disposition* **43**, 1522-1535, doi:10.1124/dmd.115.064246 (2015).

156 Cheng, Y. *et al.* Aryl Hydrocarbon Receptor Activity of Tryptophan Metabolites in Young Adult Mouse Colonocytes. *Drug Metab Dispos* **43**, 1536-1543, doi:10.1124/dmd.115.063677 (2015).

157 Cheng, Y. *et al.* Editor's Highlight: Microbial-Derived 1,4-Dihydroxy-2-naphthoic Acid and Related Compounds as Aryl Hydrocarbon Receptor Agonists/Antagonists: Structure–Activity Relationships and Receptor Modeling. *Toxicological Sciences* **155**, 458-473, doi:10.1093/toxsci/kfw230 (2016).

158 Jin, U. H. *et al.* Microbiome-derived tryptophan metabolites and their aryl hydrocarbon receptor-dependent agonist and antagonist activities. *Mol Pharmacol* **85**, 777-788, doi:10.1124/mol.113.091165 (2014).

159 Murray, I. A., Patterson, A. D. & Perdew, G. H. Aryl hydrocarbon receptor ligands in cancer: friend and foe. *Nature Reviews Cancer* **14**, 801-814, doi:10.1038/nrc3846 (2014).

160 Díaz-Díaz, C. J. *et al.* The Aryl Hydrocarbon Receptor is a Repressor of Inflammation-associated Colorectal Tumorigenesis in Mouse. *Annals of Surgery* **264**, 429-436, doi:10.1097/sla.0000000000001874 (2016).

161 Benson, J. M. & Shepherd, D. M. Aryl Hydrocarbon Receptor Activation by TCDD Reduces Inflammation Associated with Crohn's Disease. *Toxicological Sciences* **120**, 68-78, doi:10.1093/toxsci/kfq360 (2010).

162 Takamura, T. *et al.* Activation of the aryl hydrocarbon receptor pathway may ameliorate dextran sodium sulfate-induced colitis in mice. *Immunol Cell Biol* **88**, 685-689, doi:10.1038/icb.2010.35 (2010).

163 Furumatsu, K. *et al.* A role of the aryl hydrocarbon receptor in attenuation of colitis. *Dig Dis Sci* **56**, 2532-2544, doi:10.1007/s10620-011-1643-9 (2011).

164 Batlle, E. & Clevers, H. Cancer stem cells revisited. *Nature Medicine* **23**, 1124-1134, doi:10.1038/nm.4409 (2017).

165 Roper, J. *et al.* In vivo genome editing and organoid transplantation models of colorectal cancer and metastasis. *Nature biotechnology* **35**, 569-576, doi:10.1038/nbt.3836 (2017).

166 Gong, X. *et al.* LGR5-Targeted Antibody–Drug Conjugate Eradicates Gastrointestinal Tumors and Prevents Recurrence. *Molecular Cancer Therapeutics* **15**, 1580-1590, doi:10.1158/1535-7163.mct-16-0114 (2016).

167 Tofighi, R. *et al.* Non–Dioxin-like Polychlorinated Biphenyls Interfere with Neuronal Differentiation of Embryonic Neural Stem Cells. *Toxicological Sciences* **124**, 192-201, doi:10.1093/toxsci/kfr221 (2011).

168 Boitano, A. E. *et al.* Aryl hydrocarbon receptor antagonists promote the expansion of human hematopoietic stem cells. *Science* **329**, 1345-1348, doi:10.1126/science.1191536 (2010).

169 Feng, Y. *et al.* Sox9 induction, ectopic Paneth cells, and mitotic spindle axis defects in mouse colon adenomatous epithelium arising from conditional biallelic Apc inactivation. *The American journal of pathology* **183**, 493-503, doi:10.1016/j.ajpath.2013.04.013 (2013).

170 Hardiman, K. M., Liu, J., Feng, Y., Greenson, J. K. & Fearon, E. R. Rapamycin Inhibition of Polyposis and Progression to Dysplasia in a Mouse Model. *PLOS ONE* **9**, e96023, doi:10.1371/journal.pone.0096023 (2014).

171 Madison, B. B. *et al.* Cis elements of the villin gene control expression in restricted domains of the vertical (crypt) and horizontal (duodenum, cecum) axes of the intestine. *J Biol Chem* **277**, 33275-33283, doi:10.1074/jbc.M204935200 (2002).

172 Madisen, L. *et al.* A robust and high-throughput Cre reporting and characterization system for the whole mouse brain. *Nature neuroscience* **13**, 133-140, doi:10.1038/nn.2467 (2010).

173 Gormally, M. V. *et al.* Suppression of the FOXM1 transcriptional programme via novel small molecule inhibition. *Nat Commun* **5**, 5165, doi:10.1038/ncomms6165 (2014).

174 Fan, Y. Y., Davidson, L. A. & Chapkin, R. S. Murine Colonic Organoid Culture System and Downstream Assay Applications. *Methods Mol Biol*, doi:10.1007/7651_2016_8 (2016).

175 Sato, T. *et al.* Single Lgr5 stem cells build crypt-villus structures in vitro without a mesenchymal niche. *Nature* **459**, 262-265, doi:10.1038/nature07935 (2009).

176 Miyoshi, H. & Stappenbeck, T. S. In vitro expansion and genetic modification of gastrointestinal stem cells in spheroid culture. *Nature Protocols* **8**, 2471, doi:10.1038/nprot.2013.153 (2013).

177 Turk, H. F. *et al.* Inhibitory effects of omega-3 fatty acids on injury-induced epidermal growth factor receptor transactivation contribute to delayed wound healing. *Am J Physiol Cell Physiol* **304**, C905-917, doi:10.1152/ajpcell.00379.2012 (2013).

178 Angelos, M. G. *et al.* Aryl hydrocarbon receptor inhibition promotes hematolymphoid development from human pluripotent stem cells. *Blood* **129**, 3428-3439, doi:10.1182/blood-2016-07-730440 (2017).

179 Wang, I. C. *et al.* FoxM1 regulates transcription of JNK1 to promote the G1/S transition and tumor cell invasiveness. *J Biol Chem* **283**, 20770-20778, doi:10.1074/jbc.M709892200 (2008).

180 Lee, S.-Y., Jang, C. & Lee, K.-A. Polo-Like Kinases (Plks), a Key Regulator of Cell Cycle and New Potential Target for Cancer Therapy. *Development & Reproduction* **18**, 65-71, doi:10.12717/DR.2014.18.1.065 (2014).

181 Yoshida, Y., Wang, I. C., Yoder, H. M., Davidson, N. O. & Costa, R. H. The forkhead box M1 transcription factor contributes to the development and growth of mouse colorectal cancer. *Gastroenterology* **132**, 1420-1431, doi:10.1053/j.gastro.2007.01.036 (2007).

182 Fan, Y. Y. *et al.* A bioassay to measure energy metabolism in mouse colonic crypts, organoids, and sorted stem cells. *Am J Physiol Gastrointest Liver Physiol* **309**, G1-9, doi:10.1152/ajpgi.00052.2015 (2015).

183 Warburg, O. On the origin of cancer cells. *Science* **123**, 309-314 (1956).

184 Rodriguez-Colman, M. J. *et al.* Interplay between metabolic identities in the intestinal crypt supports stem cell function. *Nature* **543**, 424-427, doi:10.1038/nature21673 (2017).

185 Ema, M. *et al.* Dioxin binding activities of polymorphic forms of mouse and human arylhydrocarbon receptors. *J Biol Chem* **269**, 27337-27343 (1994).

186 Ko, C. I., Wang, Q., Fan, Y., Xia, Y. & Puga, A. Pluripotency factors and Polycomb Group proteins repress aryl hydrocarbon receptor expression in murine embryonic stem cells. *Stem Cell Res* **12**, 296-308, doi:10.1016/j.scr.2013.11.007 (2014).

187 Morales-Hernandez, A. *et al.* Alu retrotransposons promote differentiation of human carcinoma cells through the aryl hydrocarbon receptor. *Nucleic Acids Res* **44**, 4665-4683, doi:10.1093/nar/gkw095 (2016).

188 Tomasetti, C. & Vogelstein, B. Variation in cancer risk among tissues can be explained by the number of stem cell divisions. *Science* **347**, 78 (2015).

189 Xie, G., Peng, Z. & Raufman, J.-P. Src-mediated aryl hydrocarbon and epidermal growth factor receptor cross talk stimulates colon cancer cell proliferation. *American Journal of Physiology-Gastrointestinal and Liver Physiology* **302**, G1006-G1015, doi:10.1152/ajpgi.00427.2011 (2012).

190 Zhai, Z. *et al.* Accumulation of differentiating intestinal stem cell progenies drives tumorigenesis. *Nat Commun* **6**, 10219, doi:10.1038/ncomms10219 (2015).

191 Okino, S. T., Pookot, D., Basak, S. & Dahiya, R. Toxic and Chemopreventive Ligands Preferentially Activate Distinct Aryl Hydrocarbon Receptor Pathways: Implications for Cancer Prevention. *Cancer Prevention Research* **2**, 251-256, doi:10.1158/1940-6207.Capr-08-0146 (2009).

192 Ahmad, A. *et al.* 3,3'-Diindolylmethane enhances taxotere-induced growth inhibition of breast cancer cells through downregulation of FoxM1. *International journal of cancer* **129**, 1781-1791, doi:10.1002/ijc.25839 (2011).

193 Halasi, M. & Gartel, A. L. FOX(M1) News—It Is Cancer. *Molecular Cancer Therapeutics* **12**, 245, doi:10.1158/1535-7163.MCT-12-0712 (2013).

194 Metidji, A. *et al.* The Environmental Sensor AHR Protects from Inflammatory Damage by Maintaining Intestinal Stem Cell Homeostasis and Barrier Integrity. *Immunity* **49**, 353-362.e355, doi:10.1016/j.immuni.2018.07.010 (2018).

195 Arsenescu, R. *et al.* Role of the xenobiotic receptor in inflammatory bowel disease. *Inflammatory bowel diseases* **17**, 1149-1162, doi:10.1002/ibd.21463 (2011).

196 Kiss, E. A. *et al.* Natural Aryl Hydrocarbon Receptor Ligands Control Organogenesis of Intestinal Lymphoid Follicles. *Science* **334**, 1561-1565, doi:10.1126/science.1214914 (2011).

197 Liu, J. Z. *et al.* Association analyses identify 38 susceptibility loci for inflammatory bowel disease and highlight shared genetic risk across populations. *Nat Genet* **47**, 979-986, doi:10.1038/ng.3359 (2015).

198 Yamagishi, H., Kuroda, H., Imai, Y. & Hiraishi, H. Molecular pathogenesis of sporadic colorectal cancers. *Chin J Cancer* **35**, 4-4, doi:10.1186/s40880-015-0066-y (2016).

199 Carethers, J. M. & Jung, B. H. Genetics and Genetic Biomarkers in Sporadic Colorectal Cancer. *Gastroenterology* **149**, 1177-1190 e1173, doi:10.1053/j.gastro.2015.06.047 (2015).

200 Tomasetti, C., Marchionni, L., Nowak, M. A., Parmigiani, G. & Vogelstein, B. Only three driver gene mutations are required for the development of lung and colorectal cancers. *Proceedings of the National Academy of Sciences of the United States of America* **112**, 118-123, doi:10.1073/pnas.1421839112 (2015).

201 Vogelstein, B. *et al.* Cancer Genome Landscapes. *Science* **339**, 1546, doi:10.1126/science.1235122 (2013).

202 Brocardo, M. & Henderson, B. R. APC shuttling to the membrane, nucleus and beyond. *Trends Cell Biol* **18**, 587-596, doi:10.1016/j.tcb.2008.09.002 (2008).

203 Jaiswal, A. S. & Narayan, S. A novel function of adenomatous polyposis coli (APC) in regulating DNA repair. *Cancer letters* **271**, 272-280, doi:10.1016/j.canlet.2008.06.024 (2008).

204 Aoki, K. & Taketo, M. M. Adenomatous polyposis coli (APC): a multi-functional tumor suppressor gene. *Journal of Cell Science* **120**, 3327, doi:10.1242/jcs.03485 (2007).

205 Tetsu, O. & McCormick, F. Beta-catenin regulates expression of cyclin D1 in colon carcinoma cells. *Nature* **398**, 422-426, doi:10.1038/18884 (1999).

206 He, T. C. *et al.* Identification of c-MYC as a target of the APC pathway. *Science* **281**, 1509-1512, doi:10.1126/science.281.5382.1509 (1998).

207 Batlle, E. *et al.* Beta-catenin and TCF mediate cell positioning in the intestinal epithelium by controlling the expression of EphB/ephrinB. *Cell* **111**, 251-263, doi:10.1016/s0092-8674(02)01015-2 (2002).

208 Herbst, A. *et al.* Comprehensive analysis of β-catenin target genes in colorectal carcinoma cell lines with deregulated Wnt/β-catenin signaling. *BMC Genomics* **15**, 74, doi:10.1186/1471-2164-15-74 (2014).

209 Joseph, R., Little, P., Hayes, D. N. & Lee, M. S. Characterization of the number and site of APC mutations in sporadic colorectal cancer. *Journal of Clinical Oncology* **35**, 630-630, doi:10.1200/JCO.2017.35.4_suppl.630 (2017).

210 Huang, D. *et al.* Mutations of key driver genes in colorectal cancer progression and metastasis. *Cancer metastasis reviews* **37**, 173-187, doi:10.1007/s10555-017-9726-5 (2018).

211 Xie, M.-Z., Li, J.-L., Cai, Z.-M., Li, K.-Z. & Hu, B.-L. Impact of primary colorectal Cancer location on the KRAS status and its prognostic value. *BMC Gastroenterol* **19**, 46-46, doi:10.1186/s12876-019-0965-5 (2019).

212 Waters, A. M. & Der, C. J. KRAS: The Critical Driver and Therapeutic Target for Pancreatic Cancer. *Cold Spring Harb Perspect Med* **8**, a031435, doi:10.1101/cshperspect.a031435 (2018).

213 Rothhammer, V. & Quintana, F. J. The aryl hydrocarbon receptor: an environmental sensor integrating immune responses in health and disease. *Nat Rev Immunol* **19**, 184-197, doi:10.1038/s41577-019-0125-8 (2019).

214 Johnson, L. *et al.* Somatic activation of the K-ras oncogene causes early onset lung cancer in mice. *Nature* **410**, 1111-1116, doi:10.1038/35074129 (2001).

215 Shibata, H. *et al.* Rapid colorectal adenoma formation initiated by conditional targeting of the Apc gene. *Science* **278**, 120-123 (1997).

216 Hinoi, T. *et al.* Mouse model of colonic adenoma-carcinoma progression based on somatic Apc inactivation. *Cancer research* **67**, 9721-9730, doi:10.1158/0008-5472.CAN-07-2735 (2007).

217 Jackson, E. L. *et al.* Analysis of lung tumor initiation and progression using conditional expression of oncogenic K-ras. *Genes Dev* **15**, 3243-3248, doi:10.1101/gad.943001 (2001).

218 Zou, M. *et al.* KRASG12D-mediated oncogenic transformation of thyroid follicular cells requires long-term TSH stimulation and is regulated by SPRY1. *Laboratory Investigation* **95**, 1269, doi:10.1038/labinvest.2015.90 (2015).

219 Drost, J. *et al.* Sequential cancer mutations in cultured human intestinal stem cells. *Nature* **521**, 43-47, doi:10.1038/nature14415 (2015).

220 Shiizaki, K., Kido, K. & Mizuta, Y. Insight into the relationship between aryl-hydrocarbon receptor and β-catenin in human colon cancer cells. *PLOS ONE* **14**, e0224613, doi:10.1371/journal.pone.0224613 (2019).

221 Carmon, K. S., Lin, Q., Gong, X., Thomas, A. & Liu, Q. LGR5 interacts and cointernalizes with Wnt receptors to modulate Wnt/beta-catenin signaling. *Molecular and cellular biology* **32**, 2054-2064, doi:10.1128/MCB.00272-12 (2012).

222 Leung, C., Tan, S. H. & Barker, N. Recent Advances in Lgr5(+) Stem Cell Research. *Trends Cell Biol* **28**, 380-391, doi:10.1016/j.tcb.2018.01.010 (2018).

223 Leedham, S. J. *et al.* A basal gradient of Wnt and stem-cell number influences regional tumour distribution in human and mouse intestinal tracts. *Gut* **62**, 83-93, doi:10.1136/gutjnl-2011-301601 (2013).

224 Janssen, K. P. *et al.* APC and oncogenic KRAS are synergistic in enhancing Wnt signaling in intestinal tumor formation and progression. *Gastroenterology* **131**, 1096-1109, doi:10.1053/j.gastro.2006.08.011 (2006).

225 Hwang, J.-H. *et al.* A mutant KRAS-induced factor REG4 promotes cancer stem cell properties via Wnt/β-catenin signaling. *International journal of cancer* **n/a**, doi:10.1002/ijc.32728 (2019).

226 Jeong, W.-J., Ro, E. J. & Choi, K.-Y. Interaction between Wnt/β-catenin and RAS-ERK pathways and an anti-cancer strategy via degradations of β-catenin and RAS by targeting the Wnt/β-catenin pathway. *npj Precision Oncology* **2**, 5, doi:10.1038/s41698-018-0049-y (2018).

227 Lemieux, E., Cagnol, S., Beaudry, K., Carrier, J. & Rivard, N. Oncogenic KRAS signalling promotes the Wnt/beta-catenin pathway through LRP6 in colorectal cancer. *Oncogene* **34**, 4914-4927, doi:10.1038/onc.2014.416 (2015).

228 Sobhani, I. *et al.* Colorectal cancer-associated microbiota contributes to oncogenic epigenetic signatures. *Proceedings of the National Academy of Sciences* **116**, 24285-24295, doi:10.1073/pnas.1912129116 (2019).

229 Lamas, B., Natividad, J. M. & Sokol, H. Aryl hydrocarbon receptor and intestinal immunity. *Mucosal Immunology* **11**, 1024-1038, doi:10.1038/s41385-018-0019-2 (2018).

230 Wolk, K. *et al.* IL-22 increases the innate immunity of tissues. *Immunity* **21**, 241-254, doi:10.1016/j.immuni.2004.07.007 (2004).

231 Mizoguchi, A. *et al.* Clinical importance of IL-22 cascade in IBD. *Journal of gastroenterology* **53**, 465-474, doi:10.1007/s00535-017-1401-7 (2018).

232 Lindemans, C. A. *et al.* Interleukin-22 promotes intestinal-stem-cell-mediated epithelial regeneration. *Nature* **528**, 560-564, doi:10.1038/nature16460 (2015).

233 Brand, S. *et al.* IL-22 is increased in active Crohn's disease and promotes proinflammatory gene expression and intestinal epithelial cell migration. *American Journal of Physiology-Gastrointestinal and Liver Physiology* **290**, G827-G838, doi:10.1152/ajpgi.00513.2005 (2006).

234 Sugimoto, K. *et al.* IL-22 ameliorates intestinal inflammation in a mouse model of ulcerative colitis. *J Clin Invest* **118**, 534-544, doi:10.1172/jci33194 (2008).

235 Zenewicz, L. A. *et al.* Innate and adaptive interleukin-22 protects mice from inflammatory bowel disease. *Immunity* **29**, 947-957, doi:10.1016/j.immuni.2008.11.003 (2008).

236 Zwarycz, B. *et al.* IL22 Inhibits Epithelial Stem Cell Expansion in an Ileal Organoid Model. *Cellular and Molecular Gastroenterology and Hepatology* **7**, 1-17, doi:10.1016/j.jcmgh.2018.06.008 (2019).

237 Dudakov, J. A., Hanash, A. M. & van den Brink, M. R. Interleukin-22: immunobiology and pathology. *Annual review of immunology* **33**, 747-785, doi:10.1146/annurev-immunol-032414-112123 (2015).

238 Lejeune, D. *et al.* Interleukin-22 (IL-22) Activates the JAK/STAT, ERK, JNK, and p38 MAP Kinase Pathways in a Rat Hepatoma Cell Line: PATHWAYS THAT ARE SHARED WITH AND DISTINCT FROM IL-10. *Journal of Biological Chemistry* **277**, 33676-33682, doi:10.1074/jbc.M204204200 (2002).

239 Schwank, G. *et al.* Functional repair of CFTR by CRISPR/Cas9 in intestinal stem cell organoids of cystic fibrosis patients. *Cell Stem Cell* **13**, 653-658, doi:10.1016/j.stem.2013.11.002 (2013).

240 Zha, J.-M. *et al.* Interleukin 22 Expands Transit-Amplifying Cells While Depleting Lgr5+ Stem Cells via Inhibition of Wnt and Notch Signaling. *Cellular and Molecular Gastroenterology and Hepatology* **7**, 255-274, doi:https://doi.org/10.1016/j.jcmgh.2018.09.006 (2019).

241 Zenewicz, L. A. IL-22: There Is a Gap in Our Knowledge. *ImmunoHorizons* **2**, 198-207, doi:10.4049/immunohorizons.1800006 (2018).

242 Perusina Lanfranca, M., Lin, Y., Fang, J., Zou, W. & Frankel, T. Biological and pathological activities of interleukin-22. *J Mol Med (Berl)* **94**, 523-534, doi:10.1007/s00109-016-1391-6 (2016).

243 Huynh, J., Chand, A., Gough, D. & Ernst, M. Therapeutically exploiting STAT3 activity in cancer - using tissue repair as a road map. *Nat Rev Cancer* **19**, 82-96, doi:10.1038/s41568-018-0090-8 (2019).

244 Carow, B. & Rottenberg, M. E. SOCS3, a Major Regulator of Infection and Inflammation. *Frontiers in immunology* **5**, 58-58, doi:10.3389/fimmu.2014.00058 (2014).

245 Moyat, M. *et al.* IL-22-induced antimicrobial peptides are key determinants of mucosal vaccine-induced protection against H. pylori in mice. *Mucosal Immunology* **10**, 271-281, doi:10.1038/mi.2016.38 (2017).

246 Mulcahy, M. E., Leech, J. M., Renauld, J. C., Mills, K. H. & McLoughlin, R. M. Interleukin-22 regulates antimicrobial peptide expression and keratinocyte differentiation to control Staphylococcus aureus colonization of the nasal mucosa. *Mucosal Immunology* **9**, 1429-1441, doi:10.1038/mi.2016.24 (2016).

247 Zheng, Y. *et al.* Interleukin-22 mediates early host defense against attaching and effacing bacterial pathogens. *Nature Medicine* **14**, 282, doi:10.1038/nm1720 (2008).

248 Stefanich, E. G. *et al.* Pre-clinical and translational pharmacology of a human interleukin-22 IgG fusion protein for potential treatment of infectious or inflammatory diseases. *Biochemical Pharmacology* **152**, 224-235, doi:https://doi.org/10.1016/j.bcp.2018.03.031 (2018).

249 Cox, J. H. *et al.* Opposing consequences of IL-23 signaling mediated by innate and adaptive cells in chemically induced colitis in mice. *Mucosal Immunology* **5**, 99-109, doi:10.1038/mi.2011.54 (2012).

250 Powell, N. *et al.* Interleukin-22 orchestrates a pathological endoplasmic reticulum stress response transcriptional programme in colonic epithelial cells. *Gut* **69**, 578, doi:10.1136/gutjnl-2019-318483 (2020).

251 Mizoguchi, A. *et al.* Clinical importance of IL-22 cascade in IBD. *Journal of gastroenterology* **53**, 465-474, doi:10.1007/s00535-017-1401-7 (2018).

252 Lindemans, C. A. *et al.* IL-22 Is an Intestinal Stem Cell Growth Factor, and IL-22 Administration in Vivo Reduces Morbidity and Mortality in Murine GvHD. *Blood* **124**, 651-651, doi:10.1182/blood.V124.21.651.651 (2014).

253 Hanash, A. M. *et al.* Interleukin-22 protects intestinal stem cells from immune-mediated tissue damage and regulates sensitivity to graft versus host disease. *Immunity* **37**, 339-350, doi:10.1016/j.immuni.2012.05.028 (2012).

254 Aden, K. *et al.* Epithelial IL-23R Signaling Licenses Protective IL-22 Responses in Intestinal Inflammation. *Cell Reports* **16**, 2208-2218, doi:https://doi.org/10.1016/j.celrep.2016.07.054 (2016).

255 Chen, Y. *et al.* Loss of adenomatous polyposis coli function renders intestinal epithelial cells resistant to the cytokine IL-22. *PLOS Biology* **17**, e3000540, doi:10.1371/journal.pbio.3000540 (2019).

256 Yasukawa, H. *et al.* The JAK-binding protein JAB inhibits Janus tyrosine kinase activity through binding in the activation loop. *Embo j* **18**, 1309-1320, doi:10.1093/emboj/18.5.1309 (1999).

257 Sasaki, A. *et al.* Cytokine-inducible SH2 protein-3 (CIS3/SOCS3) inhibits Janus tyrosine kinase by binding through the N-terminal kinase inhibitory region as well as SH2 domain. *Genes to cells : devoted to molecular & cellular mechanisms* **4**, 339-351, doi:10.1046/j.1365-2443.1999.00263.x (1999).

258 Rigby, R. J., Simmons, J. G., Greenhalgh, C. J., Alexander, W. S. & Lund, P. K. Suppressor of cytokine signaling 3 (SOCS3) limits damage-induced crypt hyper-proliferation and inflammation-associated tumorigenesis in the colon. *Oncogene* **26**, 4833-4841, doi:10.1038/sj.onc.1210286 (2007).

259 Ortiz-Muñoz, G. *et al.* Suppressors of cytokine signaling abrogate diabetic nephropathy. *J Am Soc Nephrol* **21**, 763-772, doi:10.1681/ASN.2009060625 (2010).

260 Iwahori, K. *et al.* Overexpression of SOCS3 exhibits preclinical antitumor activity against malignant pleural mesothelioma. *International journal of cancer* **129**, 993-1005, doi:10.1002/ijc.25716 (2011).

261 Tsai, C.-H., Lee, Y., Li, C.-H., Cheng, Y.-W. & Kang, J.-J. Down-regulation of aryl hydrocarbon receptor intensifies carcinogen-induced retinal lesion via SOCS3-STAT3 signaling. *Cell Biology and Toxicology*, doi:10.1007/s10565-019-09499-z (2019).

262 Wada, T. *et al.* Aryl Hydrocarbon Receptor Plays Protective Roles against High Fat Diet (HFD)-induced Hepatic Steatosis and the Subsequent Lipotoxicity via Direct Transcriptional Regulation of Socs3 Gene Expression. *J Biol Chem* **291**, 7004-7016, doi:10.1074/jbc.M115.693655 (2016).

263 Sood, V., Lata, S., Ramachandran, V. G. & Banerjea, A. C. Suppressor of Cytokine Signaling 3 (SOCS3) Degrades p65 and Regulate HIV-1 Replication. *Front Microbiol* **10**, doi:10.3389/fmicb.2019.00114 (2019).

264 Lahvis, G. P. & Bradfield, C. A. Ahr null alleles: distinctive or different? *Biochem Pharmacol* **56**, 781-787, doi:10.1016/s0006-2952(98)00134-8 (1998).

265 Liao, G.-B. *et al.* Regulation of the master regulator FOXM1 in cancer. *Cell Commun Signal* **16**, 57-57, doi:10.1186/s12964-018-0266-6 (2018).

266 Li, S., Bostick, J. W. & Zhou, L. Regulation of Innate Lymphoid Cells by Aryl Hydrocarbon Receptor. *Frontiers in immunology* **8**, 1909-1909, doi:10.3389/fimmu.2017.01909 (2018).

267 Krishnan, V., Porter, W., Santostefano, M., Wang, X. & Safe, S. Molecular mechanism of inhibition of estrogen-induced cathepsin D gene expression by 2,3,7,8-tetrachlorodibenzo-p-dioxin (TCDD) in MCF-7 cells. *Molecular and cellular biology* **15**, 6710-6719, doi:10.1128/mcb.15.12.6710 (1995).

268 Safe, S., Wormke, M. & Samudio, I. Mechanisms of inhibitory aryl hydrocarbon receptor-estrogen receptor crosstalk in human breast cancer cells. *Journal of mammary gland biology and neoplasia* **5**, 295-306, doi:10.1023/a:1009550912337 (2000).

269 Mahe, M. M. *et al.* Establishment of Gastrointestinal Epithelial Organoids. *Curr Protoc Mouse Biol* **3**, 217-240, doi:10.1002/9780470942390.mo130179 (2013).

270 Schwank, G., Andersson-Rolf, A., Koo, B.-K., Sasaki, N. & Clevers, H. Generation of BAC Transgenic Epithelial Organoids. *PLOS ONE* **8**, e76871, doi:10.1371/journal.pone.0076871 (2013).

APPENDIX A

GENOTYPING OF AHR$^{F/F}$ MICE[18]

Goal: To determine the genotyping of AhR$^{f/f}$ mice.

Reagents:

Hot start mixture (Denville, CB4030-4)

DNA amount: 50 -100 ng

Fw2 primer (P1): GTCACTCAGCATTACACTTTCTA

Downstream Fw primer (P2): CAGTGGGAATAAGGCAAGAGTGA

Reverse primer (P3): GGTACAAGTGCACATGCCTGC

dH_2O (Gibco, 15230-170).

Reaction mix:

Reagents	stock	50 µl reaction
Hot start mix	2X	25 µl
P1 primer	10 µM	1 µl
P2 primer	10 µM	1 µl
P3 primer	10 µM	1 µl
DNA		25-100 ng
H_2O		up to 50 µl

PCR program:

94°C	3 min
35 cycles of:	
94°C	30 sec
63°C	20 sec
72°C	20 sec
72°C	5 min for extra extending

Expected result:

Excised AhR allele: 180 bp, unexcised AhR allele: 140 bp

Gel:

2% agarose gel, 3 ul of Gelred (Biotium #41003) in 100 ml, 180 V for ~45 minutes.

APPENDIX B

GENOTYPING OF KRAS$^{G12D/+}$ MICE

Purpose: Detecting wild type KRAS, LSL-G12D KRAS (floxed but not recombined) and G12D-KRAS (recombined) allele from crypts isolated from CDX2P-CreER^{T2}-APC$^{580D/+}$; KRAS$^{G12D/+}$ mouse colon.

Antibody and reagents: 2X master mix (Denville Hot Start, CB4030-4), 10 mM primers (order from https://www.idtdna.com/Primerquest/Home/Index), PCR machine (AB 2720 Thermocycler), dH_2O (Gibco, 15230-170).

Source of primers: Jackson lab (https://jacks-lab.mit.edu/protocols/genotyping/kras_cond) and Hinoi[216]

Kras Jackson F1 (P1)	5'-GTCTTTCCCCAGCACAGTGC-3′
KRAS 1AS (P2) [216]	5′-GCAGCGTTACCTCTATCGTA-3′
Kras Jackson F2 (P3)	5'-AGCTAGCCACCATGGCTTGAGTAAGTCTGCA-3′

Rxn Mix (30 µl reaction):

Reaction mix	Volume (ml)
Master mix (2X)	15
Kras P1 (10 mM)	1.5
Kras P2 (10 mM)	1.5
Kras P3 (10 mM)	1.5
DNA (50 ng)	
Water	to 30 ml
Total	30

PCR parameters:

94°C	2 min	Initialization

35 cycles of:

94°C	30 sec	Denaturation
61°C	30 sec	Annealing
72°C	45 sec	Extension/elongation

72°C	5 min	Final elongation
4°C	keep	Final hold

Amplified fragments (P1+P2+P3): WT = 700 bp ; LSL-G12D = 570 bp ; G12D (recombined) = 720 bp.

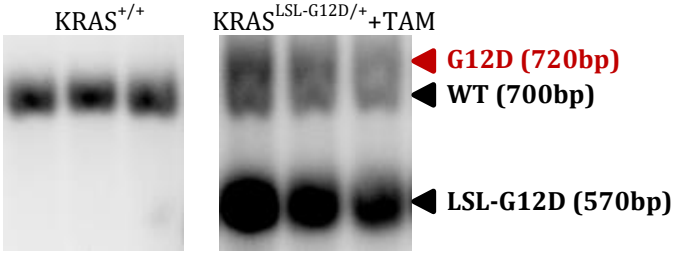

APPENDIX C

GENOTYPING OF $APC^{S580/+}$ MICE

Purpose: Detecting wild type APC, APC^{580S} (floxed but not recombined) and APC^{580D} (recombined) allele from crypts isolated from CDX2P-$CreER^{T2}$-$APC^{580D/+}$; $KRAS^{G12D/+}$ mouse colon

Antibody and reagents: 2X master mix (Denville Hot Start, CB4030-4), 10 mM primers (order from https://www.idtdna.com/Primerquest/Home/Index), PCR machine (AB 2720 Thermocycler), dH_2O (Gibco, 15230-170)

Source of primers: Shibata et al [215,216].

APC F1 (P3)	5′- GTTCTGTATCATGGAAAGATAGGTGGTC-3′
APC R1 (P4)	5′- CACTCAAAACGCTTTTGAGGGTTGATTC -3′
APC R2 (P5)	5'-GAGTACGGGGTCTCTGTCTCAGTGAA-3'

Rxn Mix (30 ul reaction):

Reaction mix	Volume (µl)
Master mix (2X)	15
Kras P1 (10 mM)	1
Kras P2 (10 mM)	1
Kras P3 (10 mM)	1
DNA	4
Water	8
Total	30

PCR parameters:

94°C	3 min	Initialization

30 cycles of:

94°C	30 sec	Denaturation
62.5	30 sec	Annealing
72°C	40 sec	Extension/elongation

72°C	2 min	Final elongation
4°C	keep	Final hold

Amplified fragments (P1+P2+P3): WT = 226 bp; APC^{580S} = 314 bp; APC^{580D} (recombined) = 258 bp

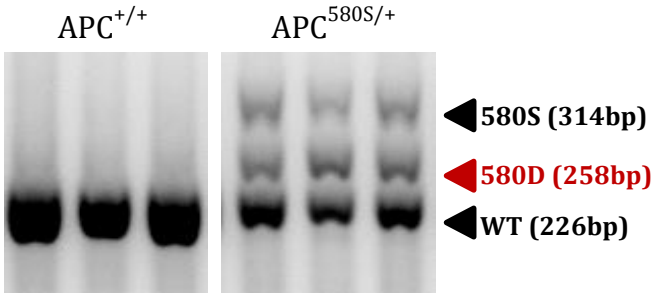

APPENDIX D

MOUSE COLON ORGANOID CULTURE PASSAGE[269]

Materials:

ADF^{+}: Advanced DMEM/F12 medium (Life Tech 12634-010), 2 mM Glutamax, 10 mM HEPES, and 1X P/S.

Matrigel (Corning 356231).

Clevers' organoid medium

For colon organoid culture	Final conc	500 µL/well	*6 Wells
		µL	
EGF (100 µg/mL) (Life Tech #PMG8044)	50 ng/mL	0.25	1.5
LDN (Noggin replacement (0.2 mM) (Stemgent #04-0074)	0.2 µM, ~ 81.3 ng/mL	0.50	3
R-Spondin conditioned medium (10x)	1x	50.00	300
N2 supplement (100x) (Life Tech #17502048)	1x	5.00	30
B27 supplement (50x) (Life Tech #17504044)	1x	10.00	60
N-Acetylcys (400 µM) (A) (Sigma #A7250-5G)	1 µM	1.25	7.5
ADF+ (w/ Gln, HEPES, P/S)		200.00	1200
Wnt conditioned medium		250.00	1500

Procedure:

Before passaging, prepare Clever's organoid medium supplemented with Y-27632 (Sigma #Y0503, 10 mM stock in ADF, 1:1000 dilution to make final concentration in medium [10 µM])

_____1. Organoids can be passaged 5-10 days after seeding. Thaw the Matrigel on ice (one day before experiment), and pre-incubate a 24-well plate in a CO_2 incubator at 37 °C at least 30 min before plating.

_____2. Remove media from wells and put the culture plate on ice. Add 1 ml of ice-cold PBS to each well. Break up the Matrigel by pipetting back and forth several times with pre-chilled P1000 tips.

_____3. Transfer the suspension into a 15 ml conical tube filled with ice-cold PBS (final volume is better to be 10 ml).

_____4. Centrifuge at 300 g for 3 minutes at 4 °C, and carefully aspirate.

_____5. Add 5 ml cold PBS to resuspend pellets, centrifuge at 300 g for 3 minutes, and carefully aspirate (50~100 µl remaining is fine) (optional).

_____6. Add 0.4~0.5 ml 0.25% Trypsin (cat# Life Tech 25200) per sample, and incubate 2~3 minutes at 37 °C.

_____7. Add 1 ml of ADF^+ supplemented 10% FBS to stop reaction. 1~10 cell clusters would be expected.

_____8. Spin down at 500 g for 3 minutes at 4°C.

_____9. Aspirate supernatant and resuspend pellet in Matrigel (1:3~1:5 split).

_____10. Apply 30~50 ul of Matrigel suspension per well on the pre-warmed 24-well plate. Slowly eject the Matrigel in the center of the well.

_____8. Place the 24-well plate in a CO_2 incubator (37°C, 5% CO_2) for 10 minutes to allow a complete polymerization of the Matrigel.

_____9. Overlay the Matrigel with 300~500 ul of Clever's organoid media supplemented with Y (1:1000 dilution).

_____10. Culture the plate in the CO_2 incubator. Every 2~3 days, replace the media with fresh Clever's organoid media.

APPENDIX E

ORGANOID FORMING EFFICIENCY FROM SORTED INDIVIDUAL CELLS

Goal: To determine the organoid forming efficiency from sorted colonic stem or progenitor cells.

Reagents: See catalog numbers and recipes on page 157.

ADF+: Advanced DMEM/F12 medium (Life Tech 12634-010) plus 2 mM Glutamax and 10 mM HEPES, and 1X P/S. 500 ml ADF media + 5 ml glutamax + 5 ml HEPES + 5 ml P/S.

Prepare before sorting:

Single cell cocktail (1.1 ml):

1 ml ADF^+ (see below) + 1.1 µl Y (stock. 10 mM) + 11 µl N2 + 22 µl B27 + 2.8 µl A + 100 µl 10% BSA.

Collection medium (1 ml; need 350 µl for each collection tube):

1 ml ADF^+ + 10 µl N2 + 20 µl B27 + 2.5 µl A +1 µl Y.

PI (10 µl/500 µl sample) (BD, 556463) is used to exclude dead cells when sorting cells (If cells contain tomato positive, do not use PI).

Materials:

Clevers's medium (see recipe below) supplemented with Y (final concentration, 10µM), Jagged-1 (final concentration 1µM) and CHIR (final concentration, 2.5 µM, Stemgent CHIR99021, 04-004-10)

Matrigel Preparation (Corning 356231): 600 µl Matrigel + 0.6 µl Y + 0.6 µl Jagged-1

Experiment:

_____ Centrifuge sorted single cells at 500xg for 3 min at 4°C.

_____ Remove supernatant, and add volume of collection medium to suspend cells (normally 50 µl/10,000 cells).

_____ Count cell density.

_____ Plate 30 µl Matrigel per well onto warm 24-well plate, immediately drip proper volume of cell suspension (2~5 µl, equivalent to 500 cells per well) on the mound, based on cell density and how many cells you want to plate.

_____ Re-warm plate in 37 °C incubator for 10 minutes to completely solidify Matrigel. During this step, warm prepared Clever's organoid medium supplemented with Y, Jagged-1 and CHIR.

_____ Apply 300 µl above medium per well.

_____ Withdraw Y, Jagged-1 and CHIR 3 days after plating. Since that, change medium every 2 days.

_____ Count organoids at Day 5.

APPENDIX F

FREEZING ORGANOIDS[269]

Prepare freezing media

ADF+: ADF + glutamax + P/S + HEPES

0.5 ml per each cryovial:

0.4 ml **ADF+** + 0.05 ml **DMSO** + 0.05 ml **FBS** (heat inactivated FBS)

Before freezing organoids, please make sure the organoids are relatively small, without many buddings (small organoids are better to recover after freezing).

1. _____Organoids can be frozen 3~4 days after passaging.
2. _____Remove the media and add 500 µl cell freezing media (80% ADF+, 10% DMSO, 10% FBS – filter sterilize before use).
3. _____Scrape Matrigel with P-1000 tip and transfer contents into cryo vial. Freeze in a Mr. Frosty unit at -80°C for at least 1 day, and transfer to liquid nitrogen.
4. _____Update Chapkin lab organoid Biobank.

The organoids can be stored at least for 1 year.

APPENDIX G

CULTURE HUMAN ORGANOIDS

Note: ADF^{++} = ADF + glutamax + P/S + HEPES

Human organoid growth factor (gf) mix:

Component	**Stock**	**Suspend in**	**Final conc in growth media**	**Source**	**µl per ml media**
WRN conditioned media	100%		50%	Homemade	500
ADF + glutamax + P/S	100%			Gibco 12634-010	462
N2	100X		1x	Gibco 17502-048	10
B27	50X		1x	Gibco 17504-044	20
EGF	100 µg/ml	PBS + 0.5% FBS	40 ng/ml	LifeTech PMG8041	0.4
SB202190	10 mM	DMSO	3 µM	Sigma S7067	0.3
A 83-01	500 µM	DMSO	500 nM	Tocris 2939	1
N-Acetyl cysteine	1 mM	di water	1 µM	Sigma A9165	1
Nicotinamide	10 M	di water	10 mM	Sigma N3376	1
Gastrin 1	10 µM	PBS+0.5% BSA	10 nM	Sigma G9020	1

To grow organoids from stock frozen in liquid N2

___ Thaw Matrigel the night before

___ Prepare 15 ml conical tube with 10 ml ADF^{++}

___ Pre-warm 24- or 48-well plate. Pre-chill centrifuge.

___ Prepare growth media: 250 µl WRN + 150 µl ADF^{++} + 100 gf mix (per well of 24-well plate)

___Thaw vial of organoids quickly by swirling in 37°C water bath

___ Pipet organoids with P1000 tip into the 15 ml vial of media

___ Spin down at 4°C for 3 min at 400 xg.

___ Discard supernatant thoroughly and resuspend organoids in Matrigel. Plate one vial into one well of a 24-well plate in 50 µl Matrigel.

___ Allow Matrigel to solidify in 37°C for ~10 min then add pre-warmed growth media with 10 µM Y.

Passaging human organoids

Should be passaged every 2-5 days. Note that human organoids prefer to be crowded. Don't plate too sparse.

___ Thaw Matrigel overnight.

___ Prepare and warm growth media. Turn on heating block to 37°C.

___ Remove media from organoid wells and add 500 µl 0.5 mM EDTA in PBS

500 µl PBS + 0.5 µl 0.5 M EDTA

___ Pipet with a P-1000 tip to break up the Matrigel and transfer to 1.5 ml low-bind eppie tube.

___ Pipet 10-20 times to thoroughly break up Matrigel.

___ Spin for 4 sec by holding down the "short" spin button on the benchtop Eppendorf centrifuge at 4 °C.

___ Remove supernatant and add 300~400 µl 0.25% EDTA-Trypsin (cat# Life Tech 25200). Pipet ~5 times.

___ Place tube in 37°C heat block for 3 minutes.

___ Pipet ~10 times before adding 1 ml 10% FBS containing WRN (or ADF+) media.

___ centrifuge at 500*g for 3 minutes at 4°C.

___ Remove sup and resuspend pellet in Matrigel (split 1:5 or 1:6).

___ Plate in 24 or 48 well plates. Incubate at 37°C for 10 min and then feed with pre-warmed complete media.

24 well plate: 50 µl Matrigel and 500 µl media

48 well plate: 25 µl Matrigel and 300 µl media

Freezing human organoids

Remove media from growing organoids

Add 500 µl cell freezing media (80% ADF++, 10% DMSO, 10% FBS – filter sterilize before use).

Scrape Matrigel with P-1000 tip and transfer contents into cryo vial.

Freeze in a Mr. Frosty unit at -80°C for at least 1 day, and transfer to liquid nitrogen.

Fill out the Organoid Biobank form at google.tamu.edu, Team Drives, Chapkin Lab, Organoid Biobank.

Typical organoid morphology at 5-7 days post passage is shown here. Usually small hollow circles with a small percentage of budding organoids.

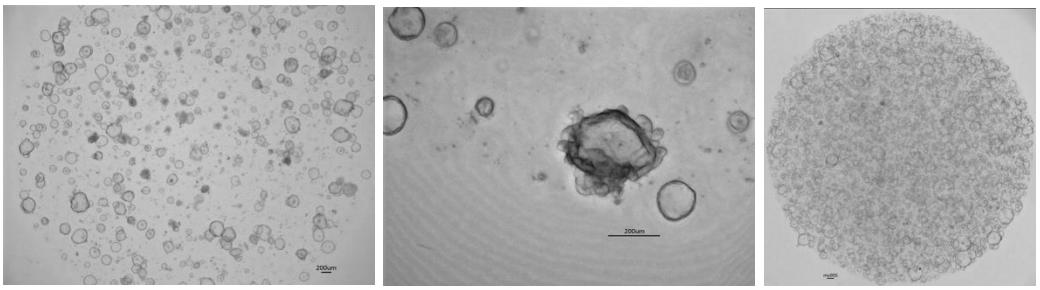

APPENDIX H

MOUSE/HUMAN ORGANOI NUCLEOFECTION[270]

Goal: To CRISPR KO target gene in organoids.

Materials:

Amaxa Mouse/Rat Hepatocyte Nucleofector Kit (VAPL-1004)

0.25% EDTA-Trypsin (cat# Life Tech 25200)

Prechilled PBS

Matrigel

Clever's organoid medium

pSpCas9 BB-2A-GFP (PX458) plasmid (GenScript, SC1678) containing guide RNA targeting AhR (AAGTCGGTCTCTATGCCGCT or AGACCGACTTAATACAGAGT).

Preparing organoids for Transfection (takes 7~10 days):

Before transfection, mouse organoids are cultured for two passages in Clever's organoid medium plus 10 mM Nicotinamide. At least 5~8 wells of organoids are needed to do transfection (~1 million cells).

Transfection using nucleofection:

1. Remove culture medium and add 0.5 ml ice-cold PBS to each well. Break up the Matrigel by pipetting up and down several times and scraping remaining Matrigel. Transfer the suspension into a 15 ml conical tube filled with 5 ml ice-cold PBS.
2. Centrifuge at 500 g for 3 minutes at 4 °C, and carefully aspirate.
3. Add 0.6~1 ml 0.25% Trypsin plus 10 µM Y per sample and incubate 10 minutes at 37 °C. Pipet cell suspension every 3 minutes. Before next step, take 2~5 µl

cell suspension and observe whether most organoids are dissociated into small clusters under microscope. It is very difficult to dissociate into single cells. 2~10 cell clusters are fine.

4. Add 5 ml 10% FBS in ADF^+ to stop reaction.
5. Filter cell suspension into another 15 ml conical tube using 70 µm filter (MACS, Cat# 130-098-462) (40 µm strainer also will be OK)
6. Spin down at 600 g for 3 minutes at 4 °C.
7. Aspirate the supernatant carefully.
8. Add 0.5 ml ADF^+ plus Y to suspend pellets. Take 10 µl cell suspension to count cell density.
9. Transfer proper volume of cell suspension to 1.7 ml non-stick tube based on cell density. Each transfection requires 0.5~0.7 million cells. I tried 0.25 million per reaction, and it worked.
10. Centrifuge at 700 g for 3 minutes at 4 °C.
11. Prepare Nucleofector solution (100 µl per sample): 82 µl of Nucleofector Solution plus 18 µl of supplement.
12. Resuspend the cell pellet carefully in 100 µl RT Nucleofector solution plus Y (very important) per sample.
13. Combine 100 µl of cell suspension with 5 µg plasmid (this is for 0.7 million cells. You can calculate how much plasmid is needed based on actual sample. Also the concentration of plasmid is crucial for transfection, not only the total amount of plasmid. The cell number and plasmid concentration may need to be titrated for best results).

14. Transfer cell/DNA suspension into certified cuvette. Close the cuvette with the cap.
15. Select the appropriate Nucleofector Program: T-028.
16. Insert the cuvette with cell/DNA suspension into the Nucleofector Cuvette Holder and apply selected program by pressing the X-button.
17. Take the cuvette out of the holder once the program is finished.
18. Incubate the sample in the cuvette for 15 minutes at RT.
19. Transfer cell suspension into a 1.7 ml non-stick tube containing 0.5 ml ice-cold ADF^+ plus Y.
20. Centrifuge at 500 *g for 3 minutes at 4 °C.
21. Aspirate the supernatant carefully, and add 130~150 µl Matrigel to resuspend the cell pellet. Split into 5 wells of a 24-well plate. Each well will be 30 µl.
22. Place the 24-well plate in a CO_2 incubator (37°C, 5% CO_2) for 10 minutes to allow a complete polymerization of the Matrigel.
23. Overlay the Matrigel with 300 ul of Clever's organoid media supplemented with Y (1:1000 dilution), Jagged-1 (1:1000 dilution) and CHIR (final concentration, 2.5 µM).
24. Culture the plate in the CO_2 incubator. Three days after transfection, we can start to add 500 µg/ml G418 to the medium (500 µg/ml G418 will definitely kill all of untransfected mouse organoids within 3 days). Two days after transfection, we can sort cells based on fluorescence.

For human organoid transfection, the procedure is the same, the only difference is the culture medium (50% WRN+30% ADF^+ +20% GF mixture)

APPENDIX I

ORGANOID TRANSFECTION USING LIPOFECTAMINE 3000[270]

Goal: To CRISPR KO target gene in organoids.

Reagent:

Lipofectamine 3000 (Life Tech #L3000008)

pSpCas9 BB-2A-GFP (PX458) plasmid (GenScript, SC1678)

Preparing organoids for transfection (takes 7~10 days):

Before transfection, mouse organoids are cultured in 24-well plates for two passages in Clever's organoid medium (recipe below) plus 10 mM Nicotinamide. At least 5~8 wells of organoids are needed to do transfection (~1 million cells).

Procedure: it will take ~6.5 hours for transfection, so it is better to perform before 10 am.

Organoid dissociation

25. Remove culture medium and add 0.5 ml ice-cold PBS to each well. Break up the Matrigel by pipetting up and down several times and scraping remaining Matrigel. Transfer the suspension into a 15 ml conical tube filled with 5 ml ice-cold PBS.
26. Centrifuge at 500 g for 3 minutes at 4 °C, and carefully aspirate.
27. Add 0.6~1 ml 0.25% Trypsin plus 10 µM Y-27632 per sample and incubate 10 minutes at 37 °C. Pipet cell suspension every 3 minutes. Before next step, take 2~5 µl cell suspension and observe whether most organoids are dissociated into small clusters under microscope. It is very difficult to dissociate into single cells. 2~10 cell clusters are fine.

28. Add 5 ml 10% FBS in ADF^{+} to stop reaction.
29. Filter cell suspension into another 15 ml conical tube using 70 µm filter (MACS, Cat# 130-098-462) (40 µm strainer also will be OK)
30. Spin down at 600 g for 3 minutes at 4 °C.
31. Aspirate the supernatant carefully.
32. Add 1.5 ml Clever's medium plus Y to suspend pellets. Take 10 µl cell suspension to count cell density.
33. Transfer the cell suspension to one well of a 6-well plate. Each transfection requires 1~1.2 million cells.
34. Place the plate into 37°C incubator, and prepare for transfection.

Prepare nucleic acid-Lipofectamine 3000 complexes.

1. Add 125 µl Opti-MEM medium and 7.5 µl of Lipofectamine 3000 Reagent into a 1.5 ml tube. Mix well.
2. Dilute 10 µg of plasmid into 125 µl Opti-MEM medium in a second 1.5 ml tube, and then add 20 µl P3000 Reagent. Mix well.
3. Add 132 µl diluted DNA to a third tube containing 132 µl diluted Lipofectamine 3000 Reagent (1:1 ratio). Mix well.
4. Incubate at RT for 15 minutes.

Transfection

1. Transfer all nucleic acid-lipofectamine 3000 complexes to cells. Mix them by gently swirling the plate.
2. Centrifuge the 6-well plate at 600*g for 1 hour at 32°C.

3. Incubate the plate for 4 hours at 37°C.

Organoid culture

1. Collect all cells into a 5 ml tube and centrifuge at 600*g for 4 minutes at 4°C.
2. Carefully aspirate the supernatant and add 300 µl Matrigel to resuspend the cell pellet. Split into 6 wells of a 24-well plate. Each well will be 50 µl.
3. Place the 24-well plate in a CO_2 incubator (37°C, 5% CO_2) for 10 minutes to allow a complete polymerization of the Matrigel.
4. Overlay the Matrigel with 500 µl of Clever's organoid media supplemented with Y (1:1000 dilution), Jagged-1 (1:1000 dilution) and CHIR (final concentration, 2.5 µM). Successfully transfected cells need to be sorted out 2 days after lipofection.

Cell sorting

1. Prepare single cell cocktail (1 ml per sample):

   1 ml ADF^+ + 1.1 µl Y-27632 + 11 µl N2 + 22 µl B27 + 2.8 µl N-Ac + 100 µl 10% BSA
2. Setup the flow cytometer.
3. Dissociate organoids following the Organoid dissociation steps 1-7 above.
4. Resuspend cells with 0.5 ml of ice-cold single cell cocktail.
5. Before sorting, filter again through 20 µm Partec filter into a 5 ml 5% FBS pre-coated BD polypropylene tube, rinsing with 200 µl of single cell cocktail.
6. Add 10 µl of 7-AAD to exclude the dead cells during sorting. Collect the top 30% GFP-expressing cells. Usually we could obtain ~300-600 cells.

Organoid culture

1. Centrifuge sorted GFP-expressing cells at 600*g for 3 minutes at 4 °C.
2. Aspirate the supernatant carefully, and add appropriate volume of Matrigel to resuspend the cells (~30 cells per 30 µl Matrigel). Split into ~10 wells of a 24-well plate. Each well will be 30 µl.
3. Place the 24-well plate in a CO_2 incubator (37°C, 5% CO_2) for 10 minutes to allow a complete polymerization of the Matrigel.
4. Overlay the Matrigel with 300 µl of Clever's organoid media supplemented with Y (1:1000 dilution), Jagged-1 (1:1000 dilution) and CHIR (2.5 µM).
5. Culture the plate in the CO_2 incubator.
6. Pick up single organoid by using P200 pipette, transfer the organoid into a new 1.5 ml tube, and passage as usual. Collect cell lysate for WB to validate the knockout efficiency or DNA sequencing.

APPENDIX J

DNA SEQUENCING FOR AHR CRISPR KO

Goal: to validate AhR CRISPR KO organoid clones at DNA level by using guide RNA against 5'-AAGTCGGTCTCTATGCCGCT-3' and 5'-AGACCGACTTAATACAGAGT-3'.

Reagents:

Phusion High-fidelity PCR master Mix (Life Technologies, F532L)

Organoid DNA: 50 -100 ng. (Isolated with Denville #740952.250)

AhR Forward primer (P1): 5'- AACATCACCTACGCCAGTCG-3'

AhR Reverse primer (P2): 5'- ATAACCTGAGCCTCTCGTGC-3'.

The primers P1 and P2 should be 200~400 bp upstream or downstream from PAM sequence, respectively.

AhR sequencing primer (P3): 5'-TGGCTGAAGTGGAGTAGCT-3'.

The sequencing primer should be within 80~200 bp away from PAM sequence.

dH_2O (Gibco, 15230-170).

QIAquick PCR Purification Kit (Qiagen, 28104)

I. PCR mixture setup

Reagents	stock	30 µl reaction
Phusion PCR master mix	2X	15 µl
P1 primer	10 µM	1 µl
P2 primer	10 µM	1 µl
DNA		50 ng
H_2O		up to 30 µl

II. PCR amplification

PCR program:

98°C	30sec
30 cycles of:	
98°C	10 sec
60°C	20 sec
72°C	15 sec
72°C	3 min for extra extending

III. PCR product purification (Follow the protocol provided by the QIAquick PCR Purification Kit)

1. Add 5 volumes Buffer PB to 1 volume of the PCR reaction and mix.
2. Place a QIAquick column in a provided 2 ml collection tube.
3. To bind DNA, apply the sample to the QIAquick column and centrifuge at 10,000*g for 30s at RT. Discard flow-through and place the QIAquick column back in the same tube.

4. To wash, add 750 µl Buffer PE to the QIAquick column and centrifuge at 10,000*g for 30s at RT. Discard flow-through and place the QIAquick column back into the same tube.
5. Centrifuge the QIAquick column once more in the provided 2 ml collection tube for 1 min to remove residual wash buffer.
6. Place each QIAquick column in a clean 1.5 ml microcentrifuge tube.
7. To elute DNA, add 30 µl dH_2O to the center of the QIAquick membrane and centrifuge the column for 1 min.

IV. Send Purified DNA for Sanger sequencing using AhR Primer P3. Some deletions or insertions should be expected in KO clones, compared with WT clones.

V. Analysis of DNA Sanger Sequences

PCR products are submitted to GeneWiz for Sanger sequencing. Sequence reads received from GeneWiz must have a QS (Quality Score) of 40 or higher and CRL (Contiguous Read Length) of 500 or higher to be analyzed. QS is calculated according to GeneWiz protocol, where it represents the average of Quality Values (QV) for each base in the sequence. The QV is derived from the formula, QV = -10log(Pe), where Pe is the Probability of Error. CRL represents the longest uninterrupted stretch of bases with quality higher than QV of 20 within a specified window. Sequence files (.ab1) files are then imported into SnapGene and aligned against a template sequence for the

target gene that is obtained from the NCBI repository. Alignments, along with chromatograms, are exported to .pdf files.

APPENDIX K

RNASCOPE

Goal: to determine the expression of RNA in situ.

Common reagents

RNAscope Target Retrieval Reagents (ACD #322000)

Pretreatment Regents (ACD #322300)

RNAscope 2.5 HD Detection Regents-RED (ACD #322360)

RNAscope Wash Buffer (ACD #310091)

Biocare EcoMount medium (Fisher #50-828-32)

Gill's Hematoxylin I (American Master Tech Scientific #HXGHE1LT)

Ammonium hydroxide 28~30% (Mallinckrodt #3256)

Fix the sample

Immediately following dissection, fix tissue in 10% NBF for 16–32 HRS at ROOM TEMPERATURE (RT). Fixation time will vary depending on tissue type and size. For the colon, I used 6h fixation at RT.

DAY 1 Work

1. **Bake Slides**
    1. Turn on regular oven to 60°C.
    2. Bake slides at 60°C for 1h.

2. Deparaffinize Paraffin-embedded tissue sections

1. Submerge slides in the first xylene-containing dish in the fume hood. Incubate for 5 min at RT. Agitate the slides by occasionally lifting the slide up and down.
2. Remove the slide rack, and immediately place in the second xylene-containing dish in the fume hood. Incubate for 5 min at RT with agitation.
3. Remove the slide rack from xylene and immediately place in the dish containing 100% ethanol. Incubate for 1 minutes at RT with agitation.
4. Remove the slide rack and immediately place in the second dish containing 100% ethanol. Incubate for 1 min at RT with agitation.
5. Remove the slides from the rack, and place on absorbent paper. Air dry slides for 5 min at RT.

(Optional step 1-6) For under-fixed tissue.

1. post-fix the slides by placing them in 4% PFA at RT for 60 min. After this, perform ethanol gradient to remove the fixative.
2. Remove the slides from the 4% PFA. Immerse slides in 50% EtOH. Incubate for 5 MIN at RT.
3. Remove the slides from 50% EtOH. Immerse in 70% EtOH. Incubate for 5 MIN at RT.
4. Remove the slides from 70% EtOH. Immerse in 100% EtOH. Incubate for 5 MIN at RT.

5. Remove the slides from 100% EtOH. Immerse in fresh 100% EtOH. Incubate for 5 MIN at RT.
6. Remove slides from 100% EtOH. Leave slides for 5 MIN at RT to dry.

3. Prepare 1X RNAscope Target retrieval Regents.

Prepare 250~700 ml of fresh RNAscope 1X Target Retrieval Regents by dilution with distilled water, depending on the container size we use.

4. Apply RNAscope Hydrogen Peroxide

1. Add ~5-8 drops of RNAscope Hydrogen Peroxide to completely cover the tissue section.
2. Incubate slides for 10 min at RT.
3. Tap the slide on absorbent paper. Immediately submerge the slide into distilled water.
4. Wash slides 3~5 times by lifting the slides up and down in the distilled water.
5. Repeat step 4 with fresh distilled water.

5. Target retrieval

1. Heat 1x RNAscope Target Retrieval buffer to sub-boiling state (~99C) in the metal pot (remove the internal strainer).
2. Place slides into sub-boiling buffer. Make sure the slides are completely submerged into buffer. Incubate for 15 minutes.

3. Remove slides from hot 1x RNAscope Target Retrieval buffer by forceps. Immediately submerge slides into distilled water.
4. Wash slides 3~5 times by lifting the slides up and down in the distilled water (about 15 sec).
5. Wash slides in fresh 100% ethanol for 3 min.
6. Air dry slides at RT.

6. Create a barrier

Draw a barrier around each section with hydrophobic barrier pen. Let the barrier dry completely overnight at RT.

Day 1 work STOP

DAY2 work

Apply RNAscope Protease Plus

1. Place a ddH_2O-drenched Gel Blot paper (MIDSCI #10-427-812) in HybEZ Humidity control Tray and put the prepared humidity control tray at 40°C oven.
2. Place dried slides on the HybEZ Slide Rack and add ~5 drops of RNAscope Protease Plus to entirely cover each section.
3. Remove the HybEZ Humidity Control Tray from oven and place the HybEZ Slide Rack in the tray. Close the lid, seal, and insert tray back into the oven. Incubate at 40°C for 30 min.

4. Remove the HybEZ Humidity Control Tray from the oven. Take the HybEZ Slide Rack out. Place tray back into oven.
5. Tap the slides to remove the excess liquid. Immediately submerge into jar filled with distilled water.
6. Wash slides 3~5 times by lifting the slides up and down in the distilled water (about 15 sec).

Equilibrate reagents

1. Remove AMP 1-6 reagents (from RNA Scope kit) from refrigerator and place at **RT for at least 20 minutes** ahead of experiment.
2. Ensure oven and prepared humidity control tray are at 40°C.
3. Before each use, warm the Target and/or Control probe for at least **10 min at 40°C** in regular oven. Swirl gently to mix.

Run the assay

Hybridize probe

1. Tap to remove excess liquid from slides. Place slides in the HybEZ Slide Rack located in the HybEZ humidity control tray. Add ~4 drops of the appropriate probe to entirely cover each section.
2. Cover the HybEZ humidity control tray with lid and insert into the oven for 2 HRS at 40°C.
3. Remove the HybEZ control tray from the oven and remove HybEZ Slide Rack. Put the HybEZ control tray back to 40°C oven.

4. Remove all slides from the rack, and quickly tap excess liquid. Put all slides into slide holder, and submerge into jar with 1X wash buffer.
5. Wash slides in 1X wash buffer for 2 min at RT. Agitate slides 3 times by lifting up and down.
6. Repeat step 5 with fresh 1X wash buffer.

After hybridizing probe, prepare the following reagents:

1. **Prepare 1X Wash buffer**

   Prepare 3L of 1X wash Buffer by adding 2.94L distilled water and prewarmed 60 ml of RNAscope Wash Buffer (50X) to a large carboy. Mix well.

Warm RNAscope 50X Wash Buffer up to 40C for 10-20 minutes before preparation. **1X Wash Buffer may be stored at RT for up to one month**.

2. **Prepare counterstaining reagents**
   1. In the fume hood, prepare 50% Hematoxylin staining solution by adding 50 ml Gill's hematoxylin I to 50 ml of ddH2O. 50% Hematoxylin staining solution can be reused for 1 week.
   2. In the fume hood, prepare 0.02% (w/v) Ammonia water by adding 0.715 ml of 28%~30% Ammonium Hydroxide to 125 ml ddH2O. Mix well.

Hybridize AMP1

1. Tap to remove excess liquid from slides. Place slides in the HybEZ Slide Rack located in the HybEZ humidity control tray. Add ~4 drops of the AMP1 to entirely cover each section.
2. Close the tray, and insert into the oven for 30 min at 40°C.

3. Remove HybEZ control tray from the oven and remove HybEZ Slide Rack.
4. Remove all slides from the rack, and quickly tap excess liquid. Put all slides into slide holder, and submerge into jar with 1X wash buffer.
5. Wash slides in 1X wash buffer for 2 min at RT. Agitate slides 3 times by lifting up and down.
6. Repeat step 5 with fresh 1X wash buffer.

Hybridize AMP2

1. Tap to remove excess liquid from slides. Place slides in the HybEZ Slide Rack located in the HybEZ humidity control tray. Add ~4 drops of the AMP2 to entirely cover each section.
2. Close the tray, and insert into the oven for 15 min at 40°C.
3. Remove HybEZ control tray from the oven and remove HybEZ Slide Rack.
4. Remove all slides from the rack, and quickly tap excess liquid. Put all slides into slide holder, and submerge into jar with 1X wash buffer.
5. Wash slides in 1X wash buffer for 2 min at RT. Agitate slides 3 times by lifting up and down.
6. Repeat step 5 with fresh 1X wash buffer.

Hybridize AMP3

1. Tap to remove excess liquid from slides. Place slides in the HybEZ Slide Rack located in the HybEZ humidity control tray. Add ~4 drops of the AMP3 to entirely cover each section.
2. Close the tray, and insert into the oven for 30 min at 40°C.

3. Remove HybEZ control tray from the oven and remove HybEZ Slide Rack.
4. Remove all slides from the rack, and quickly tap excess liquid. Put all slides into slide holder, and submerge into jar with 1X wash buffer.
5. Wash slides in 1X wash buffer for 2 min at RT. Agitate slides 3 times by lifting up and down.
6. Repeat step 5 with fresh 1X wash buffer.

Hybridize AMP4

1. Tap to remove excess liquid from slides. Place slides in the HybEZ Slide Rack located in the HybEZ humidity control tray. Add ~4 drops of the AMP4 to entirely cover each section.
2. Close the tray, and insert into the oven for 15 min at 40°C.
3. Remove HybEZ control tray from the oven and remove HybEZ Slide Rack.
4. Remove all slides from the rack, and quickly tap excess liquid. Put all slides into slide holder, and submerge into jar with 1X wash buffer.
5. Wash slides in 1X wash buffer for 2 min at RT. Agitate slides 3 times by lifting up and down.
6. Repeat step 5 with fresh 1X wash buffer.

DO not insert tray into the oven for the rest of the procedure.

Hybridize AMP5

1. Tap to remove excess liquid from slides. Place slides in the HybEZ Slide Rack located in the HybEZ humidity control tray. Add ~4 drops of the AMP5 to entirely cover each section.

2. Place the HybEZ slide rack in the HybEZ humidity control tray. Close tray and incubate for 30 min at **RT**.
3. Remove HybEZ Slide Rack from the HybEZ humidity control tray.
4. Remove all slides from the rack, and quickly tap excess liquid. Put all slides into slide holder, and submerge into jar with 1X wash buffer.
5. Wash slides in 1X wash buffer for 2 min at RT. Agitate slides 3 times by lifting up and down.
6. Repeat step 5 with fresh 1X wash buffer.

Hybridize AMP6

1. Tap to remove excess liquid from slides. Place slides in the HybEZ Slide Rack located in the HybEZ humidity control tray. Add ~4 drops of the AMP6 to entirely cover each section.
2. Place the HybEZ slide rack in the HybEZ humidity control tray. Close tray and incubate for 15 min at **RT**.
3. Remove HybEZ Slide Rack from the HybEZ control tray.
4. Remove all slides from the rack, and quickly tap excess liquid. Put all slides into slide holder, and submerge into jar with 1X wash buffer.
5. Wash slides in 1X wash buffer for 2 min at RT. Agitate slides 3 times by lifting up and down.
6. Repeat step 5 with fresh 1X wash buffer.

Detect the signal

1. Briefly spin down the contents of the Fast Red-B tube to be sure the content is at the bottom of the tube before opening the cap.
2. Prepare 120 ul of RED working solution per section by using a 1:60 ratio of Fast RED-B to Fast RED-A. For example, add 2 ul of Fast RED-B to 120ul of Fast RED-A. 4 drops of Fast RED-A can give enough 120 ul solution. **Use the mixture of Fast RED working solution within 5 min.**
3. Tap to remove excess liquid from slides. Pipette ~120 ul of RED solution onto each tissue section. Place the HybEZ slide rack in the HybEZ humidity control tray. Close tray and incubate for 10 min at **RT**.
4. Remove HybEZ Slide Rack from the HybEZ control tray.
5. Quickly tap excess liquid. Put all slides into slide holder, and submerge into jar with ddH2O.
6. Rinse again with fresh ddH2O.

Counterstain the slides

1. Submerge slides into jar containing 50% Hematoxylin staining solution for 2 min 20s at RT.
2. Immediately transfer the slides into jar with ddH2O, wash slides 4 times by lifting slides up and down. Repeat with fresh ddH2O 3 more times (4 times in total). Slides should become clear, while sections remain purple.
3. Transfer slides into jar with 0.02% Ammonia water. Move slides up and down 5 times. Section should turn blue (hard to see actually)

4. Replace Ammonia water with ddH2O. Wash slides 4 times.

Mount the samples

1. Remove the slide rack from the jar with ddH2O, and dry slides in a 60°C regular oven for at least 15 min.
2. Brief dip one slide into fresh pure xylene one time, and immediately place 1~2 drops of EcoMount on the section before xylene dries.
3. Carefully place a 1.5 thickness 24 X 50 mm coverslip (Corning #2980-245) over the tissue section. Avoid air bubble.
4. Air dry slides for >=5 min.

APPENDIX L

SECRETE-PAIR DUAL LUMINESCENCE ASSAY (GENECOPOEIA)

Goal: To determine the effect of exogenous treatment on regulating gene expression at the transcriptional level.

Reagents

Lipofectamine 3000 (Life Technologies, L3000008)

Opti-MEM (Life Technologies, 31985062)

Secrete-Pair Dual Luminescence Assay Kit (GeneCopoeia #LF031)

Gluc/SEAP plasmid (GeneCopoeia #pEZX-PG04)

Cell transfection

1. Culture cells in a 6-well plate, 2 ml medium per well.
2. When the confluence reaches 80%, transfect cells with dual-reporter constructs following Lipofectamine 3000 protocol as follows:
3. Add 125 µl Opti-MEM medium and 7.5 µl of Lipofectamine 3000 Reagent into a 1.5 ml tube. Mix well.
4. Dilute 5 µg of plasmid into 125 µl Opti-MEM medium in a second 1.5 ml tube, and then add 10 µl P3000 Reagent (not to be confused with Lipofectamine 3000 reagent). Mix well.
5. Add 132 µl diluted DNA to the diluted Lipofectamine 3000 Reagent in step 3 (1:1 ratio). Mix well.
6. Incubate at RT for 15 minutes.

7. Transfer all nucleic acid-lipofectamine 3000 complexes to the well containing cells. Mix them by gently swirling the plate. Place the plate to 37°C incubator.
8. Change to fresh medium containing treatments (such as DMSO or 10 nM TCDD) 24 hours after transfection. 2 ml fresh medium per well. Add one well of fresh medium in an empty well as a background signal.
9. Collect 0.4 ml of supernatant per sample 24 and 48 hours after experimental treatment. Store the collected medium in -20°C if not use immediately. The enzymes are stable at
   -20°C for at least one month.

Gaussia Luciferase Assay Procedure (using Secrete-Pair Dual Luminescence Assay Kit)

1. Thaw Buffer GL-S (10x) thoroughly at RT, inverting the tube several times and then vortex for 3~5 sec. Dilute 1:10 in distilled water to make 1x Buffer GL-S. Prepare 100 µl of 1x Buffer GL-S for each reaction. Duplicates for each sample are recommended.
2. Prepare the Gluc Assay Working Solution (e.g. 10 samples) by adding 10 µl of substrate GL to 1 ml of 1x Buffer GL-S. Mix well by inverting the tube several times.
3. Incubate at RT for 25 minutes (capped and protect from light) before adding to the samples.
4. Setup the luminometer (CLARIOstar). Set the measurement for 3 seconds of integration. Do not use over 6 seconds of integration.

5. Pipet culture medium samples from step 9 (10 µl per well, in duplicates) into a 96-well white (opaque) plate (Corning catalog #3912).
6. Add the Gluc Assay Working Solution from Step 2 (100 µl per well) to the samples from step 5. After finishing pipetting, gently tap the plate several times to mix the sample and substrate.
7. Centrifuge the plate briefly.
8. Proceed with the measurement.

SEAP Assay Procedure (using Secrete-Pair Dual Luminescence Assay Kit)

1. Aliquot 40 µl of each culture medium from step 9 above into eppie tube. Heat the medium at 65°C for 15 minutes in a heat block, and then place on ice.
2. Thaw Buffer AP (10x) thoroughly at RT, inverting the tube several times and then vortex for 3~5 sec. Dilute 1:10 in distilled water to make 1x Buffer AP. Prepare 100 µl of 1x Buffer AP for each reaction. Duplicates for each sample are recommended.
3. Prepare the SEAP Assay Working Solution (e.g. 10 reactions) by adding 10 µl of substrate AP to 1 ml of 1x Buffer AP. Mix well by inverting the tube several times.
4. Incubate at RT for 10 minutes (capped and protect from light) before adding to the samples.
5. Setup the luminometer (CLARIOstar). Set the measurement for 3 seconds of integration. Do not use over 6 seconds of integration.
6. Pipet heated culture medium samples (10 µl per well, in duplicates) into a 96-well white (opaque) plate (Corning #3912).

7. Add the SEAP Assay Working Solution from Step 3 (100 µl per well) to the samples from step 6. After finishing pipetting, gently tap the plate several times to mix the sample and substrate.
8. Centrifuge the plate briefly. Incubate the plate at RT for 5 minutes.
9. Proceed with the measurement.

APPENDIX M

CHROMATIN IMMUNOPRECIPITATION ASSAY

Purpose: to determine the interacting between a transcription factor of interest and the promoter of a direct target of the transcription factor.

Reagents:

ChIP-IT High Sensitivity (Active Motif #53040)

37% formaldehyde solution (Sigma #252549)

Reagent Preparation

Complete cell fixation solution

Buffer should be prepared fresh before experiment. For every 10 ml of cell growth medium used, prepare 1.25 ml of Complete Cell Fixation Solution by adding 90 µl Fixation Buffer to 0.785 ml sterile water in a 15 ml conical tube. And then add 375 µl 37% formaldehyde to the tube, and vortex to mix. Use 1/10 growth medium volume per sample.

PBS Wash Buffer

For 25 ml PBS Wash Buffer, add 21.25 ml sterile water, 2.5 ml 10X PBS and 1.25 ml Detergent. Mix well. Place PBS Wash Buffer on ice to chill.

DNA purification Wash Buffer

Add 40 ml of fresh 100% ethanol to the DNA purification wash buffer bottle. Mix well.

Section A: Cell fixation.

1. Remove organoid culture medium and add 0.5 ml ice-cold PBS to each well. Break up the Matrigel by pipetting up and down several times and scraping remaining Matrigel. Transfer the suspension into a 15 ml conical tube filled with 5 ml ice-cold PBS.
2. Centrifuge at 500 g for 3 minutes at 4°C, and carefully aspirate.
3. Add 3 ml of room temp Gibco DPBS to suspend organoids.
4. Add 0.3 ml freshly prepared Complete Cell Fixative Solution to organoids. Shake gently at RT for 15 minutes.
5. Stop the fixation reaction by adding 0.165 ml Stop Solution. Swirl to mix and incubate at RT for 5 minutes.
6. Centrifuge at 1250 g for 3 minutes at 4°C.
7. Remove the supernatant. Resuspend the pellets in 5 ml ice-cold PBS Wash Buffer by pipetting up and down. Keep samples at 4°C for the reminder of the procedure.
8. Centrifuge at 1250 g for 3 minutes at 4°C. Remove the supernatant. Resuspend the pellets in 5 ml ice-cold PBS Wash Buffer again by pipetting up and down. Centrifuge at 1250 g for 3 minutes at 4°C. Remove the supernatant.
9. Resuspend the pellet in 2 ml Chromatin Prep Buffer supplemented with 2 µl PIC and 2 µl 100 mM PMSF. Pipet up and down to mix.
10. Incubate on ice for 10 minutes.
11. Transfer the resuspended pellets individually to a chilled dounce homogenizer on ice. Use the tight fitting pestle to homogenize the sample for ~60 strokes.

Transfer the contents to a new 15 ml conical tube and centrifuge for 3 minutes at 1250 g at 4°C.

12. Remove the supernatant and discard. Resuspend each pellet in 500 µl ChIP Buffer supplemented 5 µl PIC and 5 µl 100 mM PMSF. Transfer the contents to a new 1.5 ml tube.
13. Incubate on ice for 10 minutes.

Section B. Chromatin Sonication.

1. Open Bioruptor Pico (Diagenode #B01060010) appropriately.
2. Sonicate samples by applying 12 sonication cycles 30 second ON/30second OFF.
3. Spin tubes at 4°C at 16,000 g for 2 minutes to pellet the cellular debris.
4. Transfer 25 µl of each chromatin preparation from step 3 into a 600 µl PCR tube as the Input DNA.
5. Aliquot the remainder of each chromatin preparation into two 600 µl PCR tubes. 250 µl per tube. Store at -80°C.

Input Preparation

1. To each 25 µl chromatin preparation from Step 4 above, add 175 µl TE pH 8.0 and 1 µl RNAse A. Cap the tube, and vortex to mix.
2. Incubate in a thermocycler at 37°C for 30 minutes.
3. Add 2 µl Protease K to each tube and vortex. Incubate tubes in a thermocycler at 55°C for 30 minutes, and then increase the temperature to 80°C for 2 hours.
4. Transfer each chromatin input to a 1.5 ml tube. Add 83 µl Precipitation Buffer, 2 µl Carrier and 750 µl absolute ethanol. Vortex to mix and chill at -80°C overnight.

5. Centrifuge at 16,000 g for 15 minutes at 4°C.
6. Carefully remove the supernatant. Wash the pellet with 500 µl 70% ethanol and spin at 16,000 g for 5 minutes at 4°C.
7. Carefully remove the supernatant. Leave the tubes uncapped, and incubate at 60°C for 30 minutes to allow the pellet air dry.
8. Add 25 µl DNA Purification Elution Buffer to each tube. Incubate at RT for 20 minutes. Then vortex to ensure the pellet is completely dissolved.
9. Measure DNA concentration on a Nanodrop. Store the Input DNA at -20°C.

Section C. Immunoprecipitation.

1. Thaw sonicated chromatin on ice. Spin chromatin at 16000*g for 2 minutes at 4°C.
2. Setup the ChIP reactions by adding the components in the order shown in Table 1 below to 1.5 ml tubes. Use the input DNA concentration to calculate the volume for chromatin immunoprecipitation. Recommend using 10~30 µg chromatin per reaction. However, it is very difficult to obtain for organoids. 3 µg chromatin per reaction could be used for organoids.
3. In a 600 µl PCR tube, prepare the antibodies to be used in the ChIP reactions. IgG and target antibody should be performed at the same time. IgG is a negative control for testing antibody specificity.

Use a separate tube for each antibody. To the tube, add 5 µl Blocker and 4 µg ChIP antibody (2 µg AhR antibody (Enzo, BML-SA210) used in most of literature)). Incubate Antibody/Blocker mix for 1 minute at RT and then add to the ChIP reactions.

Table 1

Reagent	1 reaction
Sheared Chromatin (3~30 µg)	X µl
ChIP Buffer	Adjust up to 200 µl
Protease Inhibitor Cocktail (PIC)	5 µl
Antibody/Blocker mix (from step 3)	Not to exceed 35 µl
Maximum volume allowed	240 µl

4. Cap tubes and incubate on an end-to-end rotator overnight at 4°C.
5. The protein G agarose beads require washing before use. Transfer 30 µl Protein G agarose beads for each ChIP reaction to a 1.5 ml tube. Add an equal volume of TE, pH 8.0 and invert to mix. Spin at 1250*g for 1 minute at 4°C. Remove the supernatant equivalent to the volume of TE added to the agarose beads.

Note: Before pipetting the Protein G agarose beads, they should be fully resuspended by inverting the tube. When pipetting the beads, cut 2 mm from the end of a pipet tip to prevent the tip from becoming clogged.

6. Wash the beads a second time with the same volume of TE, pH 8.0 and invert to mix. Spin at 1250*g for 1 minute at 4°C. Remove the supernatant equivalent to the volume of TE added to the agarose beads. The beads are now ready to use.
7. Spin the ChIP reactions at 1250*g for 1 minute at 4°C to collect liquid from the inside of the cap.
8. Using a cut pipet tip, add 30 µl washed Protein G agarose beads to each reaction. Cap tubes and incubate on an end-to-end rotator at 4°C for 3 hours.

9. Label a ChIP Filtration Column for each ChIP reaction. Remove the tab from the bottom of the column and place in a vertical rack (the side holds small tubes) sitting in an empty 1 ml pipet tip box.
10. Remove ChIP reactions from rotator and spin at 1250*g for 1 minute at 4°C to collect liquid from inside of the cap.
11. Add 600 µl ChIP Buffer to each ChIP reaction, then transfer the entire reaction (including the protein G agarose beads) to its labeled column. Allow flow-through to occur by gravity.
12. During the gravity flow, transfer 100 µl per ChIP reaction of Elution Buffer AM4 to a 1.5 ml tube and allow to pre-warm at 37°C during the wash steps.
13. Wash each column with 900 µl Wash Buffer AM1. Let stand for 3 min.
14. Repeat Step 13 four more times for a total of five washes.
15. Transfer columns to a new 1.5 ml tube and spin at 1250*g for 3 minutes at RT to remove residual Wash Buffer.
16. Following the spin, transfer the ChIP Filtration Columns to new 1.5 ml tubes. Add 50 µl 37°C Elution Buffer AM4 to each column. Incubate at RT for 5 minutes. Spin at 1250*g for 3 minutes at RT.
17. Add another 50 µl 37°C Elution Buffer AM4 to each column. Incubate at RT for 5 minutes. Spin at 1250*g for 3 minutes at RT.
18. Discard the ChIP Filtration Columns. The flow-through (~100 µl volume) contains the ChIP DNA. Proceed to Section D.

Section D. Reversal of Cross-links and DNA purification

1. Transfer each eluted ChIP DNA to a 250 µl PCR tube and add 2 µl Proteinase K. Vortex to mix and heat in a thermocycler at 55°C for 30 minutes and then increase the temperature to 80°C for 2 hours.
2. Transfer the DNA to a 1.5 ml tube and add 5 volumes (500 µl) DNA Purification Binding Buffer to each tube and vortex to mix. Adjust the pH with 5 µl 3M Sodium Acetate. The sample should be bright yellow in color to indicate a proper pH.
3. For each sample, place a DNA purification column (AM#103928) in the collection tube and add each pH adjusted sample to its own column. Close the cap on each column, place them with the collection tubes in a centrifuge, and spin them at 14000*g for 1 minute at RT.
4. Remove the column from the collection tube, then remove and discard the flow through from the collection tube. Return the column to the collection tube.
5. Prepare DNA Purification Wash Buffer (AM#103497) before the first use. Add 750 µl DNA Purification Wash Buffer to each column and cap the column.
6. Spin at 14000*g for 1 minute at RT.
7. Remove the column from the collection tube, then remove and discard the flow through from the collection tube. Return the column to the collection tube.
8. With the column cap open, spin at 14000*g for 2 minutes at RT to remove any residual Wash Buffer from the column.
9. Transfer the column to a clean 1.5 ml tube. Add 80 µl of 37°C pre-warmed DNA Purification Elution Buffer (AM#103498) to the center of the column matrix.

Incubate for 1 minute at RT. Spin at 14000*g for 1 minute at RT. Add an additional 80 µl of 37°C pre-warmed DNA Purification Elution Buffer (AM#103498) to the center of the column matrix. Incubate for 1 minute at RT. Spin at 14000*g for 1 minute at RT. Total elution volume is 160 µl.

10. Discard column. Purified DNA may be stored at -20°C for future qPCR.

Section F. Quantitative PCR (qPCR).

1. Follow the specific instructions for SYBR Green qPCR master mix (Life Technologies, A25742) and preparing triplicate or even four replicates per sample. I recommend performing linear test for each pair of target primers by using input DNA before real experiments. The known DNA quantities of Input DNA are 40 ng, 4 ng, 0.4 ng, 0.04 ng, 0.004 ng. The Ct value should be between 20 and 23 for 40 ng input, otherwise, the primers may not be sensitive to detect trace amount of ChIP DNA.

Table 2

Reagent	**15 µl PCR reactions**
2x SYBR Green master mix	7.5 µl
Primer mix (2.5 µM each primer)	3 µl what primers
qPCR quality water	0.5 µl
DNA sample (ChIP or Input)	4 µl
Total volume	15 µl

For real experiments, Input DNA should give 0.04 ng as normalization. Negative control primers (regions of the genome not bound by your protein of interest)

should be included as well. Negative control primers could be only performed in 3~4 independent samples.

2. Run SYBR Green qPCR reactions as per instructions.

Section G. Data analysis

Express data as a percentage of input.

1. Obtain the raw Ct values for all reactions including ChIP and IgG samples along with Input DNA samples using both target primers and negative control primers.
2. Calculate the amount (in ng) of ChIP DNA for each sample. Normalize ChIP DNA to corresponding Input DNA. For example, the average Ct value for ChIP DNA (Ct1) and corresponding Input DNA (Ct2) is 33 and 32 respectively, then the amount of ChIP DNA is 0.04 ng*$2^{Ct2-Ct1}$=0.04 ng* 2^{32-33}=0.02 ng.
3. Calculate the total amount of ChIP DNA in the whole reaction. Multiple the number in the Step 2 by 40 (dilution factor. The total eluted ChIP DNA in 160 µl, while 4 µl of eluted ChIP DNA is used for each well of qPCR). Therefore, the adjusted value should be 0.8 ng.
4. To express data as a percentage of input, divide the adjusted value from step 3 by the amount of DNA that went into the ChIP reaction and then multiply by 100%. For example, if 3 µg was used in the ChIP reaction per sample, it is equivalent to 3000 ng of chromatin. The calculation would be the adjusted value from step 3 divided by 3000 ng and then multiple 100. Hence, the ultimate percentage for the above example should be 0.8 ng/3000 ng*100%=0.027%. Typical percent of input recovered values are 0.05% to 1%.